RAVINDRAN MEENAKUMARI, H.N. 2024. *Modelling and analysis of vibrations in flexible cylinders subjected to internal multiphase and external single-phase flows*. Robert Gordon University, PhD thesis. Hosted on OpenAIR [online]. Available from: https://doi.org/10.48526/rgu-wt-2801155

Modelling and analysis of vibrations in flexible cylinders subjected to internal multiphase and external single-phase flows.

RAVINDRAN MEENAKUMARI, H.N.

2024

MODELLING AND ANALYSIS OF VIBRATIONS IN FLEXIBLE CYLINDERS SUBJECTED TO INTERNAL MULTIPHASE AND EXTERNAL SINGLE-PHASE FLOWS

HAREESH NARAIN RAVINDRAN MEENAKUMARI

PhD 2024

MODELLING AND ANALYSIS OF VIBRATIONS IN FLEXIBLE CYLINDERS SUBJECTED TO INTERNAL MULTIPHASE AND EXTERNAL SINGLE-PHASE FLOWS

HAREESH NARAIN RAVINDRAN MEENAKUMARI

A thesis submitted in partial fulfilment of the requirements of Robert Gordon University for the degree of Doctor of Philosophy

October 2024

Abstract

This study investigates the fluid-structure interaction phenomena of flexible straight cylinders subjected to internal two-phase slug flows and external vortex-induced vibrations (VIV) by taking into account the geometric and hydrodynamic nonlinearities. Flow-induced vibration (FIV) is a common phenomenon observed in various engineering systems such as heat exchangers, nuclear power plants, chemical process plants and hydrocarbon transportation. In many of these applications, internal flow generally occurs as multiphase flow, characterized by simultaneous flow of gas and liquid. Among different flow patterns that may emerge from multiphase flow, slug flows are widely recognised as problematic due to fluctuations in multiphase mass, velocities and pressure changes causing slug flow-induced vibrations (SIV). Most of the literature related to internal single and two-phase flow have largely focused on the use of a linearised tension beam model. Fundamental understanding of SIV in three-dimensional space and time considering in-line and axial dynamics is still lacking. A three-dimensional semi-empirical model is presented, incorporating nonlinear structural equations of coupled out-of-plane, in-plane and axial oscillations combined with equations involving centrifugal and Coriolis forces for the analysis and prediction of SIV. New dimensionless equations are derived from the dimensional model to analyse key flow features and improve overall understanding of the model. To capture forces due to VIV, the model uses a phenomenological wake oscillator model to emulate oscillatory drag and lift forces induced by VIV. An idealised slug unit model capable of capturing mass variations in the slug flow regime is utilised in this study assuming slug flows are fully developed and undisturbed by pipe oscillations. A numerical space-time finite difference scheme is implemented to analyse and solve the highly nonlinear partial differential equations present in the model. Model validations are performed by comparing the results with experimental and numerical data from literature related to SIV and VIV. Comparisons demonstrate qualitative and quantitative similarities with experimental results, highlighting the model's capability to capture similar amplitudes, frequencies and dominant modes excited by SIV and VIV. Parametric studies capture the effects of key SIV and VIV flow characteristics on the vibration responses of vertical and horizontal fluid-conveying cylinders. Results from SIV in submerged vertical straight cylinders revealed amplitude-modulation response, mean displacements, simultaneous three-dimensional oscillations and the influence of internal flow velocities. Lower flow velocities produced amplitude increase of up to 350% compared to higher velocities at specific slug formations. A new dimensionless parameter is introduced to predict scenarios of high amplitude oscillations for vertical cylinders conveying two-phase slug flows. SIV in flexible horizontal cylinders highlighted the significant effects of slug frequencies, internal flow velocities and fluid densities through large mean displacements, three-dimensional out-of-plane, in-plane and axial oscillations and parametric resonance. When the slug frequency to structure natural frequency ratio, $f_s/f_n = 1$, was observed, it generated high amplitudes with an increase of up to 4 times compared to $f_s/f_n = 2$ ratio at certain flow velocities. Additionally, frequency domain analysis revealed the presence of sub-harmonic frequencies and high frequency modulated response. Numerical results in the case of combined VIV-SIV excitation scenario exhibited variations in mean displacements and RMS amplitudes compared to VIV-only results in all three-directions of oscillations. In-line and axial oscillation amplitudes increased by up to 200% compared to VIV-only amplitude responses. Frequency domain analysis demonstrated frequency response with increased frequency components and sub-harmonics particularly in the in-line and axial oscillations. Moreover, parametric resonance conditions produced an oscillation amplitude increase of up to 2 times in the cross-flow direction and up to 8 times in the in-line direction, with increased frequency modulations, sub-harmonic frequencies and variations in obtained dominant modes.

Keywords: Slug flow, Flexible cylinder, 3-D response, Nonlinear dynamics, Fluid-structure interaction, Vortex-induced vibrations, Parametric resonance.

Acknowledgments

First of all, I would like to express my heartfelt gratitude to my PhD supervisors Dr Hossein Zanganeh and Prof Mamdud Hossain for providing me with this invaluable opportunity. Their unwavering support, guidance and patience have been instrumental in completing this journey. I extend my heartfelt appreciation for their dedication, encouragement and constructive feedback. Their mentorship has immensely shaped my academic journey, and I am genuinely thankful for the opportunity to learn and grow under their guidance. I would like to thank the School of Engineering at Robert Gordon University, Aberdeen for providing the scholarship to carry out my studies.

I would like to extend my sincere gratitude to Dr Anil Prathuru, Dr Taimoor Asim, Dr Ghazi Droubi and Dr Ketan Pancholi for their constant support and guidance throughout my doctoral journey. Their valuable insights, constant support and advice have enriched my research experience and contributed significantly to my academic growth. I am truly grateful for their mentorship.

During my time at RGU I have had the pleasure of meeting many friends who have brought happiness to my life. I am particularly grateful to Mr Vinooth Rajendran for his motivation, guidance and for making my life at RGU truly enjoyable. I am sincerely grateful for his presence throughout this endeavour.

I would also like to thank all the faculty and staff members at the School of Engineering, especially Dr Rosslyn Shanks and Mr Kiall Clark for their invaluable assistance and guidance throughout my research journey. I am truly thankful for their dedication and expertise.

Finally, I wish to express my deepest gratitude to my wife, parents and sister, whose unconditional love and support have been my source of strength and inspiration. I am forever grateful to my parents for their constant encouragement, selfless sacrifices and unwavering support.

Table of Contents

List of Figures

List of Tables

Nomenclature

Abbreviations

3-D	Three-dimensional
FSI	Fluid-structure interaction
FIV	Flow-induced vibration
SIV	Slug flow-induced vibration
VIV	Vortex-induced vibration

Roman Symbols

A_r	Cross-sectional area
A_w/D, A_u/D, A_v/D	Dimensionless out-of-plane, in-plane and axial amplitude
A_{wrms}/D, A_{urms}/D, A_{vrms}/D	RMS value of out-of-plane, in-plane and axial amplitude
C	Damping coefficient
C_D	Oscillating drag coefficient
Cd_o	Wake associated drag coefficient
$\bar{C}_d$	Mean drag coefficient
C_L	Oscillating lift coefficient
Cl_o	Wake associated lift coefficient
C_m	Added mass coefficient
D	Diameter
E	Young's modulus
EI	Bending stiffness
E_I	Dimensionless bending stiffness
EA_r	Axial stiffness
E_A	Dimensionless axial stiffness

F_D, F_L	Fluctuating drag and lift forces
f_{dm}	Frequency of the dominant mode
f_n	First natural frequency of the empty cylinder
f_{n1}	First natural frequency of the fluid containing cylinder
f_s	Slug frequency
f_{ow}, f_{ou}, f_{ov}	Oscillation frequencies in the out-of-plane, in-plane and axial directions
F_x, F_y, F_z	Hydrodynamic forces in streamwise and transverse direction
f_{vs}	Vortex-shedding frequency
g	Gravitational acceleration
G_n	Dimensionless gravitational acceleration
H_{LF}	Thin-film liquid holdup
H_{LS}	Slug liquid holdup
I	Moment of inertia
ID	Inner diameter
L	Length of the cylinder
L_D	Dimensionless length of the cylinder
L_F	Thin-film liquid length
L_S	Slug liquid length
L_U	Slug unit length
m	Mass per unit length
M	Dimensionless mass
m_a	Added mass
m_f	Mass of internal fluid
m_o	Mass per unit length plus added mass
p, q	Vortex drag and lift coefficients

S_t	Strouhal number
t_i	Dimensional time
T	Dimensional tension
t_m	Dimensionless time
T_o	Dimensional top pre-tension
T_n	Dimensionless tension
T_{no}	Dimensionless top pre-tension
u, v, w	Dynamic displacement in in-plane, axial and out-of-plane directions
U, V, W	Dimensionless displacement in in-plane, axial and out-of-plane directions
U_r	Dimensionless translational velocity
U_r'	New dimensionless translational velocity
V_e	Dimensional external flow velocity
V_r	Dimensionless external flow velocity
V_t	Dimensional internal translational velocity
V_{rel}	Dimensional external relative velocity
V_{rel}'	Dimensionless relative velocity
Y	Dimensionless cylinder span

Greek Symbols

ρ	Dimensional internal fluid density
ρ_e	Dimensional external fluid density
θ	Angle of attack of the external flow relative to the cylinder
ω_n	First natural frequency of the cylinder
$\varepsilon_u, \varepsilon_w, A_u, A_w$	Empirical wake coefficients

List of Publications

Journals (published)

Meenakumari, H.N.R., Zanganeh, H. and Hossain, M., 2024. Effect of slug characteristics on the nonlinear dynamic response of a long flexible fluid-conveying cylinder. Applied Ocean Research, 147, p.103978.

Conferences

Meenakumari, H.N.R., Zanganeh, H. and Hossain, M., 2023. Modelling and analysis of vortex-induced vibrations for flexible cylinders conveying two-phase slug flows. Proceedings of the 9th World congress on Mechanical, Chemical and Material Engineering. Brunel University, London. paper no. ICMIE 138.

Meenakumari, H.N.R., Zanganeh, H. and Hossain, M., 2023. Nonlinear dynamic response of vertical straight flexible cylinders conveying two-phase slug flows. 36th Scottish Fluid Mechanics Conference, Glasgow.

Meenakumari, H.N.R., Zanganeh, H. and Hossain, M., 2022. Three-dimensional dynamic interaction between slug flow and vertical straight flexible cylinders. Research Seminar, School of Engineering, Robert Gordon University, Aberdeen.

Journals (under preparation)

Meenakumari, H.N.R., Zanganeh, H. and Hossain, Three-dimensional vibration prediction model of horizontal flexible cylinders conveying two-phase slug flows. (manuscript in preparation).

Meenakumari, H.N.R., Zanganeh, H. and Hossain, Nonlinear dynamics of horizontal cylinders subjected to vortex-induced vibrations and internal multiphase flow. (manuscript in preparation).

Chapter 1

Introduction

1.1 Background

The importance of oil and gas in our society remains crucial, even as the global energy landscape undergoes significant transformations towards more sustainable and renewable energy resources. Despite the growing concern to reduce greenhouse gas emissions and manage climate change, oil and gas continue to fulfil a substantial portion of the world's energy needs. Globally oil and gas account for more than half of the primary energy consumption and this dominance is unlikely to reduce significantly in the immediate future. According to the Global Energy Outlook 2024, oil and gas accounts for about 53% of the world's energy consumption. In 2023, oil alone contributed approximately 29% to global energy use, making it largest source of energy followed by natural gas at 24%. These resources are not only used for electricity but also in applications such as transportation, where they fuel cars, airplanes, trucks and ships, which currently have few potent alternatives. Moreover, natural gas has become increasingly important in electricity generation due to its relatively low carbon emissions compared to coal and oil. Additionally, oil and gas remain fundamental to the petrochemical industry, which produces a variety of materials essential for modern life including plastics, fertilizers, pharmaceuticals, and synthetic fibres. It is also essential to understand the importance of oil and gas in the global economy. The global economy is highly dependent on the stability of oil and gas supplies, any sudden disruptions can have significant effects on markets and economies. For many countries oil and gas exports are an important source of revenue for essential services such as education, healthcare and infrastructure developments. For many nations, continued demand for oil and gas on the global market is essential for their economic stability.

In the last century, the surge in energy demands encouraged oil-industry pioneers to venture into offshore hydrocarbon explorations. Today, hydrocarbon sources from shallow water to ultra-deep waters collectively contribute to around one third of the total shares when it comes to supplying fossil fuels. With the advancements in technology and depletion of shallow water sources, oil rigs that were once situated few meters below the sea surface has now reached up to 2900 meters. Offshore explorations have now become a standardised practice with over 900 large-scale oil and gas platforms around the world. The pursuit into harsher and remote deep-water areas presents formidable challenges in subsea design and operation, especially for those facilities which may encounter severe environmental conditions. Marine risers and pipelines are essential structures in the oil and gas industry that play a crucial part in the production of hydrocarbons by transporting hydrocarbons from the subsea wells, several 100 meters under the sea surface, to the offshore floating unit (Maribus, 2014). Pipelines that convey internal multiphase flows are also used in several other engineering applications such as chemical, renewable energy, water management systems and nuclear industries. In chemical engineering, pipelines are used to transport multiphase mixtures during various stages of chemical processing. Pipelines often carry water mixed with air or solids in water distribution systems, hydroelectric powerplants and irrigation systems. In nuclear and thermal engineering, the safe and efficient transport of coolant is vital for operation of nuclear and thermal reactors. The presence of multiphase flow in these applications can create a dynamic environment that can cause pressure surges, blockages or even burst pipes.

Marine pipelines also play crucial role in offshore renewable energy industry, particular in wind, wave and tidal energy projects. One of the primary uses of marine pipelines in the offshore renewable industry is transporting water and other solids used for cooling systems or cleaning equipment in offshore installations. For instance, they transport seawater for cooling or other operational needs to enhance the efficiency of many mechanical systems. Another significant application for marine pipelines is in carbon capture and storage (CCS) projects associated with offshore energy productions. Many offshore projects are integrated with CCS technologies to capture carbon emissions from offshore sites and pipelines are used to to transport the captured CO_2 to subsea storage sites to mitigate environmental impact of energy production. Marine risers can be classified into rigid, flexible and top tensioned categories. Rigid risers are mainly used for shallow water explorations, whereas flexible and top tensioned risers are predominantly employed for deep-water hydrocarbon production. Flexible risers for deep-water explorations are of several configurations namely, catenary shaped, lazy wave, steep wave, lazy S, pliant wave, and Chinese lantern. Among which catenary risers are considered to be the most economical and technical solution for deep-water oil and gas production (Srinil and Bakis, 2019). However, due to their inherent flexibility and long lengths, subsea risers are likely to experience sizable flow-induced displacements when subjected to environmental loads such as waves, currents and internal flow variations. These unavoidable circumstances often lead to significant flow-induced vibration phenomena posing a critical challenge for the reliability and integrity of the entire subsea production unit. Fatigue failures due to flow-induced vibrations can be disastrous causing safety risks for personnel, environmental damage and costly repair procedures (James and Hudgins, 2016). Figure 1.1 depicts practical FIV challenges encountered in the offshore industry and the associated key flow and structural parameters considered in this study.

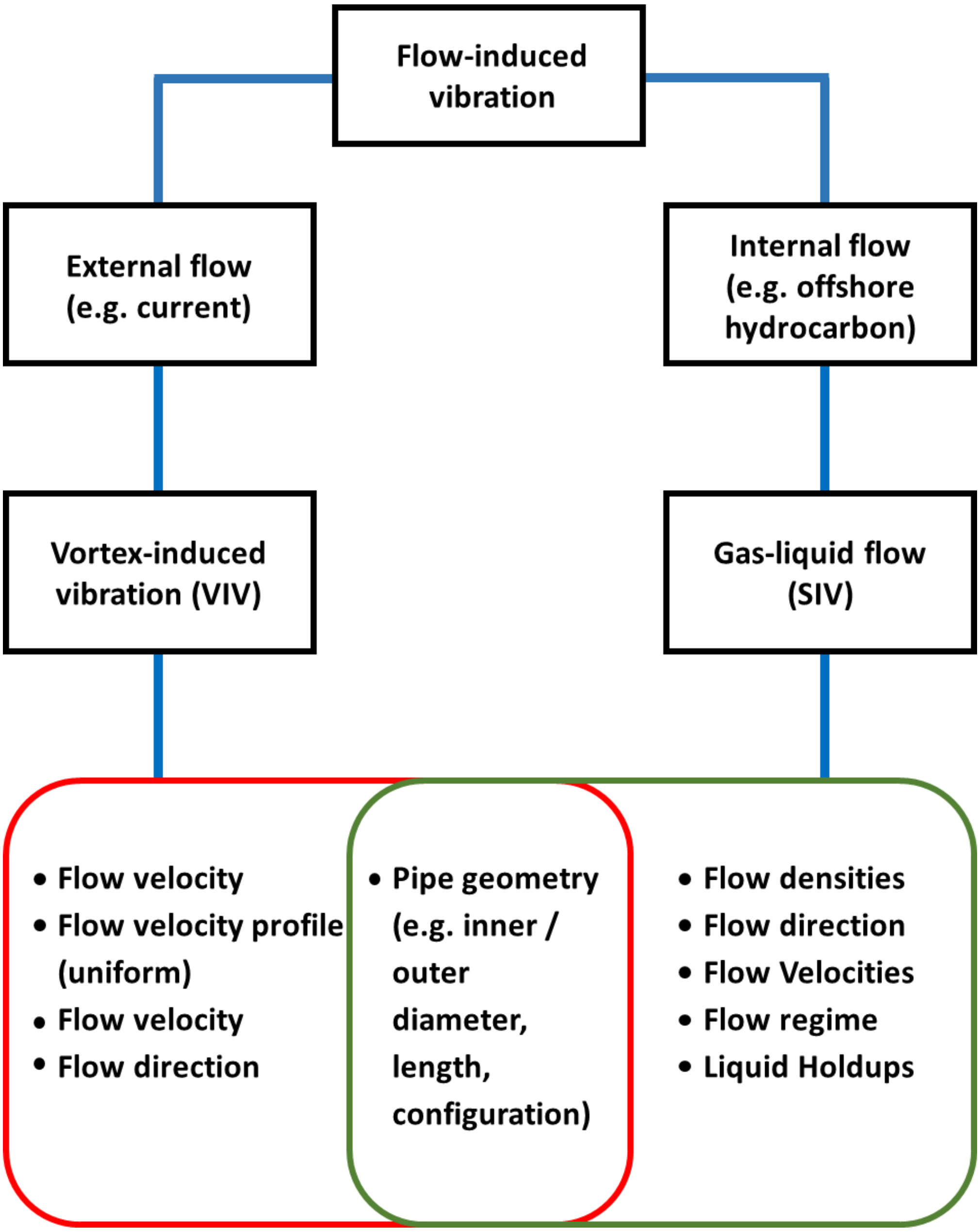

Figure 1.1: Types of FIV challenges encountered in the offshore industry considered in this study.

Flow-induced vibrations can occur in different sections of a subsea engineering unit such as platforms, marine risers, mooring cables, pipelines, umbilicals and jumpers as shown in Figure 1.2. Such a phenomena was first explored by Blevins (1977) who conducted a detailed study on FIV for offshore structures and examined models pertaining to structural vibrations due to external and internal hydrodynamic loads. Flow-induced vibrations occur as a consequence of interconnected forces exerted by the fluid on the structure and vice versa. Properties of fluids and structures include several variables, for example - fluid flows can be steady, unsteady, laminar, turbulent etc. and a structure can be rigid, flexible or can have multiple cross sections. This variation in basic FIV characteristics can lead to complex fluid-structure dynamics. The FIV phenomenon can be generally categorised into single-phase and multiphase flow-induced vibrations. Single-phase phase flow can be further classified as steady and unsteady flow. In the case of internal unsteady flows, fluid-structure interaction (FSI) is dominated by turbulent forces, while external unsteady forces are characterised by pressure forces. Alternatively, as a simultaneous flow of two or more fluids, multiphase flows may excite structure oscillations due to its inherent variations in flow properties such as mass, velocity and pressure.

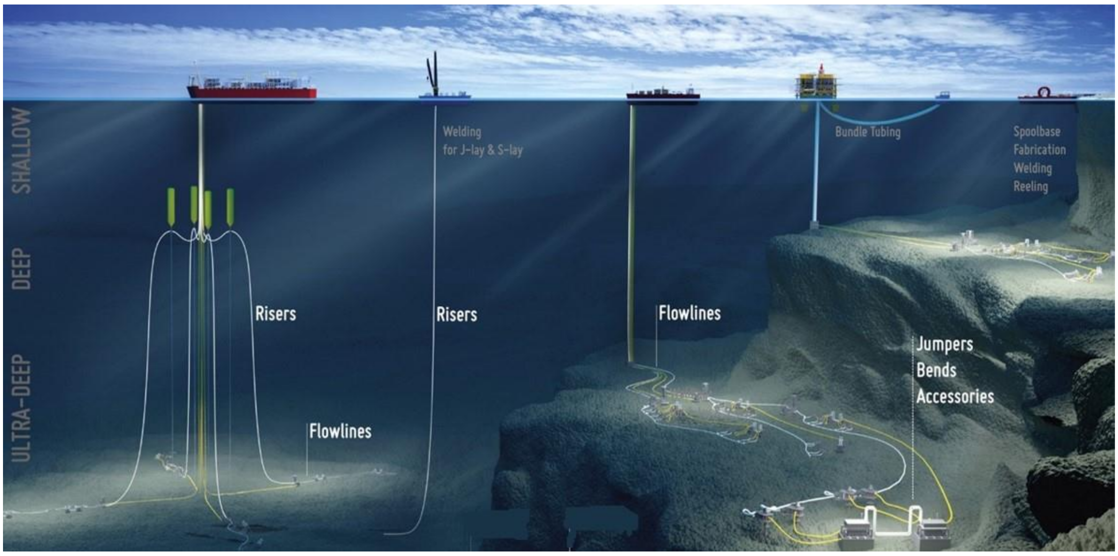

Figure 1.2: Schematic of different sections of a subsea production unit susceptible to flow-induced vibrations. (source: ArcelorMittal)

Multiphase flows can be defined as the simultaneous flow of gas, liquids (oil/water) and sometimes solid (sand). Knowledge of internal multiphase flows, characterised by fluctuating forces and dominant frequencies, is becoming increasingly important in various engineering applications such as chemical process systems, hydrocarbon transportation operations and nuclear energy extraction plants (Parameshwaran et al., 2016). Therefore, it becomes crucial during the design and operation stages to predict flow-induced forces and their interactions with the structure. Hydrocarbon flows from the subsea wells usually occur in multiphase flows, which are inherently intricate in nature because of numerous time and space varying flow variables. Depending on the nature of the reservoir, multiphase flows may consist of two leading gas and liquid (oil/water) phases also known as two-phase gas-liquid flows. In contrast to single-phase flows, the prediction of FIV due to multiphase flows are more challenging due to complex flow characteristics and unstable nature. The complexity of two-phase gas-liquid flow originates from various factors associated with flow properties, including gas and liquid superficial velocities, gas-liquid densities, viscosities, pressure, flow direction etc. Additionally, structural geometries such as pipe diameter, pipe inclination and operating conditions play significant roles potentially leading to the formation of different flow pattern phenomenon. For gas-liquid flows, some of the major flow patterns in a cylinder can be categorised as stratified, bubble and slug flows.

Among different flow patterns, slug flows have been identified as the most common flow pattern with significant force contributions. They are also considered to be the most undesirable flow regime due to its intermittent nature and fluctuations in mass and pressure. According to visual observations from experimental work by Duckler and Hubbar (1975), the process of slug liquid formation occurs in the following steps.

- As liquid and gas flow simultaneously inside the pipe, at the initial sections the liquid flows as a stratified phase below the gas phase. As liquid and gas superficial velocities increases and enters the range of velocities where slug flow is formed, the liquid phase decelerates as it moves along the pipe. This deceleration increases the level of liquid gradually approaching the top of the pipe. Around the same time waves start to develop in the liquid. As the liquid level and wave height increases, eventually it bridges the pipe cross-section and blocks the flow of gas.
- As liquid phase bridges the pipe, it is accelerated to the gas flow velocity. The acceleration of the liquid phase seems to be uniform across the pipe cross-section and acts as scoop picking up the slow-moving stratified liquid film ahead of it. This acceleration over time picks up enough volume of liquid film and forms a liquid slug as shown in Figure 3.2 in Chapter 3.

- The developed slug now sheds liquid from its back as it moves along the pipe and creates a thin film behind the slug. The shed liquid rapidly decelerates once again to much lower velocity controlled by the wall and interfacial shear.
- The liquid slug, once formed, as it traverses through the pipe sweeps all the excess liquid that entered the pipe since the final slug was developed. Beyond this point, the shed thin film liquid from the preceding slug is picked up by the newly developed slug. Since the rate of slug picking up liquid is same as the rate at which it sheds, the length of a slug unit remains consistent.
- The kinetic energy of the developed slug is higher than the preceding thin film and therefore the slug sweeps the thin film at a distance before merging with the liquid slug at slug velocity. This mechanism of slug over-running the preceding liquid film creates a mixing vortex whose length depends on the distance of merging. As the process of thin liquid film merging to the slug is chaotic in nature, gas is trapped in the mixing zone.
- As the slug and gas velocity increases, the level of gas in the slug increases. Eventually, the gas forms a sustained phase above the thin liquid film. After a point, slug begins to bypass the gas making the slug incompetent to bridge the cross-section of the pipe and block the gas phase. This point is the starting point of the transition from slug flow to annular flow. The mechanism of slug liquid formation is illustrated in Figure 1.3.

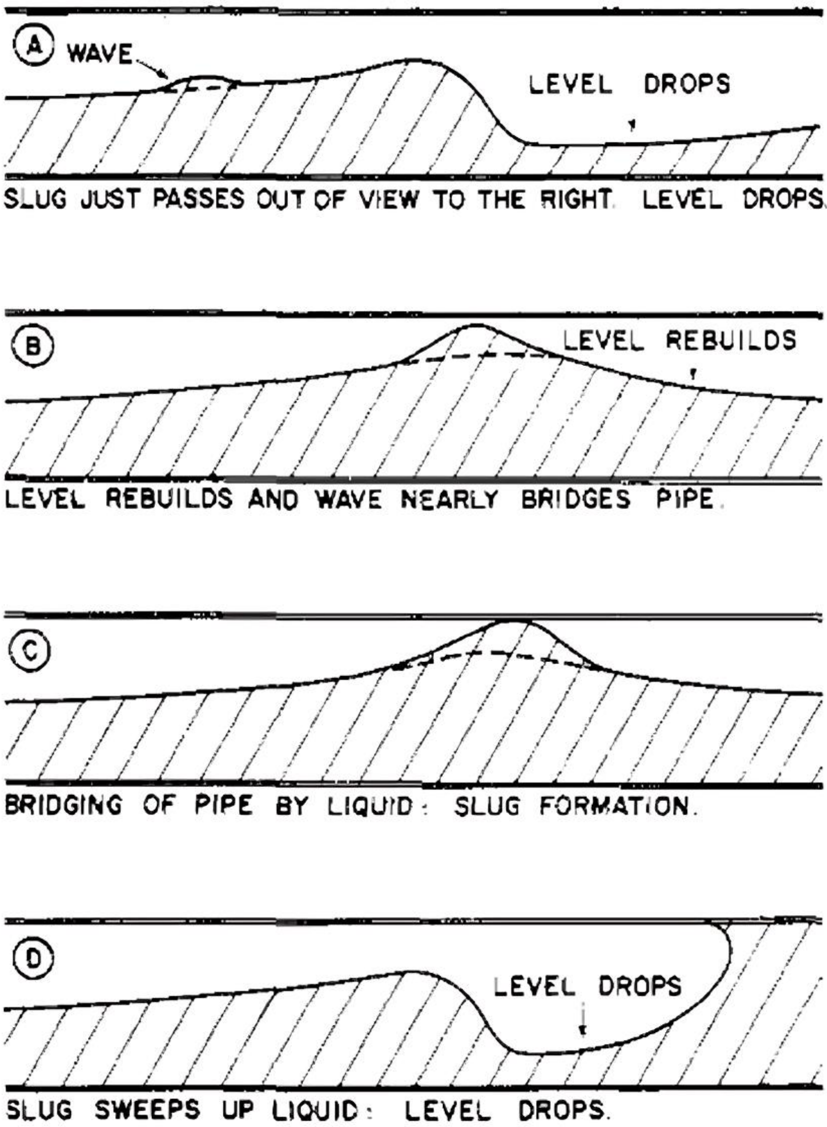

Figure 1.3: Step-by-step process of slug liquid formation inside a cylinder (Duckler and Hubbard, 1975).

The flow regime of slug flow can be characterised as an interchanging distribution of liquid and gas sections. In contrast to other homogeneous two-phase flow regimes, the slug flow regime inherently creates fluctuations in mass, pressure and flow momentum inside the pipe. Internal mass fluctuations can be attributed to the variations in two-phase densities owing to the large differences in density between the two phases. Similarly, fluctuations in velocity can be attributed to the differences in superficial velocities of the individual phases. Pressure fluctuations are caused due to the turbulence in the flow and momentum variations are caused due to a combination of momentum and velocity variations (Haile et al., 2022). In consequence, slug flow can develop fluctuating forces within the pipe with excitation frequencies, which could result in significant flow-induced vibrations when slug frequencies are close to the structure's natural frequencies (Hara, 1973). Furthermore, space-time varying forces could also be induced as a consequence of change in direction of flow in elbows, bends and steeply curved catenary risers. Two-phase flows are complex in nature and challenging to analyse as the forces created instigates structural oscillations and in turn the structural vibrations could cause changes in the internal flow properties. In the oil and gas industry, slug flow-induced vibrations are considered to be a major cause of concern as it could cause large and cyclic stresses on the structure reducing its fatigue life and sometimes causing devastating accidents. For example, Zaldivar (2010) reported that a major reason for the breakdown of a riser during the Macondo incident was caused due to internal slug flows when the slugging frequencies was close to the oscillation frequencies of the cylinder.

Subsequently, in the case of external FIV, vortex-induced vibrations is one of the largest and critical sources of vibrations for subsea production systems. This phenomenon occurs when a fluid particle during its flow encounters a bluff body along its path and is compelled to flow around the cylinder because of high stagnation pressure across the edges, thus forming a boundary layer. The developed boundary layer, because of excessive curvature separates from the surface of the cylinder forming vortices. These shed vortices alter the pressure distribution across the cylinder surface and cause increased lift and drag forces on the cylinder. The structure experiences resonance condition with increased hydrodynamic forces when the vortex shedding frequencies are close to or matches the natural frequency of the structure leading to large oscillation amplitudes. Complications due to VIV-induced forces amplify when long and flexible structures are considered, as these structures are susceptible to three-dimensional oscillations in directions perpendicular to the flow, in-line to the flow and longitudinal to the flow. Even after decades of research analysing the FIV due to external flows, VIV still remain a challenging subject due to the complexity in the hydrodynamic behaviour of fluid forces and the associated structural nonlinearities (Sumer and Fredsoe, 2006).

Considering the nature of oil and gas production systems, a scenario of combined VIV and SIV is highly probable. Hydrodynamic forces due to simultaneous VIV and SIV can generate greater challenges and uncertainties in the design and operation of subsea systems. Especially, long marine risers with high aspect ratios (length/diameter ratios) used at deeper water depths (>1000 m) are susceptible to enhanced oscillation amplitudes and stresses potentially leading to flow assurance problems and operational disruptions. Internal slug flows can possibly alter the structure dynamics and cause increased three-dimensional vibrations when VIV is active. A deeper understanding of SIV characteristics in three-dimensional space and time, along with combined external-internal excitation can be beneficial for the design and operation of offshore subsea systems. This study recognises this gap and presents a novel vibration prediction model for the analysis of combined VIV and SIV on the dynamic response of flexible straight vertical and horizontal cylinders.

1.2 Aims and Objectives of the Thesis

The present thesis aims at developing an advanced three-dimensional vibration prediction model to investigate the effects of key two-phase slug characteristics on the nonlinear vibration responses of a submerged straight vertical cylinder, unsubmerged horizontal cylinder and submerged horizontal cylinder subjected to combined internal (SIV) and external (VIV) excitations taking into account the geometric and hydrodynamic nonlinearities. These configurations are chosen as they have been previously studied experimentally, providing a basis for validation of the developed model. To achieve this, a semi-empirical theoretical model is developed comprising of nonlinear structural equations combined with equations involving centrifugal and Coriolis forces to emulate internal two-phase slug flows. The developed nonlinear model is capable of capturing mass variations in the slug flow regime. The model will be used for parametric studies to analyse the individual effects of SIV and combined effects VIV-SIV. Additionally, the model is validated through comparing published experimental and numerical results for SIV and VIV. To achieve these purposes, a finite difference scheme in the space and time domains is employed effectively solving the highly nonlinear equations present in the model. The key slug characteristics utilised in this study include the slug frequency, slug translational velocity, slug liquid holdup, thin-film liquid holdup, slug liquid length, thin-film liquid length, slug unit length and mass quotient. In the VIV front, the model includes variations in lift and drag coefficients through two coupled wake oscillator models. To achieve deeper understanding of the model during parametric study, dimensionless equations are introduced and analysed. In more specific detail, the objectives of the present thesis are as follows:

- To develop a three-dimensional fully nonlinear vibration prediction model comprising of coupled out-of-plane, in-plane and axial structural motions along with equations involving centrifugal and Coriolis forces for the analysis of SIV and VIV on vertical and horizontal straight flexible cylinders.

- To derive new dimensionless equations in the model to analyse the individual effects of key dimensionless terms through parametric studies and enhance overall understanding of the presented model.
- To compare numerical results from this study with published experimental and numerical results to verify the prediction capabilities of the model and to support key findings and observations discussed in the analysis of SIV-only and combined VIV-SIV.
- To perform a parametric study to analyse the effect of key slug characteristics, including slug translational velocity, slug liquid holdup, thin-film liquid holdup, liquid slug length, thin-film liquid length, slug unit length and mass quotient on the three-dimensional vibration response of a submerged straight vertical cylinder.
- To explore the influence of various slug frequency ratios, mass quotient ratios and parametric resonance conditions on the nonlinear vibration responses of an unsubmerged horizontal cylinder.
- To numerically investigate the three-dimensional structural motions of a submerged long horizontal cylinder under various VIV-SIV scenarios and explore the effects of parametric resonance on the combined external-internal excitation phenomena.

1.3. Outline of the Thesis

The thesis is structured as follows:

- In Chapter 2 the research studies performed on various two-phase flow regimes, SIV numerical and experimental investigations and the influence of internal single and two-phase flow on the VIV of flexible cylinders are reviewed.
- Chapter 3 presents the 3-D dimensional and dimensionless vibration prediction model taking into account the geometric and hydrodynamic nonlinearities for the analysis of SIV and VIV. The ability of the model to emulate numerically observed phenomena of SIV in submerged vertical cylinders is demonstrated through comparisons of natural frequencies against varying internal flow velocities. The significant effects of individual slug properties on the three-dimensional response of a submerged vertical cylinder are discussed. Finally, a new dimensionless parameter is introduced to predict large amplitude scenarios for long vertical cylinders transporting two-phase slug flows.
- In Chapter 4, the model is validated for unsubmerged horizontal cylinders through comparisons with published experimental results. The significance of considering geometric nonlinearities to predict vibrations due to slug induced forces are exhibited

through a parametric study exploring various slug frequency and mass quotient ratios. The phenomena of parametric resonance and subharmonics due to internal two-phase slug flows are explored.

- Chapter 5 presents the models capability to predict vibrations due to VIV-only through dominant modes and oscillation amplitude comparisons with published experimental results. The chapter further explores the three-dimensional responses of a submerged horizontal cylinder subjected to various VIV-SIV scenarios through a parametric study. Results from the numerical study highlight the significant effects SIV during the combined VIV-SIV scenario through enhanced mean displacements, harmonic and sub-harmonic frequencies, alterations in excited dominant modes and large 3-D oscillations due to parametric resonance.
- Chapter 6 summarises the conclusions of the present study and suggestions are made for future work in the research field.

Chapter 2

Literature Review

Fluid flow is a fundamental and important phenomenon in numerous engineering applications such as hydrocarbon production, nuclear power plants, heat exchangers and chemical process plants. Internal multiphase flow, in particular, has captured the attention of researchers in the recent years due to its common occurrence and associated challenges related to initial design, operational efficiency and reliable analysis. Multiphase flows can be further categorised into two-phase flows, which include gas-liquid, liquid-liquid, gas-solid and liquid-solid flows. Among these, gas-liquid two-phase flows are the most prevalent flow combination in the majority of the aforementioned engineering applications. Within the scope of this thesis, this chapter provides a review of previous research concerning gas-liquid flow characteristics and their influence on the vibration characteristics of flexible cylinders, slug flow-induced vibrations and the impact of internal flow on the combined external-internal excitation scenarios. The following sections cover the formation of gas-liquid flow patterns and two-phase flow pattern prediction maps, followed by numerical and experimental approaches to investigating SIV of flexible cylinders. Finally, literature investigating the influence of internal single-phase flows and two-phase slug flows on the combined excitation scenarios is reviewed.

2.1 Two-phase gas-liquid flow characteristics

2.1.1 Gas-liquid flow patterns in horizontal and vertical cylinders

Two-phase gas-liquid flow regimes are an important parameter when analysing vibrations of flexible cylinders induced by internal flow. Over the past two decades, numerous researchers have pursued the task of studying in detail the effects of different flow pattern on the vibration response of a cylinder through experimental and numerical approach. Different flow patterns may emerge during two-phase flows as a consequence of varying flow properties and structure orientation. Flow pattern prediction approaches in the early stages can be categorised into direct observations through high-speed photography (Vince et al., 1980) or X-ray attenuation (Hewitt and Roberts, 1969) and indirect approach through electrical impulses (Barnea et al., 1980), pressure fluctuations (Matsui, 1984), and ultrasound methods (Liang et al., 2016). When it comes to two-phase flows in horizontal pipes, flow patterns are classified into stratified smooth flows, stratified wavy flows, plug flows, slug flows, annular flows, and bubble flows. The schematic diagram of different flow patterns in horizontal pipes is described in Figure 2.1. Stratified flows are generally characterised by homogenous smooth flows, where gas and liquid flow separately at the top and bottom of the pipe. This type of flow occurs at low liquid and gas flow rates and as the gas flow rates slowly increases, the flow may transition into stratified wavy flow, during which smooth gas-liquid flows are replaced by wave-like flows.

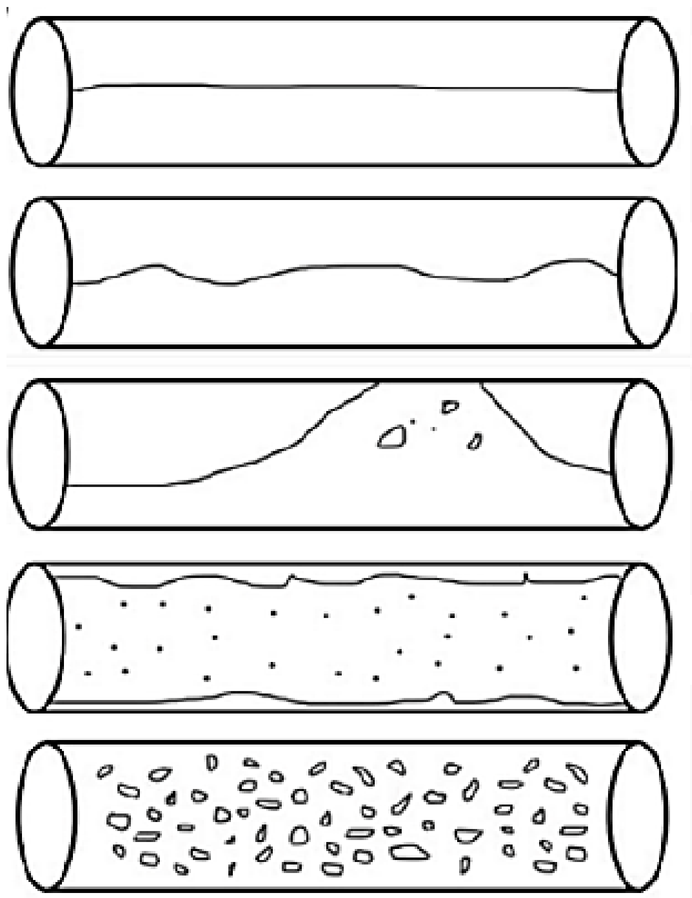

Figure 2.1: Two-phase gas-liquid flow patterns in horizontal cylinders (Umair et al., 2022).

On the other hand, as the liquid flow rates increase at constant gas flow rates, the flow pattern transitions to plug flow where the liquid region is separated by long gas bubbles. With further increase in liquid flow rates, the liquid region starts to incorporate small gas bubbles creating a flow regime popularly known as slug flows. When compared to plug flows, slug flows are generally associated with severe intermittency and longer gas bubbles. Upon further increase in gas flow rates, a liquid film region is formed in either side of the walls of the cylinder with gas bubbles at the centre forming the annular flow regime. At higher liquid rates and constant gas flow rates, the pipe becomes predominantly filled with liquid, while gas exists as small bubbles within the liquid region, creating a flow pattern referred to as bubble flow. Compared to two-phase flows in horizontal cylinders, flow pattern regimes exhibit slight variations in the case of two-phase flows in vertical cylinder. Among which bubble, plug and slug flow patterns are observed in both horizontal and vertical channels. Nevertheless, during plug and slug flow regimes in vertical channels, the liquid region forms a thick boundary layer on either side of the cylinder, while elongated bullet shaped gas bubbles, known as Taylor bubbles, form in the centre. These Taylor bubbles forms a nose-like shape with flatter tails as they occupy nearly the entire cross-section of the cylinder, with thin film liquids formed at either ends of the bubble. The schematic diagram of different flow patterns in vertical pipes is described in Figure 2.1. The difference between slug and plug flows in vertical cylinders is similar to that in horizontal pipes. At higher gas flow rates, a new regime termed churn flow is developed, identified by the formation of highly turbulent liquid slugs from the preceding slug flow regime (Fernandes et al., 1983).

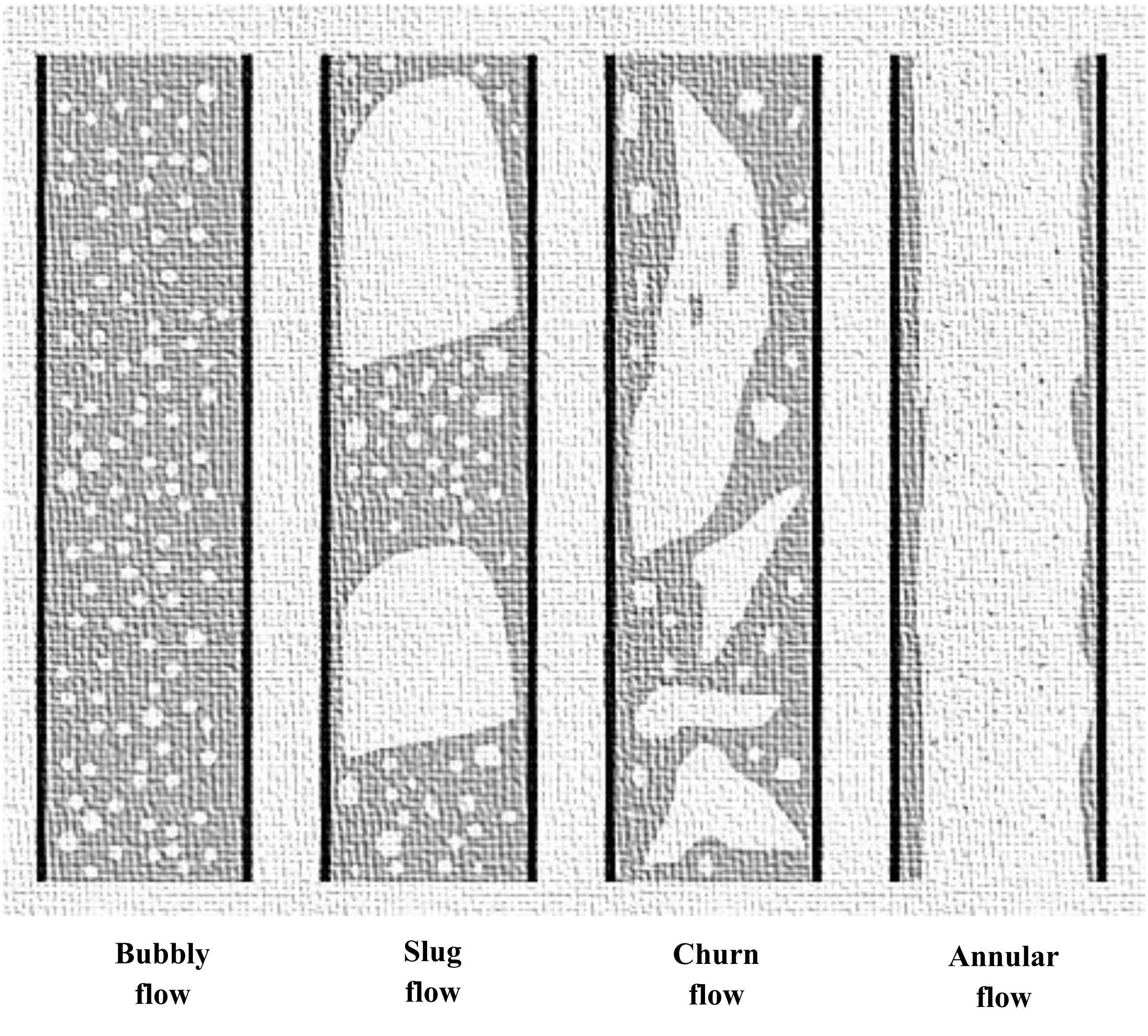

Figure 2.2: Two-phase gas-liquid flow patterns in vertical cylinders (Haile et al., 2022).

Two-phase flow regimes become a crucial parameter when it comes to internal flow-induced vibrations as different flow regimes lead to different amplitudes of vibration. Liu et al., (2012) investigated the force fluctuations of a vertical cylinder due internal two-phase flow through experimental techniques. Internal flow-induced forces were measured as superficial gas and liquid velocity were varied for a total of 36 cases, which included bubbly, slug, churn and annular flow regimes. Results from the experiment revealed that the RMS of force fluctuations exhibited maximum values during slug and churn flow regimes, while bubbly flow generated the lowest values. Cargnelutti et al., (2009) and Cargnelutti et al., (2010) performed experiments to analyse the effect of two-phase flow characteristics in different pipe configurations. The measured absolute forces were observed to be the highest during the slug flow regime, while the lowest forces were observed in the annular regime. Riverin and Pettigrew (2007) conducted experiments on a U-shaped pipe to study the vibration excitation mechanism for different flow regimes. Severe oscillations were noticed due to a resonance phenomenon caused between internal momentum fluctuations and the first natural frequency of the pipe. The slug flow regime exhibited force signals in the form of regular impulses describing the flow of liquid slugs. In contrast, the bubbly flow regime showed a narrow band force signal. Recently, Khan et al., (2022) reviewed in detail the two-phase flow-induced vibration phenomenon over a range of pipe and flow configurations. The study stated that among all the developed two-phase flow regimes, large amplitude oscillations were observed to occur during the slug and churn flow regimes.

2.1.2 Gas-liquid flow pattern prediction maps

Concurrently, numerous research studies have been performed to develop flow regime maps as a guide to predict the occurrence of different flow patterns in vertical and horizontal tube channels. Two-phase flow maps are essentially developed as a two-dimensional graph with sections separating the flow regimes. They can be classified as empirical or theoretical depending on the approach taken. Empirical flow maps are based on experimental observations, while theoretical maps are developed using mechanistic models describing fluid and structure characteristics. Baker (1954) developed one of the first flow pattern prediction map for horizontal pipe-flows through experimental observations and summarised the mechanism of all the flow-patterns observed. In the following years several other researchers developed other empirical flow pattern maps for horizontal air-water pipes (Hoogendoorn and Buitelaar, 1961; Govier and Omer, 1962).

However, Mandhane et al., (1974) developed one of the most influential flow pattern maps for horizontal pipes conveying two-phase gas-liquid flows shown in Figure 2.3. Through experimental approach, two-dimensional flow maps were developed by using gas-liquid superficial velocities as the coordinate system. Compared to other horizontal flow maps at the time, the developed map was found to provide better results with the air-water information. Similarly, the need for predicting flow patterns in vertical and inclined pipes was growing rapidly in the oil and gas industry. One of the most influential studies in developing vertical flow pattern maps was performed by Hewitt and Roberts (1969). They employed an experimental approach to observe different flow regimes, utilising superficial momentum fluxes as the coordinate system.

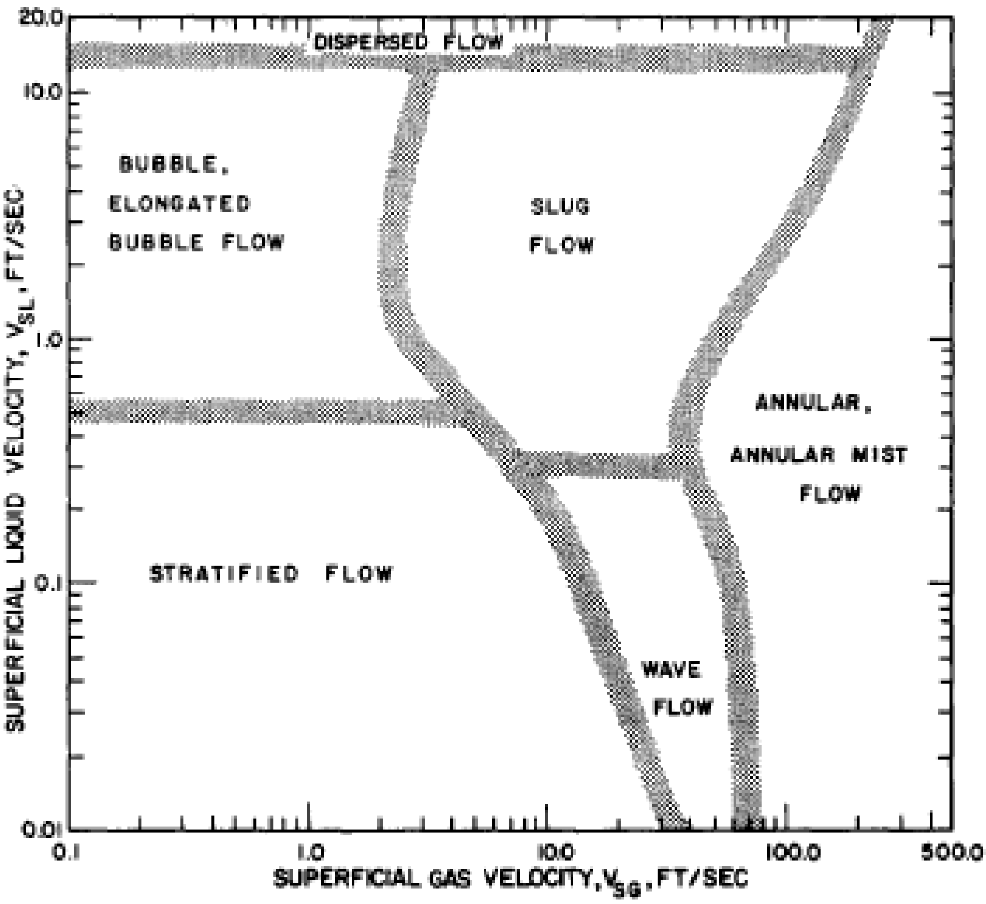

Figure 2.3: Two-dimensional flow pattern map developed by Mandhane et al., (1974) for varying superficial gas and liquid velocities.

However, flow patterns and their respective transition boundaries heavily depend on several fluid and structural parameters. Experimental approach for developing flow pattern maps poses numerous limitations when it comes to constructing maps for a wide range of flow conditions. This limitation can cause challenges during practical applications, as a wide range of flow conditions may arise during real-time production of gas and liquid. Therefore, huge efforts were made to design mechanistic flow pattern maps using dimensionless parameters to accommodate wide range of flow scenarios. The semi-empirical model developed by Taitel and Duckler (1976) was one of the first and most influential theoretical model designed for two-phase flow pattern prediction in horizontal and slightly-inclined cylinders. This theoretical approach allowed the consideration of several dimensional parameters as coordinate systems.

The model was then used for analysing the effects of several structural and fluid variables such as pipe diameter, liquid and gas superficial velocities etc. The developed model also appeared to provide identical results when compared to Mandhane et al., (1974). Subsequently, the theoretical model was further developed to predict flow pattern prediction for upward gas-liquid flows in vertical pipes (Taitel et al., 1980). Furthermore, numerous other researchers in the past have made efforts to design semi-empirical flow pattern maps by using wide range of coordinate systems. Among these, the most frequently used are volumetric gas and liquid flow rates, along with their corresponding densities, viscosities, and surface tension. Zhang et al., (2003) developed a unified mechanistic model for the prediction of flow pattern transitions, pressure variations and slug flow variables in gas-liquid flows across all pipe orientations. In this model equations for slug flow are not only used for the calculation of various slug characteristics such as liquid holdups, slug liquid lengths and slug translational velocity, but also to predict flow-pattern transitions by using the entire thin liquid film zone as the control volume. In a further study, Zhang et al., (2003) validated the developed mechanistic model with detailed experimental analysis for different pipe diameters, inclination, and fluid properties. The advancements in constructing flow transition maps over the years for gas-liquid flows across all pipe inclinations have paved the way for the developments in multiphase mathematical modelling (Danielson, 2012).

2.2 Slug Flow-Induced Vibrations

Among all the different flow patterns, the slug flow regime is found to be the most common and problematic flow pattern encountered in various engineering applications due its unstable and intermittent nature. This flow pattern can create random variations in mass distributions and pressure differences along the pipe, which may induce large amplitude oscillations when the slugging frequency is close to the structure natural frequency. Such oscillations result in cyclic stresses on the pipe over time, leading to fatigue failures, buckling and excessive curvature. These consequences have the potential to disrupt normal operations and cause severe internal damage. The accumulation of liquid slugs in the steam pipeline of a chemical plant led to a rupture accident due to increased pressure perturbations (Gong, 2010). Considerable efforts have been made by researchers in the past to study to investigate this complex fluid-structure interaction phenomena through numerical modelling and experimental techniques.

2.2.1 Investigation of slug flow-induced vibrations using mathematical models

Theoretical approach involves the development of mathematical models using governing equations and the use of computational fluid dynamics techniques to predict the oscillation response of a cylinder under the influence internal two-phase slug flows. Hara (1973) developed a semi empirical model capable of predicting the vibration response of a horizontal flexible piping system subjected to excitation by two-phase gas-liquid. The equation of motion developed includes forces due to inertia, elastic restoring force, centrifugal force, and Coriolis force of travelling liquid slugs. This influential study concludes by stating that two-phase slug flow-induced vibrations occur due to periodic fluctuations in the mass, centrifugal force, and Coriolis force of liquid slugs in the pipeline. The vibration response was described through a Mathieu type equation, and it was found that high amplitude oscillation occurs when the ratio of the liquid slug frequency to the structure's natural frequency is 1, 2, 2/3 and so on. In further study Hara (1977) validated the semi-empirical model by conducting an experimental analysis on a piping system conveying air-water two-phase flow with similar configurations. Results from the experiments were found to be in good agreement with the obtained theoretical results. Patel and Syed (1989) investigated the effects of internal slug flow on straight flexible risers with larger diameter and longer lengths. A governing equation comprising the dynamic excitation due to fluctuating internal mass was developed and compared with results from experimental arrangements. Results from the study showed that as gas and liquid flow velocities increase, the internal pressure of a riser also increases. Furthermore, this increase in internal pressure was found to alter the tension of the system. The study concludes by stating that the observed increase in internal pressures and mass variations due to slug flows can lead to large displacements and induce cyclic stresses on the system. Wu and Lou (1991) investigated the lateral motion of a marine riser conveying internal flow by developing a mathematical model. The model includes steady internal flow with factors such as currents and wave hydrodynamic loads. The dimensionless equation of the riser-fluid system is as follows:

$$\varepsilon\frac{d^4\eta}{d\xi^4}+\frac{d^2\eta}{d\tau^2}+\frac{kd\eta}{d\tau}+\frac{2\beta^{\frac{1}{2}}\alpha d^2\eta}{d\xi d\tau}+[-A+\gamma(1-\xi)]\frac{d^2\eta}{d\xi^2}-\gamma\frac{d\eta}{d\xi}=v^2+w^2+\mu\frac{dw}{d\tau}$$

Where, $\xi = w/L, \eta = u/L, \varepsilon = EI/MgL^3, \tau = \left(\frac{g}{L}\right)^{\frac{1}{2}}, k = \left(\frac{C_{eq}}{M}\right)\left(\frac{L}{g}\right)^{\frac{1}{2}}, \alpha = \left(\frac{m_f}{MgL}\right)^{\frac{1}{2}} V_t, \beta = \frac{mf}{M},$
$\gamma = 1-(m_a/M)(1+1/C_d), v = \left(\frac{\rho_e C_d D}{2Mg}\right)^{\left(\frac{1}{2}\right)} V, w = \left(\frac{C_{eq}}{Mg}\right)u, \mu = \left(\frac{\pi C_m \rho_e D^2}{4C_{eq}}\right)\left(\frac{g}{L}\right)^{\frac{1}{2}}, M = m +$

$m_a + m_f$, C_{eq} is the damping coefficient, g is the acceleration due to gravity, L is the length of the pipe, ρ_e is the external fluid density, C_d and C_m are the drag and inertia coefficients, D is the pipe external diameter, EI is the flexural rigidity and w and u are oscillations in the cross-flow and in-line direction respectively. The study concluded that the displacements and bending stress are sensitive to bending stiffness and that stiffness becomes an influencing parameter in the dynamic response at high internal velocities. Monprapurson et al., (2006) studied the effects of internal pulsatile flow on the static and dynamic response of an extensible flexible marine riser. Results from the study revealed that internal flow accelerations could displace vibration equilibrium positions of the marine riser, and fluctuations in internal flow could lead to large amplitude displacements and a decrease in natural frequencies.

Liu and Wang (2018) performed a mathematical analysis to investigate the effect of slug flow intermittence on a horizontal piping system. This study focused on integral functions describing variations in flow parameters due to a stable slug flow varying with position and time through a linear structural model. The natural frequency of the system was observed to decrease with an increase in gas superficial velocities when liquid superficial velocities and pipe lengths are large enough. Bordalo and Moorka (2018) proposed a slug flow load model that represents mass distributions of gas and liquid phases flowing through a pipe. Large amplitude oscillations were noticed when slug frequency is close to one of the natural frequencies of the pipeline. Wang et al., (2018) developed a mathematical model to investigate the dynamic response of pipeline-riser system subjected to severe slugging. Numerical results stated that when the flow pattern transitions to severe slugging phenomena, significant oscillation amplitudes were observed.

Slug flow-induced vibrations of a steel lazy wave marine riser was studied by Miranda and Paik (2019) using a space-time varying rectangular pulse train mass. The study observed vibration frequencies excited at slug frequencies. During low slug frequencies and long liquid slugs the amplitude of motion was found to be large and vice-versa during high slug frequencies and short liquid slugs. Bowen and Srinil (2020) investigated the planar dynamics of a catenary shaped riser conveying two-phase slug flows. The study aimed at analysing the individual and combined effects of slug flow properties utilizing a mechanistic slug unit concept. The flexible cylinder in the study was observed to experience mean and oscillatory displacements when slug flow was introduced, attributed to gravity and momentum effects. Furthermore, a multi-mode response with several harmonic contents was noticed at high internal flow velocities, whereas a single mode response was noticed at lower flow velocities. The dynamic responses of a simply-supported horizontal pipe conveying gas-liquid two-phase slug flow was explored by Liu et al., (2021). The study analysed the effects of different pipe materials and superficial velocities. Results from the study revealed that different pipe materials exhibit different vibrating patterns, ranging from a periodic like motion to a motion where oscillation amplitudes increase with time. More recently, the effect of water-cut and gas superficial velocities on the natural frequency of a horizontal piping system conveying low-viscosity oil-water-gas slug flows were investigated by Mi et al., (2022). It was found that the natural frequency decreased with increase in water-cut in the oil-based slug flow and vice versa for water-based slug flow. It was concluded that the relationship between effective viscosity and water cut (viscosity increases or decreases with water-cut) is the main reason for the variations in natural frequency.

2.2.2 Investigation of slug-flow induced vibrations using numerical methods.

Research on slug flow-induced vibrations in flexible cylinders using numerical methods are very limited, as very few researchers in the past have employed CFD techniques to analyse SIV due to the complexities involved in modelling and the significant computational time required. Jia (2012) investigated the SIV phenomenon in a pipeline span, jumper and riser section using computation fluid dynamics approach. Numerical results presented insights into the process of slug formation and decay in conjunction with pipe displacements due to slug flow. In a following study, Jia (2013) analysed the effect of different boundary conditions, flow rate, slug length and slug frequency on the dynamic response of a straight horizontal pipe. Slug induced vibrations were found to be the highest at higher liquid flow rates and long slug lengths. A free vibration natural frequency analysis was performed by Henandez et al., (2014) on a marine riser transporting internal multiphase flow using numerical techniques. The study demonstrated the contributions of centrifugal and Coriolis forces to the dynamic behaviour of the riser as internal flow velocity increases. Mamdud et al., (2019) investigated the flow-induced excitation forces at pipe bends due to slug-churn flow using CFD techniques. A VOF method was employed to model the multiphase flow patterns and turbulence. Simulation results showed that the predominant frequencies of force fluctuations reduced, and the RMS force fluctuations increased with increase in superficial gas velocity. Additionally, both predominant frequencies and RMS force fluctuations increased with increase in liquid superficial velocities. Wenhua Li et al., (2023) analysed properties of gas-liquid slug and its associated flow-induced vibrations in an M-shaped subsea jumper using CFD and experimental techniques. Results from the study observed when the gas-liquid mixture velocity was larger than 1.5 m/s, slug characteristics such as slug lengths and slug velocity increased with increase in mixture velocity. The associated vibration amplitude response of the M-shaped jumper was noticed to increase with increase in mixture velocities. Resonance was also observed when the slug frequency was close to the natural frequency of the jumper, causing the jumper to exhibit large amplitude vibrations.

2.2.3 Investigation of slug flow-induced vibrations using experimental methods

Over the years, experimental investigations have also been conducted to understand two-phase flow-induced problems. Few experiment studies have been performed to analyse slug flow-induced vibrations in straight cylinders. The effect of superficial velocities on the vibration responses of a horizontal pipe conveying air-water slug flows was described through experimental investigations conducted by Al-Hashimy et al., (2016). The study showed that the vibration amplitudes gradually increase with increase in liquid superficial velocities at fixed gas superficial velocities, whilst oscillation frequencies decreased with increase in liquid superficial velocities. Additionally, it was noticed that vibration displacement increased up to 64% when liquid superficial velocities increased from 0.65 m/s to 1 m/s. Wang et al., (2018) validated the developed semi-empirical model using in-house experiments for different slug flow properties such as liquid slug lengths, gas bubble length and translational velocities. Results from the study showed that vibrations due to slug flows were due to the sudden changes structure mass, stiffness and loading when liquid slugs pass through the system indicating the significant influence of centrifugal and Coriolis force on the structure. Vibration responses were also noticed to be high when the longest slug passed through the system.

Ortiz et al., (2017) conducted experiments to study the flow-induced vibration response of a clamped-clamped horizontal pipe under various two-phase flow regimes. Two-phase slug flows were observed to excite a wide range of frequencies at constant excitation magnitudes. It was also observed that the cylinder oscillations increased with increase in internal mixture velocities with excited dominant frequencies having strong relations with flow regimes and void fraction values. Liu and Wang (2018) performed an experimental and mathematical study to analyse the natural frequencies of a horizontal piping system carrying two-phase slug flows. Initial displacement values at six different points in the piping system were compared with the displacement value obtained from theoretical model. Experiment results produced quantitative similarities with displacement values from the theoretical model. In addition, a critical gas velocity was noticed which altered the excited frequencies depending on varying liquid velocities, pipe lengths and stiffness. Mohmmed et. al., (2019) analysed the stresses induced on a horizontal pipeline conveying two-phase slug flow. The study conducted experiments to investigate the effect of slug frequency on the mechanical stress of the pipe. Multivariable regression analysis was performed to develop the slug frequency stress prediction model based on the gravitational load of slug flow. Coriolis and centrifugal forces were neglected in the study. It was noticed that the slug frequency increased with increase in liquid superficial velocities at constant gas superficial velocity and vice vera at constant liquid superficial velocity. The developed model showed agreement with the recorded experiment results with a deviation of 0.7%.

Additionally, experiments have also been performed to analyse slug flow-induced vibrations in catenary shaped cylinders. Bordalo et al., (2008) conducted laboratory experiments to study the influence of internal two-phase flow on the vibration responses of a catenary riser. The investigation observed annular and slug flow patterns and showed that large oscillation amplitudes occur during the slug flow regime when compared with annular flows. At constant liquid superficial flow velocities, the oscillation amplitudes were observed to increase with increase in gas superficial velocities. The author also highlights the influence of oil and gas flow rates on the dynamic loading of the riser. A series of laboratory experiments were carried out by Zhu et al., (2018) for small-diameter tubes to investigate SIV of a free hanging elastic riser. Superficial velocity ranges of liquid and gas were varied from 0.1 m/s to 0.6 m/s for the liquid and 0.06 m/s to 0.3 m/s for gas respectively. During low liquid superficial velocities severe slugging was noticed with liquid slug lengths smaller than the length of the pipe. As liquid superficial velocities increased, varying slug length with chaotic oscillations was noticed. In a further study Zhu et al., (2018) observed that the in-plane response of the riser was predominantly first mode dominant with multiple excitation frequencies. However, at higher gas-liquid ratios, multi-mode oscillation responses were noticed. At lower mixture velocities, longer liquid slugs were observed, leading to high oscillation amplitudes. With gradual increase in mixture velocities, the accumulation of long liquid slugs seemed to be difficult due to increased gas superficial velocities. Furthermore, the study noted that vibration responses of the riser subsequently influenced the characteristics of slug flow through pressure fluctuations and seemed to impact the depletion of long liquid slugs.

Recently, Zhu et al., (2021) conducted experiments to investigate slug flow-induced vibrations of a catenary riser with high aspect ratio, across a range of gas-liquid velocity ratios from 1 to 4.5. Results from the study observed first mode dominant responses in the in-plane direction across all flow velocity ratios considered. In addition, the study observed mode switching over time from first mode to second mode due to variations in slug length and frequency. Among different cases considered, a predominant first mode response was noticed to be excited for longer liquid slug lengths, while a second mode response was excited in the case of shorter slug lengths. Second mode responses were associated with flow velocity ratios less than 2.5 generating low oscillation amplitudes. In contrast, flow velocity ratios greater than 2.5 produced large oscillation amplitudes with a first mode dominant response. In a following study Zhu et al., (2022) made use of the same pipe specifications to investigate spanwise mode contributions in both in-plane and out-of-plane directions of motion at a fixed gas-liquid ratio. Slug flows were observed to excite multi-mode behaviour with modal weights of each mode increasing with increase in gas and liquid flow velocities. Different modes were observed to excite at different pipe locations demonstrated through variations in dominant frequencies and modal weights. Out-of-plane oscillations were observed to be severe when the mixture velocity is greater than 2 m/s. In-plane dominant frequencies were observed in the out-of-plane direction as secondary frequencies, suggesting a strong coupling between the two directions of oscillations.

Furthermore, Zhu et al., (2022) conducted experiments to investigate vibrations of a catenary riser subjected to air-water severe slugging conditions. The superficial velocities of gas were varied from 0.177 m/s to 1.415 m/s at fixed liquid flow velocity of 0.094 m/s. Two different severe slugging cases with varying processes of slug development was analysed. The slug formation and blowout stages in both cases generated large amplitude oscillations due to the presence of long liquid slugs and pressure fluctuations. Severe slugging conditions were observed to generate a first mode dominant response across all flow velocities considered due to lower slug frequencies and the presence of short liquid slugs. Additionally, multiple resonance frequencies were noticed to co-exist due to the accumulation of varying slug lengths across the span of the cylinder. More recently, Porter et al., (2023) performed an experiment study of two-phase flow-induced vibrations in a horizontal pipe section to analyse and relate flow characteristics to the structure dynamic response. The study observed greater excitation frequencies with an increase in slug frequencies. Pipe midpoint oscillations were noticed to increase with increase in slug liquid holdups. Oscillations were also observed to increase with increase in liquid superficial velocities and decrease with increase in gas superficial velocities. Furthermore, centrifugal forces were noticed to be major contributors to the cylinder deflections at high translational velocities due to sudden variations in fluid densities across the cylinder span. The dominant excitation frequencies for all test cases considered were found to be close to the incoming slug frequencies with gravitational forces of the fluid controlling the transverse vibrations.

2.3 Influence of internal flow on the combined VIV and internal FIV phenomena

Flexible straight and catenary shaped fluid-conveying cylinders are also prone to vibrations due to VIV in numerous engineering applications, including heat exchangers, water service providers, marine risers and subsea pipelines. A schematic depiction of offshore structures subjected to VIV due to ocean currents is shown in Figure 2.4. As a common fluid-structure phenomenon VIV of rigid (Sarpkaya, 2004) and flexible (Williamson and Govardhan, 2004; Wu et al., 2012) cylinders have been extensively explored and reported in the literature. A flexible cylinder presents more complexities compared to a rigid one due to its inherent property of containing an infinite degree of freedom associated with immeasurable natural frequencies and vibration modes. In the past, most researchers have largely focused on studies involving rigid cylinders with very few studies conducted on flexible cylinders due to practical limitations despite their widespread use. One main challenge in the use of flexible cylinders is the presence of an infinite number of natural frequencies, potentially leading to continuous high-amplitude oscillations. In addition, lock-in ranges for rigid cylinders typically end after reaching certain reduced velocities, however, for elastic cylinders the vortex shedding frequency may latch onto another natural frequency after disconnecting from one resulting in a shift in dominant vibration modes and multi-mode responses. Another distinguishing feature between rigid and elastic cylinders is their geometry and configuration. Elastic cylinders are available in various configurations, such as straight, catenary shaped, lazy S and lazy wave, while rigid cylinders are generally straight. (Morooka and Tsukda, 2013; Santillan and Virgin, 2011). Additional research on elastic cylinders has highlighted the importance of considering three-dimensional cross-flow, in-line and axial oscillations for a more accurate prediction of VIV. (Srinil et al., 2009; Zanganeh and Srinil, 2016). These studies have also emphasized the significance of parameters such as tension and bending stiffness on VIV. In recent years, CFD approaches have also been utilised by researchers to study VIV in elastic cylinders (Huang et al., 2010; Wang and Xiao, 2016). However, CFD techniques are costly and require high computational sources. Therefore, the development of semi-empirical models found relevance to analyse and predict VIV of elastic cylinders.

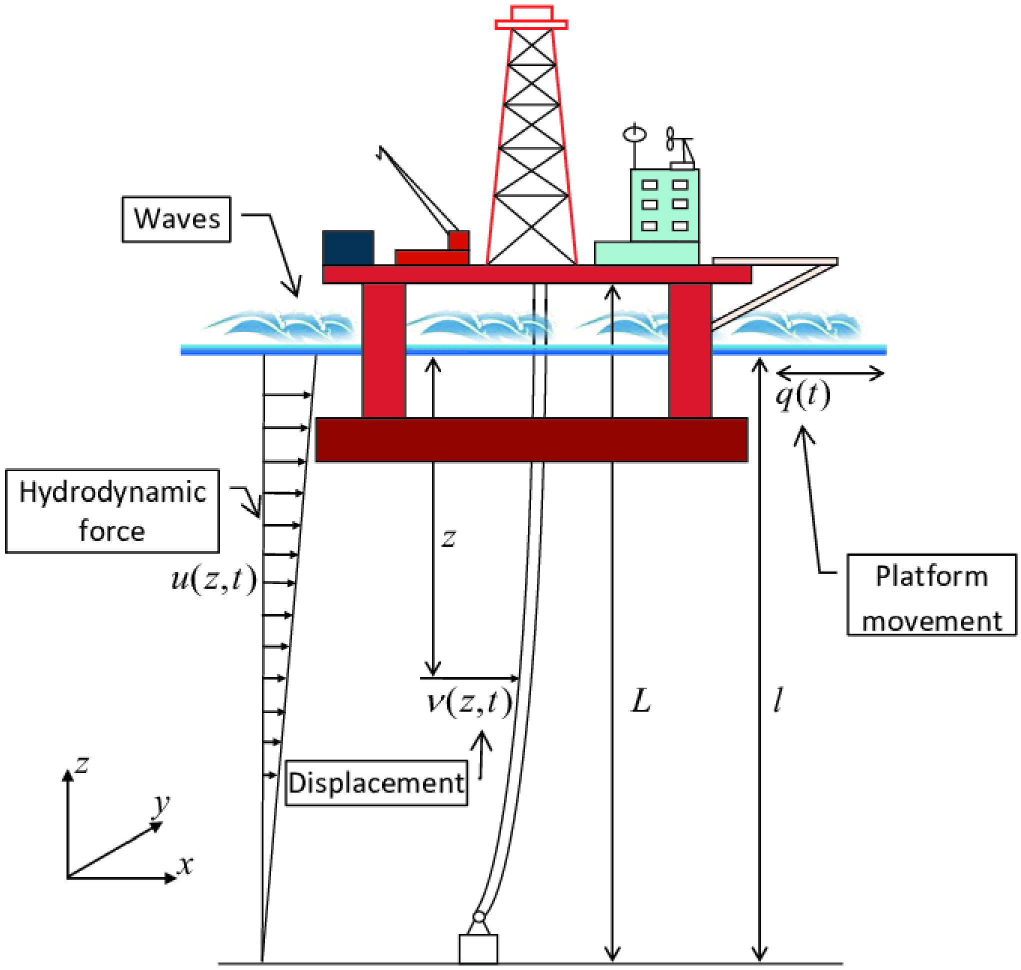

Figure 2.4: Schematic diagram of a marine riser subjected to external hydrodynamic loads (VIV) (Torres et al., 2014).

However, to optimise the design of flexible cylinders in such engineering applications, it is crucial to analyse forces resulting from a combination of external and internal excitations. This would ensure more practical and accurate predictions of flow-induced vibrations. A schematic illustration of marine risers subjected to simultaneous external and internal excitations is showed in Figure 2.5. When fluid flows within a cylinder, centrifugal and Coriolis forces have been found to contribute to cylinder oscillations due to the relative movement between the fluid and the structure. Centrifugal force contributes to the pressure load across the pipe wall, leading to a reduction in tension and natural frequencies. Conversely, Coriolis forces initiates extra damping during vibrations and add complexity to the coupling response (Meng et al., 2017). In addition, the structure could potentially experience enhanced resonance conditions when its oscillation frequencies closely align with the vortex-shedding frequency and internal flow excitation frequency, resulting in large deflections and increased stresses. Over the past decade, in response to the practical challenges faced in the industry, several studies have been conducted to investigate the vibration characteristics of flexible cylinders under combined external-internal excitation scenarios.

2.3.1 Effect of internal single-phase flow on the VIV of flexible cylinders

Guo and Lou (2008) performed experiments to investigate the effect of internal single-phase flow on the VIV of vertical straight risers. The natural frequencies of the cylinder were observed to decrease with increase in internal flow velocities in still water conditions. When external currents are introduced, cross-flow and in-line oscillations were observed to be significantly large at high internal flow velocities with in-line oscillation frequencies excited at twice the cross-flow frequencies. The fluid-structure interaction phenomena of an upward fluid-conveying cylinder under uniform external flow was investigated by Chen et al., (2012) using CFD techniques. Results from the study indicated that at high external-to-internal flow ratios, the influence of internal flow becomes significant as it determines the excited vibrations modes, oscillation amplitudes and frequencies. In addition, at higher flow velocity ratios multi-mode phenomena is observed with the reduction of oscillation frequencies in the presence of internal flow. The effect of internal flow velocities ranging from subcritical to supercritical regions on the dynamic response of a pined-pined flexible cylinder exposed to vortex-induced vibrations was investigated by Dia et al., (2013). Results from the study revealed that internal flow velocities in the supercritical regions have considerable impact on the nonlinear dynamic response of the cylinder. In the subcritical regions the cylinder is found to generate periodic motion with oscillation amplitudes gradually decreasing with increase in internal flow velocity. However, chaotic motions are observed when the flow velocities reach supercritical region. Additionally, the internal flow is found to have significant influence when the vortex shedding frequency is close to the structure natural frequencies.

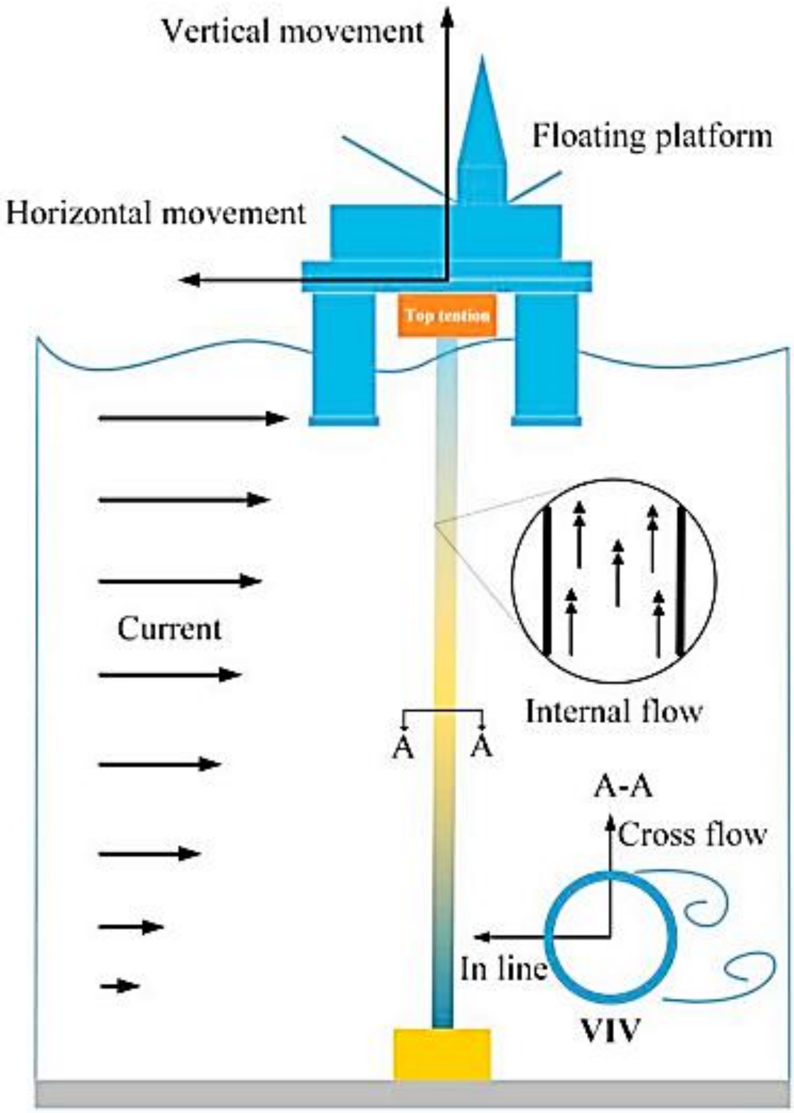

Figure 2.5: Schematic illustration of marine risers exposed to combined external and internal hydrodynamic loads (Liu et al., 2020).

In a further study, Dia et al., (2014) investigated the effects of internal single-phase fluctuating flows on the vibration response of a flexible cylinder subjected to VIV. Compared to internal steady flows, results from the study showed that cylinder deflections are amplified in the case of internal fluctuating flows. In addition, during lock-in conditions when the internal fluctuating frequencies coincide with structure natural frequencies, the cylinder is observed to experience resonance, resulting in large oscillation amplitudes. Meng et al., (2017) explored cross-flow VIV of flexible risers subjected to internal single-phase flows. The governing equations were solved using a Galerkin based finite element approach combined with the

Houbolts’s finite difference scheme. The model also adopts a distribution of van der Pol oscillators to create the VIV effect. Simulations were conducted for different internal flow velocities at two uniform external flow velocities. The analysis revealed that internal flow can induce new natural modes and may replace the predominant mode with these new natural modes. Yang et al., (2018) developed a three-dimensional nonlinear model to investigate the combined effects of internal fluid velocity and VIV of a flexible fluid-conveying cylinder, taking to account the geometric and hydrodynamic nonlinearities. A finite element approach was utilised in the study to solve the highly nonlinear equations present in the model. Internal single-phase fluid velocities and external cross-flow velocities were chosen as the varying parameters to analyse the vibration phenomena of the cylinder. A frequency domain analysis showed the significant effects of internal fluid velocity on the oscillating dynamics of the cylinder. An increase in fluid velocities leads to a decrease in the natural frequency of the cylinder and this decrease occurs more rapidly when excited dominant modes are altered. Variations in displacement amplitudes and stresses were observed at high internal flow velocities. Additionally, the critical flow velocity was noticed to be different for different external flow velocity. Rapid changes in amplitudes and stresses were also observed when internal fluid velocity reached the critical flow velocity leading to alterations in the excited dominant modes.

Xie et al., (2019) developed a mathematical model to investigate the effect of spatially and temporally varying fluid densities on the vibration characteristics of vertical straight flexible cylinder subjected to VIV. The variable density fluid is formulated using a mathematical model that follows the fluid mass conversation law. Results from the study indicate that the pipe becomes unstable and is subjected to parametric resonance as amplitudes of internal fluid density fluctuations increases. Furthermore, the study observed that when the internal fluid fluctuation frequency aligns closely with the VIV dominating mode, the pipe experiences large amplitude oscillations with variations in deflections along the pipe span and excited dominant frequencies. The effect of high density internal single-phase flow on the vibration response of a vertically straight ocean mining riser experiencing VIV was studied through the development of a novel FSI framework by Thorsen et al., (2019). The riser was subjected to external uniform flows with internal flow modelled as a time-varying steady state flow consisting of different wavelengths along the riser span. Results from the study revealed noticeable changes in the VIV oscillating pattern when the pipe span length to VIV dominant mode ratios were close to the wavelength of the internal fluid density. However, for wavelengths lesser than the aforementioned ratio, VIV oscillating patterns were noticed to be undisturbed by internal flow. The variations observed in the cylinder oscillating patterns resulted in the decrease of the overall fatigue life of the structure. Furthermore, in comparison to fatigue damages caused by vessel motion induced VIV, forces generated due to high density internal flow were observed to inflict greater fatigue damage.

More recently, Duan et al., (2021) developed a mathematical model to analyse the combined effects of internal single-phase flows and external shear currents on a vertical flexible cylinder. With an increase in internal flow velocity and density, the in-line RMS displacements were observed to decrease while cross-flow RMS amplitudes increased. Frequency domain analysis revealed multi-frequency response in both cross-flow and in-line directions at high internal flow velocity and densities. Furthermore, variations in the excited oscillation frequencies triggered new dominant modes in both directions of motion at high internal flow velocities and densities. In a further investigation, Duan et al., (2022) studied the dynamic response of a vertical flexible fluid-conveying cylinder subjected to external and internal oscillatory flow. A parametric study was performed by varying a combination of non-dimensional ratios between internal flow velocity, densities and external flow velocities. The study observed higher vibration modes excited with an increase in internal flow velocities and densities compared to modes excited by VIV-only. Additionally, the oscillation frequencies of the flexible cylinder were observed to decrease with increase in internal flow velocities and densities.

2.3.2 Effect of two-phase gas-liquid slug flows on the VIV of flexible cylinders

Blanco and Casanova (2010) developed a mathematical model to investigate the fatigue of a marine riser exposed to combined external and internal excitations. The developed model was based on the established wake oscillator model and the slug flow was modelled as series of liquid plugs and gas bubbles. Different slug flow properties were varied for parametric study, keeping the external flow velocity constant. In some of the test cases, internal slug flows were observed to alter the excited dominated modes, in-turn modifying the predicted fatigue life of the fluid-conveying cylinder. Finally, the authors recommended further investigations in horizontal and inclined pipes by varying external current velocities and tension distribution across the pipe span. Bossio et al., (2014) investigated the dynamic response of a horizontal pipeline subjected to simultaneous VIV and SIV excitations using a novel fluid-structural mode. A finite difference scheme was implemented using space and time discretisation.

Parametric study involved varying a range of external current velocities under lock-in conditions and slug flows were modelled as large and small slug units based on practical reference. Results from the study observed an 10% increase in the mid-point vibration amplitudes compared to VIV-only results in the case of smaller slug unit sizes. In the case of slug unit lengths larger than the pipe span length, significant vibrations were noticed with amplitudes almost 20 times greater than those observed in the VIV-only case.

Slug flows in a riser can modelled as a waveform known as pulse train which includes non-symmetric square waves used to describe sudden changes in flow properties. Safrendyo and Srinil (2018) incorporated similar ideas for the prediction of vibration responses of a catenary riser conveying slug gas-liquid flows subjected to external VIV. In this study flow-induced behaviour is investigated through random and steady-state slug excitations. Depending on the slug flow properties, multi-mode and multi-frequency oscillations are generated with large cross-flow and in-line deflections due to amplified mean drag values in the combined VIV-SIV scenario. Resonance due to SIV was observed to further increase the slug unit lengths determined by locked-in vibration modes and current velocity. Zhu et al., (2019) conducted experiments to investigate the coupling vibration response of a catenary riser exposed to combined external shear flow and internal two-phase slug flows. Oscillations in the out-of-plane and in-plane directions and internal flow behaviours were measured using a non-intrusive technique of high-speed picturing approach. Vibrations due to internal flow was mainly observed at the curvature of the pipeline. However, both out-of-plane and in-plane vibrations were dominated by forces due to external shear flow. The developed internal slugs were observed to undergo alterations as a result of strong cylinder oscillations in the out-of-plane directions. The liquid slugs were noticed to divide into smaller lengths, transitioning from perfect slugs with equal lengths, while the cross-section filled with gas bubbles. The combination of internal and external excitations generated a travelling wave response in contrast to standing wave characteristics observed in the case of internal FIV only. Furthermore. the out-of-plane and in-plane responses were observed to increase with increase in gas-liquid ratios. This increase in gas-liquid ratios resulted in a decrease in liquid slug lengths and overall mass of the system. Recently, Meng et al., (2021) in continuation to their previous work, analysed the effect of slug flows on the VIV of a flexible horizontal riser experiencing uniform cross-flows. Results from the study demonstrated that cylinder oscillations are more significant in the presence of two-phase slugs compared to single-phase internal flows. This is attributed to the inherent fluctuating nature of two-phase slug flow, even though the overall mass of the system is greater in the case of single-phase flow. In addition, amplitude-modulations were observed in the vibration response of the cylinder when exposed to a combination of internal two-phase slug flows and VIV as a consequence of new dominant modes excited in this scenario.

2.4 Conclusions

This chapter provides a literature review of several topics relevant to the scope of this research work. These include two-phase gas-liquid flow patterns in horizontal and vertical tube channels, flow pattern prediction maps, numerical and experimental studies on slug flow-induced vibrations and the impact of internal single-phase and two-phase slug flows on combined external-internal excitation scenarios. The investigation on two-phase flow regimes and maps gives an insight into conditions necessary for the development of two-phase flow regimes and their effects on the vibration response of a flexible cylinder. It was seen that vibrations induced due to slug flows caused large amplitude oscillations and variations in excited vibration modes and frequencies, compared to other two-phase flow regimes, due to its inherent space-time varying fluctuations in mass, velocity and pressure. In addition, the majority of literature discussing two-phase flow-induced vibrations has predominantly utilised a simplified linearised tension beam model. Fundamental understanding of slug flow-induced vibrations in three-dimensional space and time considering in-line and axial dynamics is still lacking. This shows the need for the development of a three-dimensional model to analyse and predict slug flow-induced vibrations in horizontal and vertical straight flexible cylinders taking into account the geometric and hydrodynamic nonlinearities. Moreover, the influence of SIV on the combined external-internal excitation scenarios, which could be of practical importance in various engineering applications, remain limited in the literature. Within the context of this thesis, forces due to VIV is considered as an external excitation to identify key features of SIV on the combined excitation scenario.

To achieve these objectives and address limitations in previous SIV models, this study presents a fully nonlinear three-dimensional vibration prediction model for the analysis of internal two-phase SIV and external VIV. The model includes equations involving centrifugal and Coriolis forces to emulate SIV and captures mass variations in the slug flow regime. In addition, an idealised space-time varying slug unit concept is utilised in this study, wherein slug properties are assumed to be fully developed and undisturbed by pipe oscillations. Furthermore, dimensionless equations are derived to analyse the impact of key individual slug properties and improve overall understanding of the FSI phenomena. A space-time finite difference scheme is employed to solve the highly nonlinear equations present in the model. Subsequently, the presented model is validated through comparisons with numerical and experimental results pertaining to SIV and VIV of flexible cylinders. A parametric study is then performed to analyse the individual and combined effects of key slug characteristics on submerged and free-hanging flexible straight cylinders.

Chapter 3

Three-dimensional SIV Model of Flexible Cylinders Conveying Two-Phase Slug Flows

Hydrocarbon flows in a marine riser may appear in multiple phases with varying flow patterns, among which, slug flows are known to exhibit complex flow characteristics due to fluctuations in multiphase mass, velocities, and pressure changes. Bulk of the literature concerning internal single and two-phase flow-induced vibrations has largely focused on the use of a linearised tension beam model. In this chapter, the fluid-structure interaction phenomena of a submerged long flexible cylinder conveying two-phase slug flows is investigated taking into account the geometric and hydrodynamic nonlinearities. A semi-empirical theoretical model which consists of nonlinear structural equations of coupled out-of-plane, in-plane and axial structural motions is presented for the analysis and prediction of two-phase slug flow-induced vibrations (SIV). The model includes equations involving centrifugal and Coriolis forces to capture mass variations in the slug flow regime. A numerical space-time finite difference approach combined with a frequency domain analysis is used for analysing the highly nonlinear three-dimensional responses. Model validations are performed through comparisons with published internal flow-induced vibrations results. Furthermore, a parametric study is performed to analyse the effect of key slug characteristics on the vibration response of a long vertical fluid-conveying cylinder and a new dimensionless parameter is presented to predict high amplitude scenarios.

3.1. Three-dimensional SIV phenomenological model

Marine risers with high aspect (length-to-diameter, L/D) ratios are usually employed for deep-water explorations which are susceptible to high amplitude oscillations due to external hydrodynamic loads and internal multiphase flows. Figure 3.1 depicts the schematic model of long flexible cylinder in a fixed global Cartesian ($X - Y - Z$) system subjected to internal two-phase slug flow travelling through the cylinder and single-phase external flow. The cylinder in this study is considered to be vertical and fully submerged with two-phase internal flows in the axial direction. Two different conditions of the riser are described, the initial equilibrium subjected to internal loading and the dynamic response configuration experiencing travelling internal slug flows from static equilibrium in the vertical direction. The flexible cylinder is assumed to be linearly elastic with constant Young's modulus (E) and have uniform structural properties such as mass per unit length (m), still water added mass ($m_a = \rho \pi D^2/4$ *with* ρ being external fluid density, per length (L), mass of internal fluid (m_f), per length (L), outer diameter (D), bending stiffness (EI), axial stiffness (EA_r), cross-sectional area (A_r), damping coefficient (c) and moment of Inertia (I). The cylinder is capable of further displacements in the X direction due to nonlinear coupling terms in the equation. Also, for realistic predictions of SIV for offshore operations, it is crucial to take into consideration 3-D vibration response and geometric nonlinearities (Zanganeh and Srinil, 2016). Figure 3.2 illustrates the application of the slug unit cell concept in this study originally introduced by Wallis (1969). In this concept, one slug unit is divided into a liquid phase (slug holdup, H_{LS}) containing small gas bubbles, along with a gas phase over a thin liquid film (H_{LF}), passing through the cylinder with a translational velocity, V_t. The travelling slug liquid holdup and liquid film experience shear stresses at the gas-wall, liquid-wall or liquid-gas interfaces. The slug liquid holdup is assumed to completely fill the cross-section of the cylinder over a length L_S, while the thin film liquid holdup partially occupies the cross-section over a length L_F. Together, these lengths constitute one slug unit with a total length L_U.

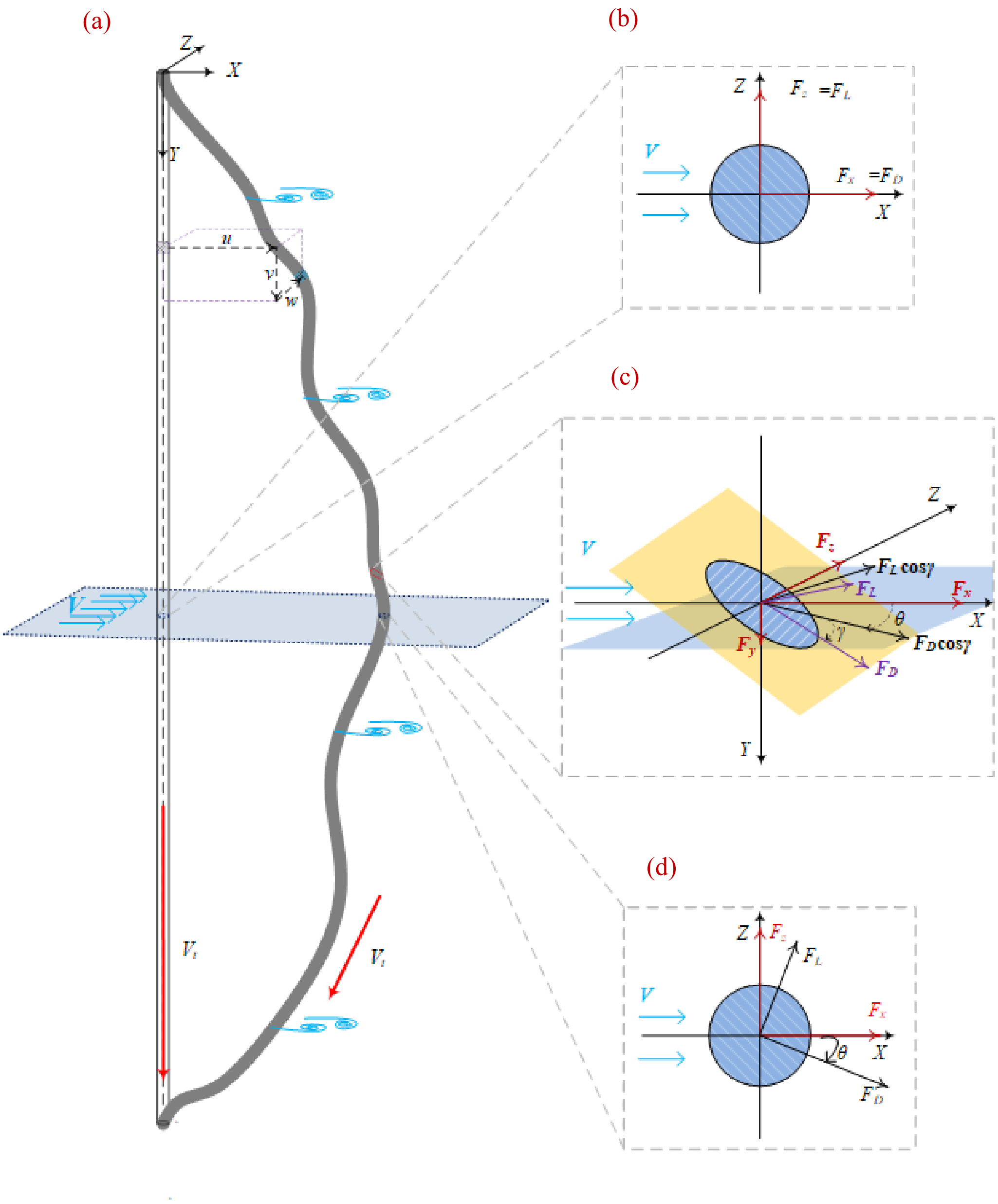

Figure 3.1: Schematic 3-D model of a flexible cylinder subjected to external loads and internal two-phase slug flows.

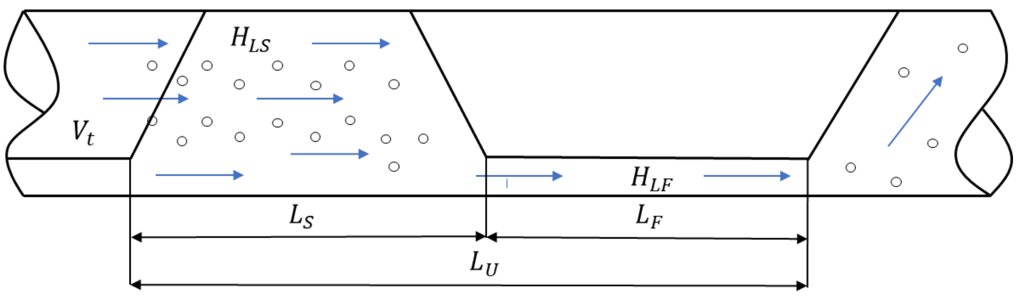

Figure 3.2: Schematic view of an idealised slug unit cell.

3.1.1 Three-dimensional nonlinear structural model:

The partial-differential equations of the riser response satisfying the Euler-Bernoulli beam hypothesis in three-dimensional space and time in general dimensional form can be expressed as (Hara, 1973; Srinil et al., 2009; Zanganeh and Srinil, 2016):

$$\begin{aligned}(m+m_a+m_f)\ddot{u}+c\dot{u}+EIu^{(IV)}+2m_fV_t\dot{u}'+m_fV_t^2u'' \\ +\left(\dot{m}_f\dot{u}+V_t\dot{m}_fu'+V_tm_f'\dot{u}+V_t^2m_f'u'\right)-(Tu')' \\ =EA_r(v''u'+v'u'') \\ +\frac{1}{2}EA_r\left(3u''u'^2+u''v'^2+2v''v'u'+u''w'^2+2w''w'u'\right)+F_x\end{aligned} \tag{3.1}$$

$$\begin{aligned}(m+m_a+m_f)\ddot{v}+c\dot{v}+EIv^{(IV)}+2m_fV_t\dot{v}'+m_fV_t^2v'' \\ +\left(\dot{m}_f\dot{v}+V_t\dot{m}_fv'+V_tm_f'\dot{v}+V_t^2m_f'v'\right)-(Tv')' \\ =EA_rv''+2EA_rv''v'+EA_r(u''u'+v''v'+w''w') \\ +\frac{1}{2}EA_r\left(v''u'^2+2u''u'v'+3v''v'^2+v''w'^2+2w''w'v'\right)+F_y\end{aligned} \tag{3.2}$$

$$\begin{aligned}(m+m_a+m_f)\ddot{w}+c\dot{w}+EIw^{(IV)}+2m_fV_t\dot{w}'+m_fV_t^2w'' \\ +\left(\dot{m}_f\dot{w}+V_t\dot{m}_fw'+V_tm_f'\dot{w}+V_t^2m_f'w'\right)-(Tw')' \\ =EA_r(v''w'+v'w'') \\ +\frac{1}{2}EA_r\left(w''u'^2+2u''u'w'+w''v'^2+2v''v'w'+3w''w'^2\right)+F_z\end{aligned} \tag{3.3}$$

where u, v, and w represent structural displacements in in-plane (X), axial (Y) and out-of-plane (Z) directions, F_x, F_y, and F_z are the corresponding hydrodynamic forces respectively and V_t is the internal slug translational velocity. The overdot and prime in the equations denote derivatives with respect to time t_i and space y, and T represent tension in space. For risers with varying inclination angles, the change in tension (T) across the length of the cylinder can be expressed as:

$$T=T_0-g\left(m-\frac{\rho\pi D^2}{4}\right)(L-y)sin\theta \tag{3.4}$$

Where T_0 is the top pre-tension, g is acceleration due to gravity and L is the total length of the cylinder. The overall structure geometric nonlinearities, mean displacements and 3-D vibrations are accounted for through quadratic and cubic coupling terms in the Eqs. (3.1-3.3). The semi-empirical model also takes into account the centrifugal force and the Coriolis force along with inertial and momentum change effects to emulate vibrations due to hydrodynamic slug flows which have been found to be key in describing two-phase flow-induced vibrations (Hara, 1973).

3.1.2 Nonlinear hydrodynamic forces

Vortices are shed when the submerged cylinder oscillates due to internal two-phase slug flows causing hydrodynamic drag and lift forces with frequencies $2\Omega_f$ and Ω_f respectively, resulting from the symmetric and asymmetric nature of vortex shedding. The respective drag and lift forces caused by the shed vortices induce oscillations in the in-plane and out-of-plane directions. The oscillations in the in-plane and out-of-plane directions instigate oscillations in the axial direction (Eq. 3.2) due to the nonlinear coupling terms in the equations. The fluctuating and self-exciting drag and lift forces can be modelled using the van der Pol wake oscillator equation by introducing wake variables $p = 2C_D/Cd_o$ and $q = 2C_L/Cl_o$, where C_D, C_L, Cd_o and Cl_o are oscillating drag, oscillating lift, wake associated drag and wake associated lift coefficients respectively. Van der Pol oscillators are widely used to model self-sustaining oscillations and effectively represents the limit cycle behaviour observed in VIV systems, providing a more accurate reflection of real-world phenomena (Facchinetti et al., 2004). The wake oscillator model can be expressed as:

$$\ddot{p} + 2\varepsilon_u \Omega_f (p^2 - 1)\dot{p} + 4\Omega_f^2 p = \frac{\Lambda_u}{D}\ddot{u} \tag{3.5}$$

$$\ddot{q} + \varepsilon_w \Omega_f (q^2 - 1)\dot{q} + \Omega_f^2 q = \frac{\Lambda_w}{D}\ddot{w} \tag{3.6}$$

Where $\Omega_f = \frac{2\pi S_t V_e}{D}$, S_t is the Strouhal number (assumed to be 0.18 following Song et al., 2011) and V_e is the external flow velocity. For a stationary cylinder, the drag and lift forces align with in-plane and out-of-plane directions, dictating $F_x = F_D$ and $F_Z = F_L$ whose projection is shown in Figure 3.1. During cylinder oscillations, the drag and lift forces become random and no longer correspond to the X and Z direction due to the cylinder relative motion. By following Zanganeh and Srinil (2016), the total and drag and lift forces acting with a clockwise horizontal angle of θ and γ as shown in Figure 3.1(c) considering structure and external flow relative velocities, V_{rel} and wake variables, the associated three-dimensional fluid forces can be expressed as:

$$F_x = \frac{1}{4}\rho D V_{rel} C_{l0} q\dot{w} + \frac{1}{4}\rho D V_{rel} C_{d0} p(V - \dot{u}) + \frac{1}{2}\rho D V_{rel} \bar{C}_d (V - \dot{u}) \tag{3.7}$$

$$F_y = \frac{1}{4}\rho D V_{rel} C_{l0} q\dot{v} + \frac{1}{4}\rho D V_{rel} C_{d0} p\dot{v} + \frac{1}{2}\rho D V_{rel} \bar{C}_d \dot{v} \tag{3.8}$$

$$F_z = \frac{1}{4}\rho D V_{rel} C_{l0} q(V - \dot{u}) - \frac{1}{4}\rho D V_{rel} C_{d0} p\dot{w} - \frac{1}{2}\rho D V_{rel} \bar{C}_d \dot{w} \tag{3.9}$$

In which, V_{rel} =

$$V_{rel} = \sqrt{(V_e - \dot{u})^2 + (\dot{v})^2 + (\dot{w})^2}. \tag{3.10}$$

Where $\bar{C}_d$ is the mean drag coefficient. The corresponding values for C_{d0}, C_{l0}, $\bar{C}_d$, ε_u, ε_w, A_u, A_w are empirical coefficients calibrated by Zanganeh and Srinil (2016) using results from experimental study conducted by Song, et al., (2011) are 0.2,0.3 1.2, 0.3,0 0.3, 12 and 12 respectively (Dai et al., 2013). It should be mentioned that the presented model is also capable of predicting vibrations due to external flow (vortex-induced vibrations), however, the focus of this study is to investigate the three-dimensional response of a submerged flexible cylinder subjected to internal two-phase slug flow.

3.1.3 Dimensionless nonlinear SIV model

Dimensionless terms such as $U = u/D,\ V = v/D,\ W = w/D, Y = y/D, T_m = \omega_n t_i,$ are introduced to the developed equations to achieve better understanding of the model during parametric study. The 3-D dimensionless nonlinear partial differential equations of coupled out-of-plane, in-plane, and axial motions combined with the equation of motion for two-phase internal flow can be expressed as:

$$
\begin{aligned}
(1+M)\ddot{U} + 2\zeta\dot{U} + E_I U^{(IV)} + 2U_r M\dot{U}' + U_r^2 M U'' \\
+ \left(\dot{M}\dot{U} + U_r\dot{M}U' + U_r M'\dot{U} + U_r^2 M'U'\right) - (T_n U') \\
= \frac{E_A}{L_D}(V''U' + V'U'') \\
+\frac{1}{2}\frac{E_A}{L_D}\Big(3U''U'^2 + U''V'^2 + \frac{2}{L_D}V''V'U' + U''W'^2 \\
+\frac{2}{L_D}W''W'U'\Big) + F_x
\end{aligned}
\tag{3.11}
$$

$$
\begin{aligned}
(1+M)\ddot{V} + 2\zeta\dot{V} + E_I V^{(IV)} + 2U_r M\dot{V}' + U_r^2 M V'' \\
+ \left(\dot{M}\dot{V} + U_r\dot{M}V' + U_r M'\dot{V} + U_r^2 M'W'\right) - (T_n V')' \\
= E_A V'' + 2\frac{E_A}{L_D}V''V' + \frac{E_A}{L_D}(U''U' + V''V' + W''W') \\
+\frac{1}{2}\frac{E_A}{L_D}\Big(V''U'^2 + \frac{2}{L_D}U''U'V' + 3V''V'^2 + V''W'^2 \\
+\frac{2}{L_D}W''W'V'\Big) + F_y
\end{aligned}
\tag{3.12}
$$

$$
\begin{aligned}
(1+M)\ddot{W} + 2\zeta\dot{W} + E_I W^{(IV)} + 2U_r M\dot{W}' + U_r^2 M W'' \\
+ \left(\dot{M}\dot{W} + U_r\dot{M}W' + U_r M'\dot{W} + U_r^2 M'W'\right) - (T_n W')' \\
= \frac{E_A}{L_D}(V''W' + V'W'') \\
+\frac{1}{2}\frac{E_A}{L_D}\Big(W''V'^2 + W''V'^2 + \frac{2}{L_D}U''U'W' + \frac{2}{L_D}V''V'W' \\
+ 3W''W'^2\Big) + F_z
\end{aligned}
\tag{3.13}
$$

Where, $M = \frac{m_f}{m_0}$, is the dimensionless mass quotient defined as the ratio of internal fluid mass (m_f) to the mass of the cylinder with added mass ($m_0 = m + m_a$), and $L_D = L/D$ is the span ratio. ζ is the damping ratio described as $\frac{1}{m_0\omega_n}c = 2\zeta$, where ω_n is the first natural frequency of the cylinder. Bending stiffness of the cylinder in dimensionless form is defined as $E_I = EI\frac{1}{m_0\omega_n^2 D^4}$. Likewise, axial stiffness is expressed as the normalised product of modulus of elasticity and cross-sectional are $E_A = \frac{EA_r}{m_0\omega_n^2 D^2}$. U_r is the dimensionless internal translational velocity expressed as, $U_r = \frac{V_t}{\omega_n D}$. Variation of tension in dimensionless form is expressed as:

$$T_n = T_{n0} - G_n(1+M)(1+Y)sin\theta + G_n\frac{\pi}{4\mu}(1+C_m)(1-Y)sin\theta \tag{3.14}$$

Where, $T_{n0} = \frac{T}{m_0\omega_n^2 D^2}$ and C_m is the added mass coefficient. Non-dimensional tension equation gives rise to a unique parameter $G_n = \frac{g}{w_n^2 D}$. Applying dimensionless terms to the wake oscillator model and the three-dimensional hydrodynamic force equations, the corresponding equations become:

$$\frac{\partial^2 p}{\partial T_m^2} + 2\varepsilon_u\Omega(p^2-1)\left(\frac{\partial p}{\partial T_m}\right) + 4\Omega^2 p = A_u\left(\frac{\partial^2 U}{\partial T_m^2}\right) \tag{3.15}$$

$$\frac{\partial^2 q}{\partial T_m^2} + \varepsilon_w\Omega(q^2-1)\left(\frac{\partial q}{\partial T_m}\right) + \Omega_f^2 q = \Lambda_w\left(\frac{\partial^2 W}{\partial T_m^2}\right) \tag{3.16}$$

$$F_x = \frac{1}{4\mu}V'_{rel}C_{l0}q\dot{W} + \frac{1}{4\mu}V'_{rel}C_{d0}p\left(\frac{V_r}{2\pi} - \dot{U}\right) + \frac{1}{2\mu}V'_{rel}\bar{C}_d\left(\frac{V_r}{2\pi} - \dot{U}\right) \tag{3.17}$$

$$F_y = \frac{1}{4\mu}V'_{rel}C_{l0}q\dot{V} + \frac{1}{4\mu}V'_{rel}C_{d0}p\dot{V} + \frac{1}{2\mu}V'_{rel}\bar{C}_d\dot{V} \tag{3.18}$$

$$F_z = \frac{1}{4\mu}V'_{rel}C_{l0}q\left(\frac{V_r}{2\pi} - \dot{U}\right) - \frac{1}{4\mu}V'_{rel}C_{d0}p\dot{W} - \frac{1}{2\mu}V'_{rel}\bar{C}_d\dot{W} \tag{3.19}$$

$$V'_{rel} = \sqrt{\left(\frac{V_r}{2\pi} - \dot{U}\right)^2 + \left(\dot{V}\right)^2 + \left(\dot{W}\right)^2} \tag{3.20}$$

Where $\mu = \frac{m_0}{\rho_e D^2}$ and ρ_e is the external flow density. V'_{rel} is the dimensionless relative velocity and V_r is the dimensionless external flow velocity. In reality, two-phase flows may develop into different flow patterns in a riser based on the pipe-fluid properties (Bordalo et al., 2008). The flow patterns may be further modified during pipe oscillation. In this study, attention is given to the slug flow regime, assuming that the slug properties analysed remain undisturbed by pipe oscillations. According to Zhu et al., (2018) slug flow is inherently transient and unsteady. Bowen and Srinil (2020) and several other researchers have suggested that the randomness of slug flow in a flexible cylinder may be approximated by average properties. Therefore, a steady time-varying slug flow is assumed in this study, indicating that the slug sheds liquid from the back at the same rate that the liquid is gathered from the front. This implies that the slug lengths remain constant as each slug unit travels along the pipe. Furthermore, the slug flow is assumed to be fully developed and is modelled as a fluid with time-varying mass using a rectangular pulse train model, implemented with MATLAB codes and functions (Miranda and Paik, 2019). The highly nonlinear partial differential equations (11) – (20) are numerically solved for 3-D dynamic responses of the flexible cylinder by using a finite difference approach in both space and time domain (see Appendix A). Other popular approaches for solving differential equations include the finite element method, finite volume method and Galerkin method. In this thesis, the finite difference method was chosen for its straightforward implementation and effectiveness in solving highly nonlinear partial differential equations (Zanganeh and Srinil, 2016). Convergence tests of numerical simulations have been performed and the results in Sections 3.2 and 3.3 are based on the dimensionless time step of 0.001 and 100 spatially discretised elements.

3.2 Model validation with numerical comparisons

Since experimental studies concerning slug flow-induced vibrations of submerged vertical cylinders are sparse, numerical results of the present model is compared with theoretical model results of vertical straight drilling riser by Meng et al., (2018). The drilling riser is a fully submerged long flexible straight cylinder with length, $L = 500$ m, outer diameter, $D = 0.583$ m and inner diameter, $ID = 0.489$ m, density $= 7850$ kg/m^3, young's modulus, $E = 210$ GPa. The density of the surrounding fluid is 1025 kg/m^3. The riser is subjected to internal single-phase flow with a density of 1600 kg/m^3. It should be mentioned that single-phase flows in the model is achieved by considering a constant fluid density along the length of the cylinder.

Figure 3.3 displays the comparison between the first six natural frequencies obtained using FFT approach from the present model with results obtained by Meng et al., (2018) for varying flow velocity ranging from 5 to 60 m/s. Free vibration frequency response results are obtained through low amplitude initial condition with hydrodynamic damping and pinned-pinned end conditions, allowing the structure to vibrate at its natural frequencies. A low amplitude initial condition was used to create oscillations in the out-of-plane direction and minimize oscillations in the other two directions caused by the nonlinear couplings in the equations. It can be seen from the figure that the developed model follows similar trends of reducing natural frequencies as internal flow velocities increase from 5 to 60 m/s. The model is seen to obtain identical natural frequency values at lower flow velocities. However, natural frequency values at higher flow velocities and higher modes (4^{th}, 5^{th} and 6^{th}) are found to be slightly higher than the compared results. Furthermore, an uncertainty analysis is carried out to measure the root mean square errors at each natural frequency. The analysis was conducted by calculating the difference between model and theoretical natural frequency values at each internal flow velocity. The sum of the squared differences is obtained which is then divided by the total number of data points, and the square root of that value gives the root mean square errors (RMSE). The RMSE values for the 1^{st}, 2^{nd}, 3^{rd}, 4^{th}, 5^{th} and 6^{th} natural frequencies were calculated to be 0.038, 0.069, 0.098, 0.138, 0.176 and 0.228, respectively. It could be seen that model predictions of natural frequencies produce low RMSE with errors increasing with the increase of the natural frequencies. The discrepancies in the predicted natural frequencies and the increasing RSME is due to the fact that the developed model takes into account the geometrical nonlinearities (i.e., spring nonlinear stiffness) as opposed to linear structural equation approach adopted by Meng et al. (2018). Zanganeh and Srinil (2016) previously have observed that models excluding geometric nonlinearities tend to overestimate dominant modes, natural frequencies and in-plane and out-of-plane amplitude results, which is common for a linearised model (Srinil, 2010). The model also captures parametric instabilities at similar flow velocities ($V_t = 50$ m/s) for all the 6 modes observed in the literature. It can be seen that the natural frequencies switch to the lower frequencies at flow velocities above 50 m/s indicating the existence of parametric instabilities. Overall, it can be concluded that the presented 3-D model provides quantitative similarities when compared with results from previous numerical simulations for submerged vertical flexible risers.

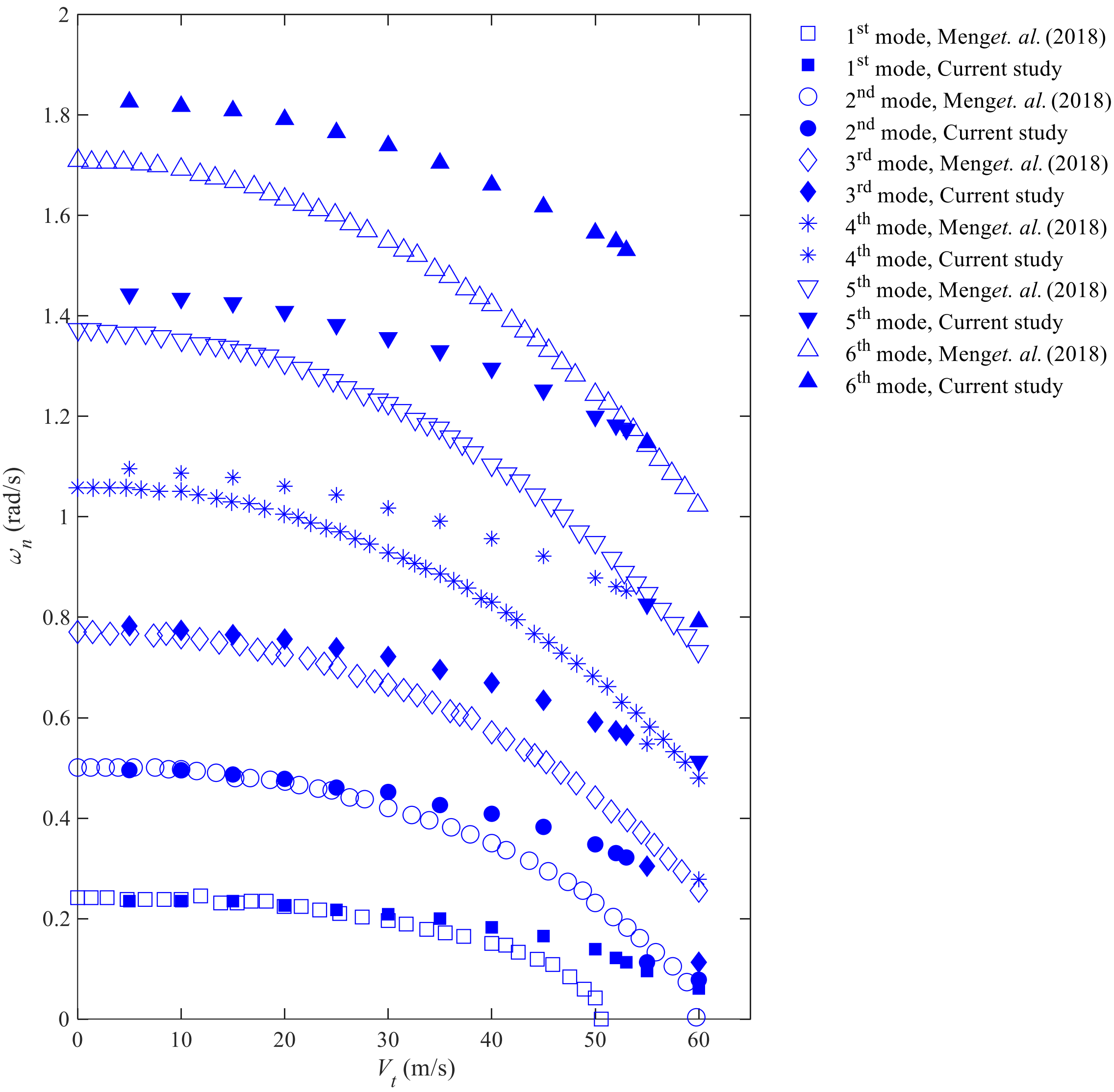

Figure 3.3: Comparison between numerical results of obtained natural frequencies for increasing internal flow velocities.

3.3 Numerical results of a long vertical cylinder conveying two-phase slug flows

The long drilling riser used for validation in the previous section is considered for parametric study. The vertical cylinder has an aspect ratio of 858 and is assumed to be submerged in water with no external flow. The effect of the slug flow characteristics mentioned in the previous section, in addition mass quotient, M, which is the ratio of internal fluid mass over the mass of empty pipe with added mass, on the dynamic response of the vertical riser, is investigated in this section. In addition, four dimensionless translation velocities (U_r $= 47.3$, 94.6 ,141.8 and

189.1) is considered for each varying slug parameter to capture maximum features of slug flow-induced vibrations.

Table 3.1 presents the details of all the slug characteristics that are varied for the parametric study. Four cases for each slug property are considered at four different translational velocities. A total of 16 cases are considered to analyse the effect of one slug property. The slug liquid holdup (H_{LS}), and the thin liquid film holdup (H_{LF}), are varied in quotient of 15 from 0 to 1. Where the value 0 denotes empty pipe and 1 indicate completely-filled liquid slug holdup (H_{LS}) and thin film holdup (H_{LF}) respectively. When varying H_{LS}, H_{LF} is considered to be 0 for all 16 cases and while varying H_{LF}, the H_{LS} parameter is considered be 1. The slug liquid length, L_S, is varied as a function of a constant slug unit length L_U ($17D$) where 0.1, 0.35, 0.6 and 0.85 represent percentages of L_U. The L_U parameter is varied as a function cylinder diameter from $5D$ to $40D$, during which L_S and L_F are divided into equal halves for every case of L_U considered. Similarly, the mass quotient cases are varied as half, two and four times the fluid density considered during validation, while L_S and L_F values correspond to the highest amplitude observed during the L_S case study. For all the cases of L_S, L_U and M the H_{LS} and H_{LF} values are 1 and 0 respectively to capture maximum momentum exchange between the two phases.

Table 3.1: Slug flow properties considered in cases of varying (a) H_{LS} (b) H_{LF} (c) L_S (d) L_U (e) M.

(a)

U_r	H_{LS}	H_{LF}	L_S/D	L_F/D	L_U	M
47.3, 94.6, 141.8, 189.1	0.55	0	16	14	30D	1.788
	0.7	0	16	14	30D	1.788
	0.85	0	16	14	30D	1.788
	1	0	16	14	30D	1.788

(b)

U_r	H_{LF}	H_{LS}	L_S/D	L_F/D	L_U	M
47.3, 94.6, 141.8, 189.1	0	1	16	14	30D	1.788
	0.15	1	16	14	30D	1.788
	0.3	1	16	14	30D	1.788
	0.45	1	16	14	30D	1.788

(c)

U_r	L_S/D	H_{LS}	H_{LF}	L_F/D	L_U	M
47.3, 94.6, 141.8, 189.1	0.1	1	0	0.9	30D	1.788
	0.35	1	0	0.65	30D	1.788
	0.6	1	0	0.4	30D	1.788
	0.85	1	0	0.15	30D	1.788

(d)

U_r	L_U	H_{LS}	H_{LF}	L_S/D	L_F/D	M

47.3, 94.6, 141.8, 189.1	5D	1	0	0.5	0.5	1.788
	10D	1	0	0.5	0.5	1.788
	20D	1	0	0.5	0.5	1.788
	40D	1	0	0.5	0.5	1.788

(e)

U_r	M	H_{LS}	H_{LF}	L_S/D	L_F/D	L_U
47.3, 94.6, 141.8, 189.1	0.894	1	0	0.35	0.65	30D
	1.788	1	0	0.35	0.65	30D
	3.576	1	0	0.35	0.65	30D
	7.151	1	0	0.35	0.65	30D

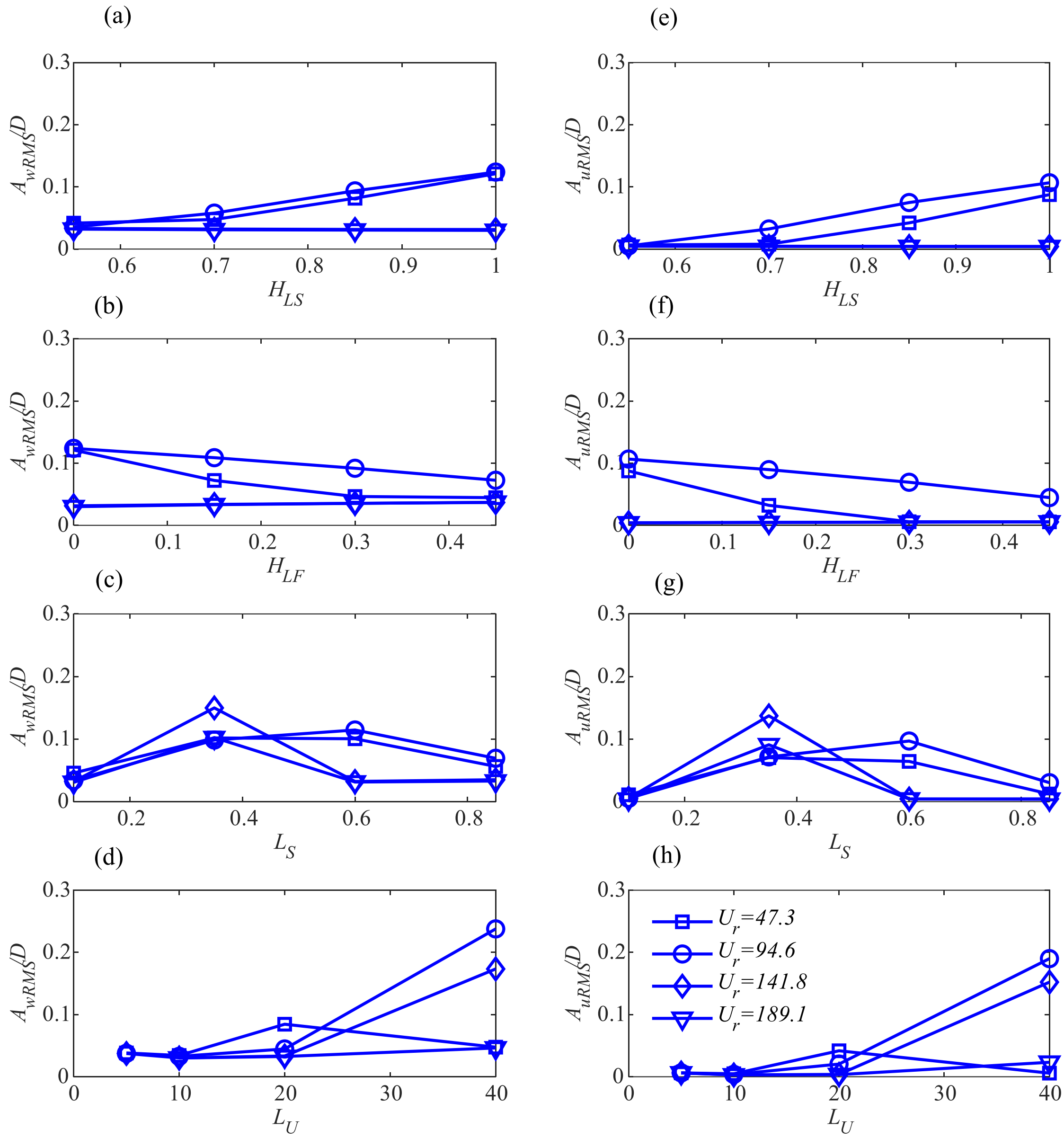

Figure 3.4: Comparison of maximum (a-d) out-of-plane and (e-h) in-plane RMS amplitudes for varying (a-e) H_{LS}, (b-f) H_{LF}, (c-g) L_S, (d-h) L_U.

3.3.1 Slug flow-induced amplitude response and mean displacements

Figure 3.4 (a-d) and (e-h) displays out-of-plane and in-plane maximum RMS amplitude response of the riser for all the slug flow parameters considered. While varying H_{LS} (Table 3.1(a)), it was observed that during low internal flow velocities (U_r = 47.3 and 94.6), the maximum RMS amplitude increased linearly with every increase in the slug holdup value, H_{LS} as seen in Figure 3.4(a) and (e). The maximum amplitude increases up to four times in the out-of-plane direction and up to eight times in the in-plane direction when H_{LS} =1 (completely-filled), compared to when H_{LS} = 0.55 (Half-filled). At higher translational flow velocities (U_r = 141.8 and 189.1), vibration amplitudes are observed to be much lower, and no changes in amplitude is observed as H_{Ls} increases. This may be due to the fact that at higher flow velocities, the slug travels through the pipe much faster, leaving very little time for the fluid to exert forces on the structure, thereby making it insignificant. This feature has also been previously observed by Bowen and Srinil (2020) for catenary pipes conveying two-phase slug flows. At lower flow velocities the increase in amplitude with increase in H_{LS} may be attributed to the overall increase in the mass of the cylinder, allowing for greater mass and momentum fluctuations over time.

In the case of varying H_{LF} (Table 3.1(b)), at lower flow velocities, the maximum amplitude decreases with an increase in H_{LF} as seen in Figure 3.4(b) and (f). This decrease is expected as the interaction between the liquid and gas phases becomes minimal, resulting in lower overall fluctuations of the two-phase flow. At higher flow velocities, the maximum amplitude trends are similar to those previously discussed for H_{LS}, with negligible changes in amplitude.

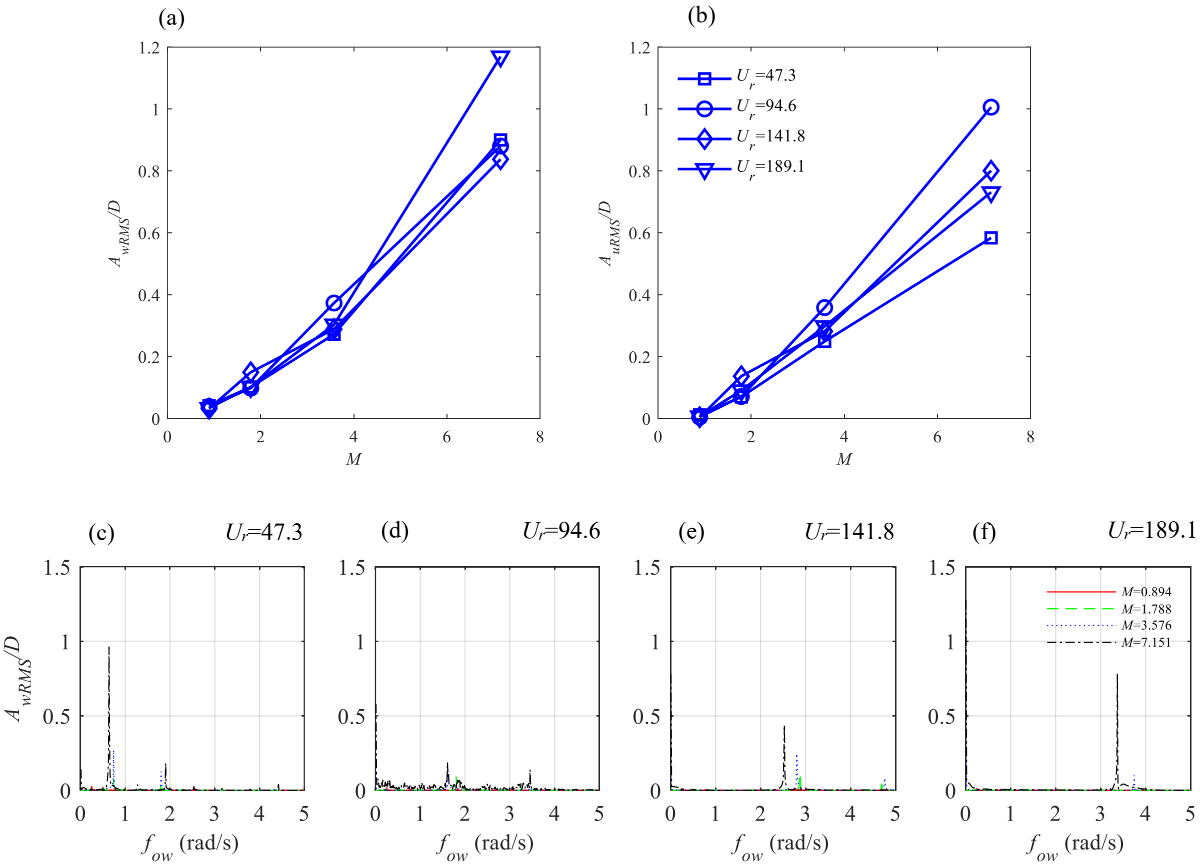

Figure 3.5: Maximum (a) out-of-plane and (b) in-plane RMS amplitudes and (c-f) frequency response plots for cases of varying mass quotient (M).

Furthermore, in the case of varying L_S (Table 3.1(c)), the out-of-plane and in-plane RMS amplitudes are found to be highest when L_S is approximately half of L_U for all four flow velocities considered. It can be observed from Figure 3.4(c) and (g) that the maximum amplitude increases with an increase in L_S and then decreases significantly when L_S is almost the same length as L_U. As mentioned earlier, this can be attributed to the minimal interaction between the two phases when L_S is close to zero or almost equal to L_U, resulting in inadequate mass and momentum fluctuations.

However, as the length of one slug unit L_U increases (Table 3.1(d)), the maximum amplitude remains low and constant for the first three cases and then increases for the fourth case in which L_U is the largest. For flow velocities 94.6, 141.8, and 189.1, the maximum amplitude is observed at L_U = 40D as seen in Figure 3.4(d) and (h). Highest amplitude response during the accumulation of the longest liquid slug has been previously observed by Miranda and Paik (2019) and Wang et al., (2018). During the lowest flow velocity case, U_r = 47.3, the maximum amplitude is observed at L_U = 20D, which is half the maximum amplitude observed when L_U = 40D (Longest liquid slug).

The highest amplitude response among all the slug properties considered in this study is observed when the mass quotient, M, (Table 3.1(e)) is three times the mass quotient previously considered, as seen in Figure 3.5(a) and (b). The RMS amplitude is observed to linearly increase with every increase in the mass quotient parameter. The highest amplitude observed is almost 50 times higher (0.03 to 1.6 in the out-of-plane direction and 0.018 to 1.4 in the in-plane direction) than the maximum amplitude noticed during the lowest mass quotient case. This increase can be attributed to the significant increase in fluid density, which leads to increased mass-momentum fluctuations in the two-phase slug flow and internal forces on the riser.

In addition, at high mass quotient cases (M = 3.58 and 7.15) during internal flow velocities U_r = 94.6, 141.8, and 189.1, the riser is observed to experience mean displacements in both the out-of-plane and in-plane directions, as shown in Figure 3.6(b-d) and (f-h) respectively. The riser drifts from its original XY position and reaches a high amplitude steady-state oscillation from the attained curved configuration in both directions. This can be observed in the colour bars associated with Figure 3.6(a-d) and (e-h). This mean drift can be a consequence of slug-induced high amplitude oscillations, which lead to disturbances in the external fluid surrounding the riser. These disturbances create oscillating drag and lift forces on the pipe due to the nonlinear external fluid forcing terms in the developed model (Zanganeh and Srinil, 2016).

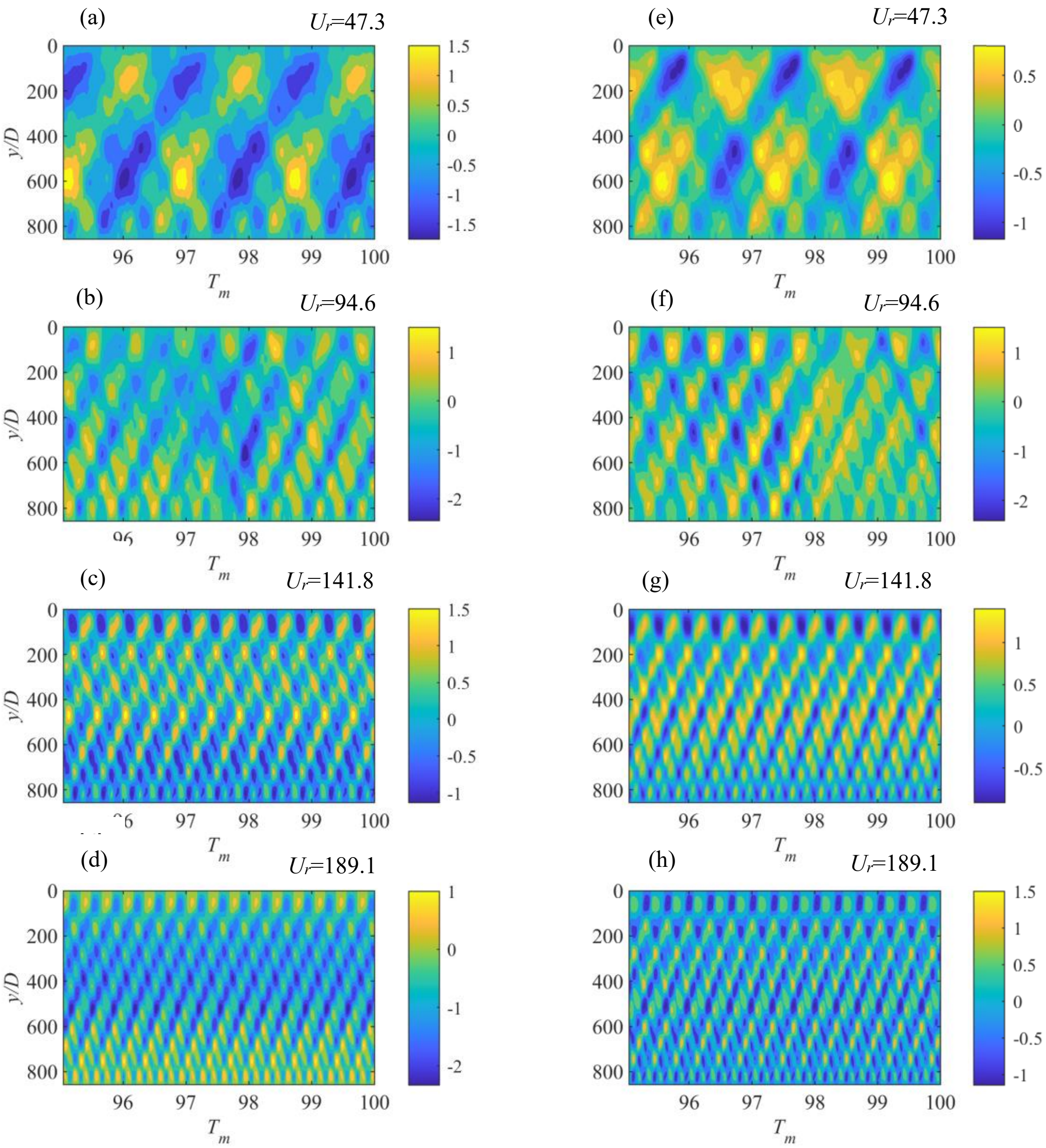

Figure 3.6: Space time varying (a-d) out-of-plane and (e-h) in-plane responses of the cylinder experiencing mean drifts during the highest mass quotient case (M =7.15).

Among all the slug flow properties considered amplitude-modulation responses are observed when the riser is exposed to the longest slug unit at L_U = 40D and U_r = 94.6, 141.8, and 189.1, respectively, as shown in Figure 3.7(a) and (b). This phenomenon occurs when multiple dominant frequencies of vibration occur over time, as previously observed by Zhu et al., (2018b) during an experimental study of slug-induced oscillations of long catenary pipes and Meng et al., (2020) for flexible marine risers subjected to simultaneous VIV and internal slug flow forces. Such amplitude-modulation response can lead to severe fatigue damage and should be considered during the life cycle analysis of pipelines conveying two-phase slug flows at higher L_U values.

Furthermore, comparison of maximum amplitudes obtained during single and two-phase slug flows for varying internal flow velocities are shown in Figure 3.7(c) and (d). It can be observed that the maximum amplitude obtained for two-phase slug flows at lower flow velocities $U_r = 47.3$ and 94.6 is significantly higher than the maximum amplitudes obtained for single-phase flow during similar flow velocities. However, at higher flow velocities ($U_r =$ 141.8, 189.1), the maximum amplitudes are found to be closer to each other. It should also be mentioned that for all the cases considered in this study, an initial condition was introduced to the riser such that the cylinder oscillates freely (self-excited without time-dependent force) in the out-of-plane direction only. However, simultaneous out-of-plane and in-plane oscillations are observed as seen in Figure 3.7(a-b), where oscillations in the in-plane direction, except for high mass quotient cases, starts several seconds after the riser begins to oscillate in the out-of-plane direction. This occurrence is attributed to the nonlinear couplings present in the developed equations, resulting from the consideration of geometric and hydrodynamic nonlinearities.

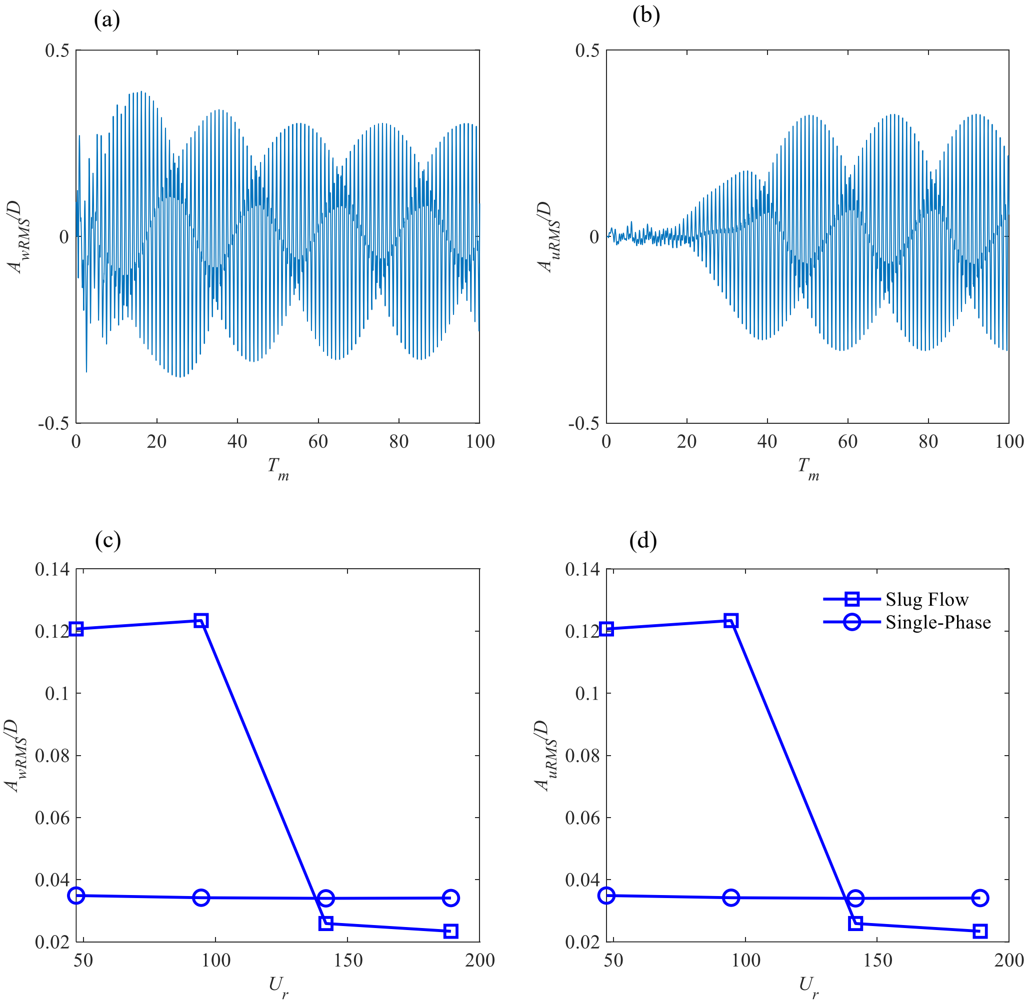

Figure 3.7: (a) Out-of-plane and (b) in-plane time-history amplitude-modulation response for $L_U = 40D$ at $U_r = 94.6$ and comparison of maximum (c) out-of-plane and (d) in-plane amplitudes of two-phase slug flows and single-phase flows at varying internal velocities.

3.3.2 Slug flow-induced oscillation frequencies

Frequency domain analysis of the above-mentioned riser displacements due to variations in slug flow characteristics is carried out using the fast Fourier transform (FFT) approach and depicted in Figure 3.8(a-p). It is observed that the natural frequencies of the first six excited modes, except in the cases of varying mass quotient, remain unchanged during two-phase slug flow when compared to the natural frequencies obtained during single-phase flow for all four internal flow velocities considered. The oscillation frequencies, f_0, shown in Figure 3.8 can be associated with the natural frequencies shown in Figure 3.3 to obtain dominant oscillation frequencies during each case considered in the parametric study. The results of the frequency domain analysis indicate that, although the obtained natural frequencies remain consistent during the parametric study for all six modes, the dominant modes and their corresponding dominant oscillation frequencies vary when the slug flow characteristics are altered.

Figure 3.8(a-p) illustrates frequency analysis of out-of-plane riser displacements using FFT. The figure describes oscillation frequency, f_0, vs amplitude plots at varying internal flow velocities. It was observed that the oscillation frequencies in the in-plane direction were the same as the frequencies in the out-of-plane direction and hence, Figure 3.8 plots show oscillation frequencies in the out-of-plane direction. The dominant modes and their corresponding frequencies are found to switch to higher modes and frequencies when the riser experiences high amplitudes of oscillations at specific slug formations. In cases where the amplitude initially increases and then decreases or vice versa, such as H_{LS} , L_S, and L_U cases, the dominant mode and frequency follow the same trend as the oscillation amplitudes as seen in Figure 3.8. When there is minimum or no change in the oscillation amplitudes, for example, H_{LF} cases, the dominant oscillation frequency and mode also remain constant.

It should also be mentioned that the same trends can be observed for every increase in the internal flow velocity. For the mass quotient (M) cases, Figure 3.5(c-f), it can be observed that the dominant mode transitions to a lower mode when the amplitude increases with an increase in the mass quotient value for all four internal flow velocities considered. Similarly, the excited oscillation frequencies are seen to decrease as the mass quotient value increases. This decrease in frequency is expected and has been observed in previous studies related to internal flow-induced vibration due to the effect of increased overall mass of the riser in high mass quotient cases. Additionally, it should be noted that the mode switching phenomenon over time does not occur for all the cases considered in this study. Overall, the results of the frequency domain and modal analysis show that the dominant modes and frequencies alter when the considered slug flow properties are varied at different flow velocities.

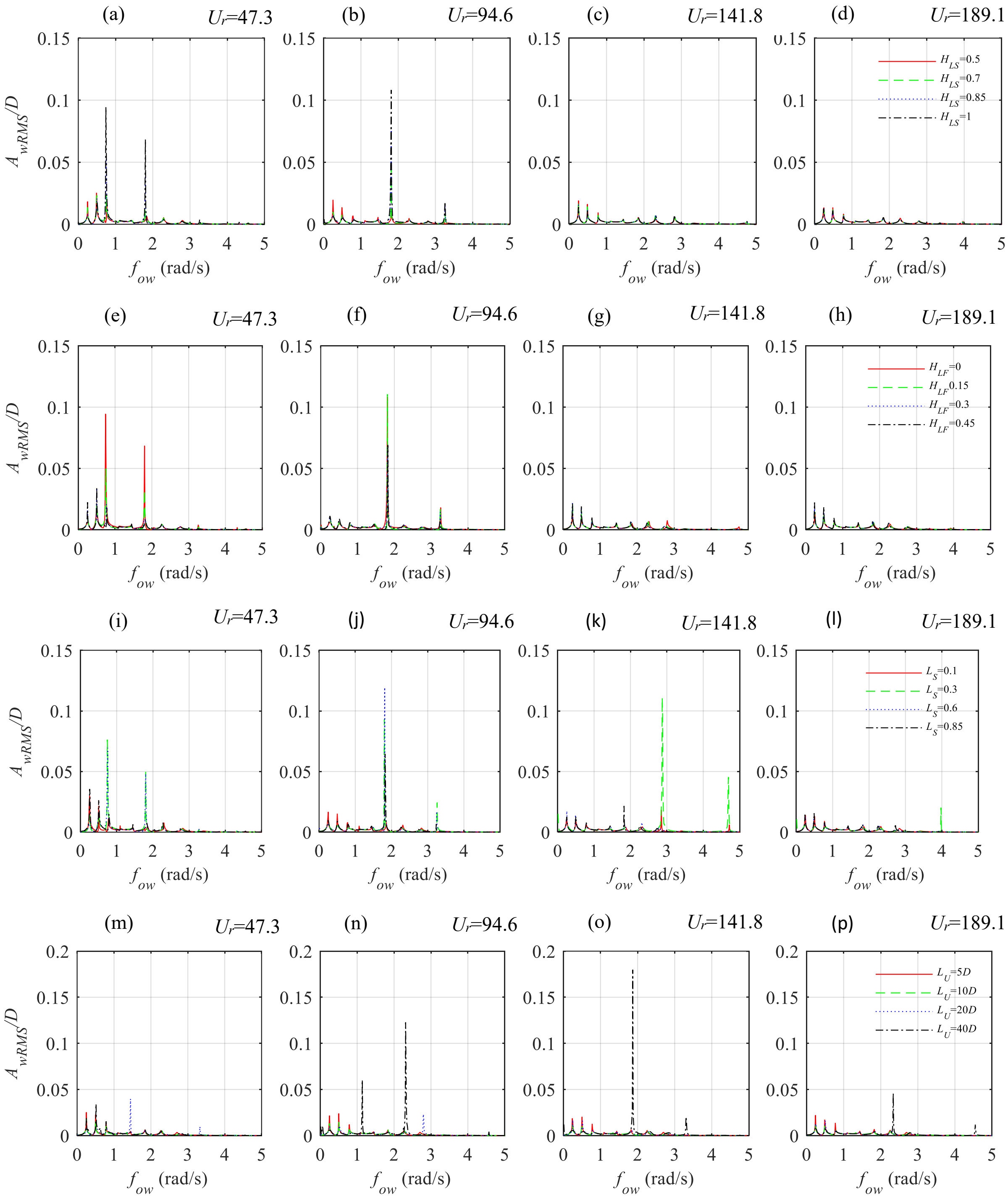

Figure 3.8: Out-of-plane frequency response plots of varying internal slug characteristics, (a-d) H_{LS} (e-h) H_{LF} (i-l) L_S (m-p) L_U at increasing internal flow velocities.

3.3.3 Axial oscillation responses and large amplitude scenarios

In addition to the two-dimensional out-of-plane and in-plane oscillations observed in the previous sections, pipe oscillations in the axial direction and mean displacements could be noticed at high mass quotient cases ($M = 3.576$, 7.151) for all the internal flow velocities considered, as shown in Figure 3.9(a-d). However, the oscillation amplitudes in the axial direction are observed to be low but considerable when compared to the out-of-plane and in-plane amplitudes. It should also be mentioned that mean displacements during oscillations in the axial direction could also be observed from the colour bars in Figure 3.9(a-d). The oscillations in the axial direction at high mass quotient can be attributed to the effect of mean displacements and high oscillation amplitudes in both the out-of-plane and in-plane directions, leading to hydrodynamic forces in the axial direction and three-dimensional (out-of-plane, in-plane and axial) oscillations arising from nonlinear couplings present in the equation. The effect of axial oscillations due to mean drag amplifications and high oscillation amplitudes has been previously observed by Zanganeh and Srinil (2016) for flexible oscillating cylinders experiencing vortex-induced vibrations.

Table 3.2: Specified slug flow parameters for verification.

U_r'	Dominant Mode	f_{dm}	H_{LS}	H_{LF}	L_S	L_F	M	D	U_r
10	1	0.235	1	0	6.1	11.4	1.788	0.583	94.46
73	3	0.730	1	0	6.1	11.4	1.788	0.583	293.98

Furthermore, it can be observed from the previous sections that oscillation amplitudes of the cylinder and the corresponding frequency and dominant modes increase with increase in smaller velocities ($U_r = 47.3, 94.6$) and decrease at higher flow velocities ($U_r = 141.8, 189.1$) for H_{LS}, H_{LF} and L_S study cases. For L_U and mass quotient, M, cases, it is vice-versa, where $U_r = 94.6$ is observed to be the flow velocity experiencing highest vibration response among all the flow velocities considered. A noticeable aspect of the presented model apart from three-dimensional oscillations and the consideration of geometric and hydrodynamic nonlinearities is the low computational effort required to perform each simulation. Simulations with reliable results of oscillation amplitudes, frequencies and mode numbers of each case discussed in this study could be completed within 48 hours.

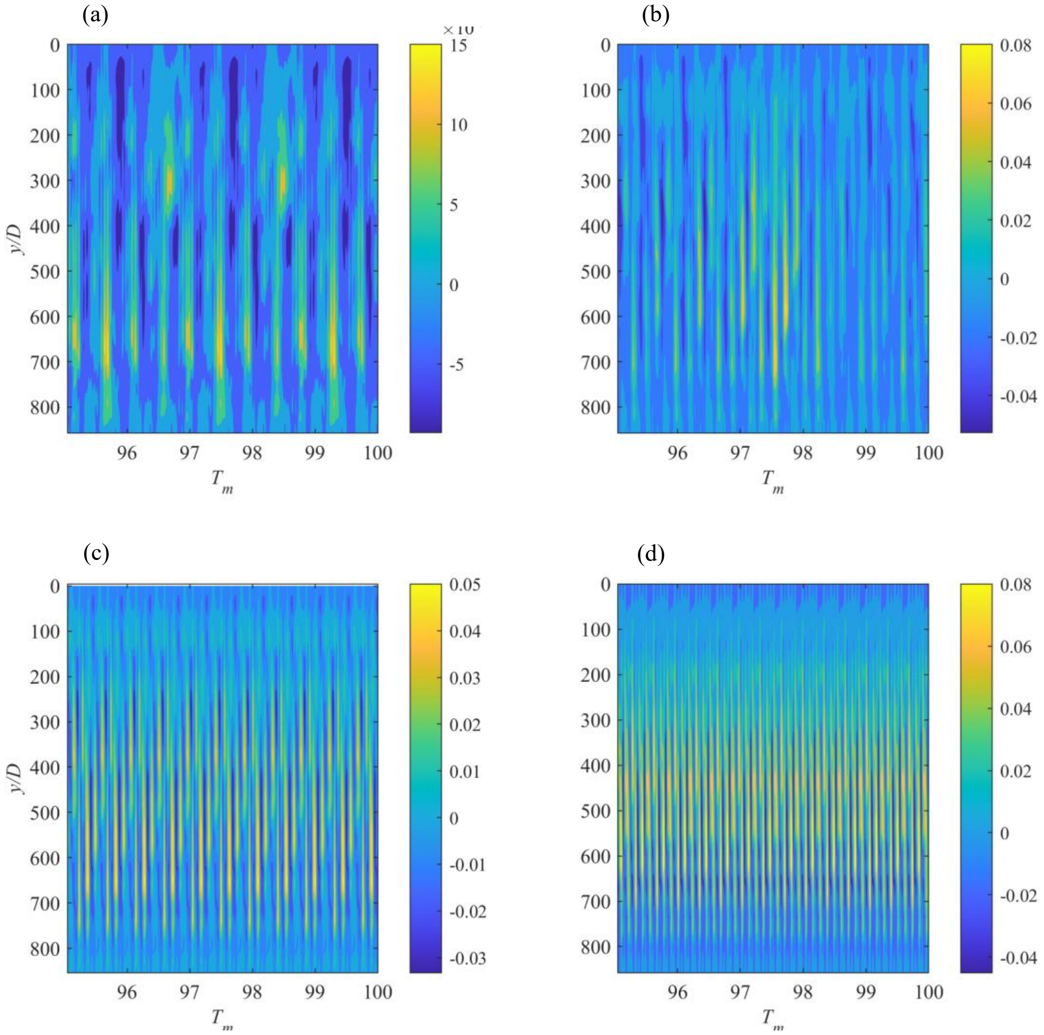

Figure 3.9: Space time varying displacements in the axial direction at mass quotient, M = 7.151 and varying internal flow velocities. (a) $U_r = 47.3$ (b) U_r =9 4.6 (c) U_r =141.8 (d) $U_r = 189.1$.

A new non-dimensional parameter, similar to the Strouhal number, is introduced to predict high oscillation amplitudes scenarios. This parameter is derived based on the results obtained from the parametric study conducted in this paper. The maximum RMS amplitude responses in the out-of-plane, in-plane and axial direction is compared using the dimensionless parameter described as:

$$U_r' = \frac{V_t}{f_{dm} * D}$$

Where, f_{dm} is the frequency of the dominant mode resulting from each case and D is the outer diameter of the cylinder. Figure 3.10 (a-b) displays the maximum RMS out-of-plane and in-plane amplitude and its associated U_r' obtained for all the 80 cases considered for parametric study. Results of this comparison reveal that high maximum RMS amplitudes due to internal two-phase slug flow occur between the U_r' range of 2 - 18. It can be inferred from Figure 3.10 that all U_r' cases outside this range produce low amplitude oscillations. This inference is plausible because, as observed in the previous sections for cases experiencing high amplitude oscillations, the corresponding dominating mode and frequency of the cylinder are also noticeably high. To verify this finding one case of U_r' outside the mentioned range and one case within the high amplitude range were examined. The f_{dm}were arbitrarily chosen and its equivalent translational velocity was calculated. The slug properties for these cases were chosen based on previous high amplitude response parameters as shown in Table 3.2. Results from the simulation show similar trends of high RMS amplitude response for case 1 where U_r' is within the high amplitude range and similarly case 2 show low RMS amplitude response in both out-of-plane and in-plane directions as shown in Figure 3.10(a) and (b).

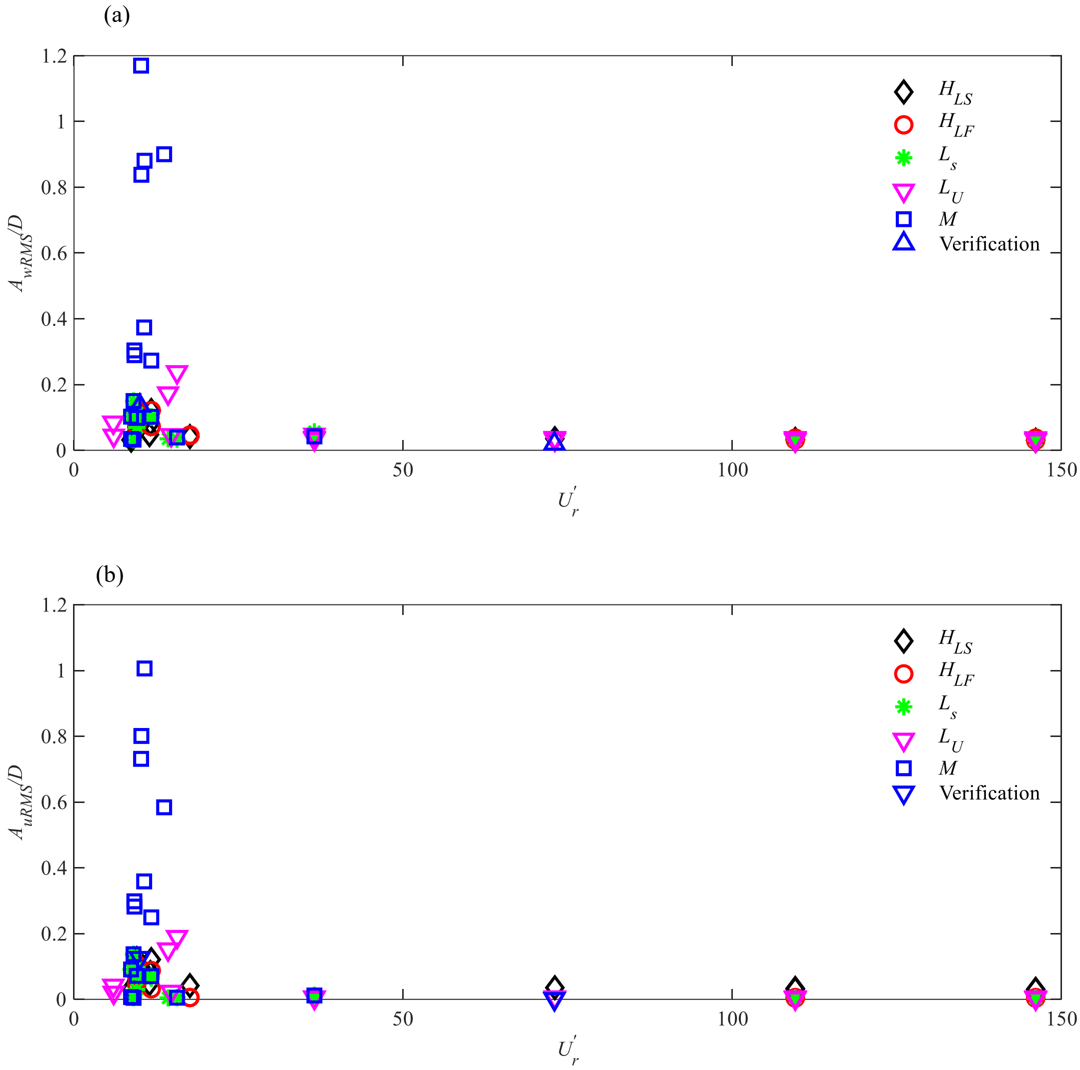

Figure 3.10: Comparison of maximum RMS (a) out-of-plane and (b) in-plane amplitude response of all the cases considered for parametric study using new dimensionless parameter U_r'.

3.4 Conclusions

A three-dimensional phenomenological model for the analysis and prediction of coupled out-of-plane, in-plane and axial slug flow-induced vibrations of a long vertical cylinder is presented in this study. The developed model accounts for both geometric and hydrodynamic nonlinearities and is capable of capturing mass variations in the slug flow regime. Through cubic and quadratic nonlinear terms, the model is coupled with equations involving centrifugal and Coriolis force for the prediction of two-phase SIV. The model combines external nonlinear fluid forcing terms through oscillatory lift and drag forces. A space-time finite difference approach has been used to solve the highly nonlinear partial differential equations present in the model. The parametric study explores the effects of key slug characteristics and provides insights into several SIV nonlinear dynamic phenomena dictating the response of a long flexible cylinder. The key features are summarised as follows.

- The slug flow-induced RMS amplitudes are observed to increase linearly at lower slug translational velocities and be constant at higher translational velocities. Lower slug velocities produce increased amplitudes up to 350% compared to higher flow velocities at specific slug formations.
- Simultaneous three-dimensional out-of-plane, in-plane and axial oscillations are observed due to nonlinear coupling terms in the presented model.
- The longest slug unit generate large amplitude-modulation response which can lead to increased fatigue damages over time.
- Mean displacements due to high internal fluid density and large amplitude response in the out-of-plane and in-plane directions induces external hydrodynamic forces on the cylinder leading to oscillations in axial direction because of nonlinear couplings.
- Changes in the two-phase slug flow oscillation frequencies were found to be negligible when compared to the single-phase oscillation frequencies for all the internal translational velocities considered. However, the dominant modes and oscillation frequencies vary according to distinct slug formations and are found to exhibit a linear relationship with the overall amplitude response.
- A dimensionless parameter U_r' is introduced for the purpose of predicting high oscillation amplitude scenarios corresponding to the cases considered in this study. U_r' values ranging from 2 to 18 were found to generate high amplitude responses while the other values outside this range generate low oscillation amplitudes.

Model validations are performed through comparisons with published numerical and experimental results. Results exhibit quantitative similarities with minor discrepancies, attributed to the consideration of a more inclusive model that takes into account the structural and geometric nonlinearities.

Chapter 4

Nonlinear Dynamic Response of a Horizontal Flexible Cylinder Conveying Two-Phase Slug Flows

In the previous chapter, several key SIV features were observed for the case of a vertical cylinder. Utilising the three-dimensional SIV model introduced earlier, this chapter investigates the dynamic response of horizontal flexible cylinders carrying two-phase slug flows by taking into account the geometric nonlinearities. The numerical model is solved using a finite difference scheme, and the three-dimensional results are analysed in the time and frequency domain. Model validation is conducted through comparisons of time-history amplitude and frequency response with experimental results from the literature. A parametric study is carried out to explore the effects of key slug characteristics on the vibration response of a horizontal cylinder surrounded by air. The significance of considering geometric nonlinearities to predict vibrations resulting from internal two-phase slug flows is discussed through three-dimensional large out-of-plane, in-plane, and axial oscillations, parametric resonance, identification of subharmonics, and high frequency modulated response.

4.1 SIV Model Validation

The developed three-dimensional prediction model is compared with the experimental tests conducted by Wang et al., (2018) for a horizontal cylinder conveying two-phase slug flows. The fluid-conveying cylinder is surrounded by air with properties $D = 0.063$ m, $L = 3.81$ m, young's modulus, $E = 750$ MPa, density $= 926$ kg/m^3 with internal liquid density $=$ 1000 kg/m^3 and viscosity $= 0.001$ Pas. The steady-state internal slug flow is modelled as a rectangular pulse train, where a single slug unit (LU) includes liquid slug (L_S) and an elongated gas bubble over a thin film of liquid (L_F), thin film liquid holdup (H_{LF}), slug liquid holdup (H_{LS}), and translational velocity, (V_t). as shown in Figure 3.2 in Chapter 3. The model follows rectangular waves with flat peaks, where area under the flat peak indicate liquid slug, whose length is L_S. The thin liquid film in the model is represented as the area under the remaining slug unit whose length is L_F. A fixed-pinned boundary conditions is assumed to facilitate comparisons and replicate experimental vibration results. Figure 4.1 compares the time-history amplitude responses of numerical simulation and experiment results at the midpoint of the cylinder. It is worth mentioning, since the focus of the present comparison is to validate the capabilities of the model in predicting key SIV features, the oscillations in Figure 4.1 are depicted around zero and their mean value has been removed. The time-history plot obtained from this study shows that the present model is capable of accurately capturing the SIV out-of-plane amplitude and frequencies compared to the experimental results. The minor discrepancies observed in Figure 4.1 are due to differences in slug frequencies between the experiment tests and the simulation. Wang et al., (2018), varied the slug frequencies of each slug unit passing through the cylinder. In their work, the slug length L_S and translational velocity, V_t, for each slug unit vary as 1.19 m, 1.09 m, 0.73 m and 1.19 m and 3.50 m/s, 3.03 m/s, 3.64 m/s and 2.33 m/s, respectively. However, this study employs a steady-state slug flow, where the slug frequencies of all the slug units passing through the cylinder over time remain constant. Therefore, the values for L_S, L_F, and V_t, obtained from the literature, are fixed at 1.19 m, 10.53 m, and 3.5 m/s, respectively, for all the slug units travelling along the cylinder. Secondly, the details of H_{LS} and H_{LF} values are absent in Wang et al., (2018), which may further affect the mean deflection at the cylinder midpoint. In the present study, these key slug flow characteristics were calculated using the *iSLUG* model (Zanganeh et al., 2021). An uncertainty analysis is performed to measure the error differences between experiment and simulation values. An RSME error of 0.00178 was obtained from calculating the square root of the mean difference in amplitude values at each time step. The low RMSE value, along with the similar trends of amplitude and frequency response observed in Figure 4.1, indicates that the model exhibits quantitative similarities when compared with previous experimental results.

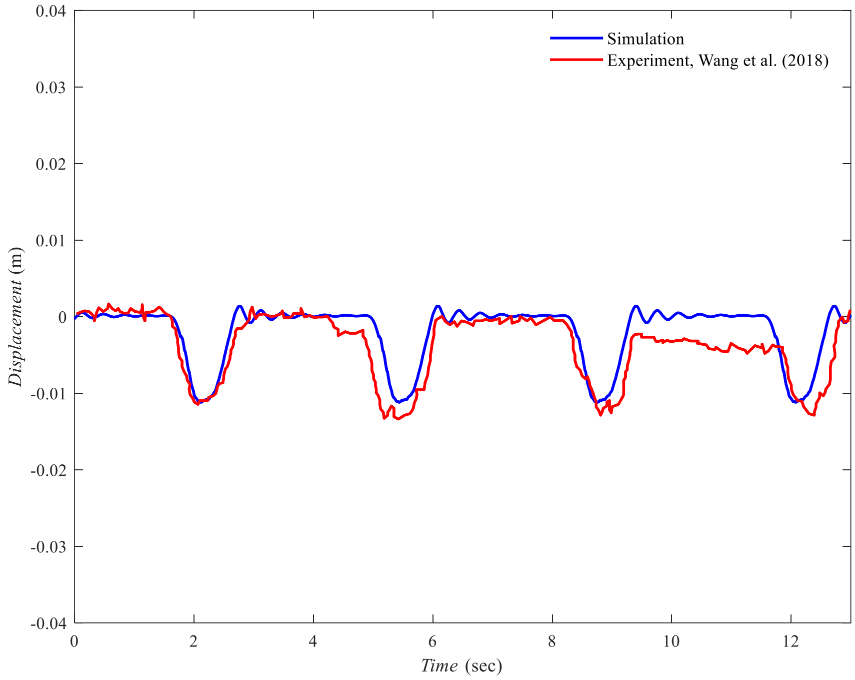

Figure 4.1: Time-history amplitude comparison between numerical and experimental results (Wang et al., 2018).

4.2 Numerical Results and Discussion

The experimentally tested horizontal cylinder used in the previous section for validation is employed here to perform a parametric study to analyse the influence of key slug characteristics on the dynamic response of the cylinder.

4.2.1 Effect of f_s/f_n ratio on the dynamic response of a horizontal fluid-conveying cylinder

Following the findings of Hara (1973), this chapter aims at analysing the effect of different f_s/f_n ratios, where f_n is the dimensional first natural frequency of the cylinder in Hertz and f_S is the incoming slug frequency expressed as $f_s = V_t/L_U$, on the time-varying response of a horizontal cylinder taking into account the associated geometric nonlinearities. The slug parameters considered for this study are illustrated in Table 4.1. The first natural frequency of the cylinder, f_n, was analytically calculated to be 3.093 H_Z (Song et al., 2011) and accordingly four slug frequencies were calculated such that the f_s/f_n ratios are 2, 1, 0.66 and 0.5 (Hara, 1973). To analyse the effects of internal flow velocities, seven slug translational flow velocities (V_t) are considered for each f_s/f_n ratios. The length of one slug unit (L_U) for each case can be estimated using the relation, $f_s = V_t/L_U$ (Bowen and Srinil, 2021). Following Chapter 3, the slug liquid holdup, H_{LS}, and the thin film liquid holdup, H_{LF}, for all 28 cases in this parameter study are factored as 1 and 0 to capture maximum SIV features, where 1 denotes completely-filled and 0 indicates completely-empty holdups of H_{LS} and H_{LF} respectively. The slug liquid length, L_S, and thin film liquid length, L_F, are considered to be equal halves of L_U for all the cases considered in this study. For a horizontal cylinder, the theta value associated with eq. 3.14 is set to zero, indicating that the cylinder is horizontal, in contrast to a value of 90 degrees for the vertical cylinder studied in Chapter 3. It should be noted that, in the parametric study, the cylinder under consideration is assumed to be surrounded by air, as discussed in the previous section.

Table 4.1: Slug flow parameters considered in cases of varying f_s/f_n ratios.

U_r	f_s/f_n	L_U/D
4.08	2	12.70
	1	25.56
	0.66	38.41
	0.5	51.27
6.12	2	19.21
	1	38.41
	0.66	57.62
	0.5	76.83
8.16	2	25.56
	1	51.27
	0.66	76.83
	0.5	102.54

10.2	2	32.06
	1	64.13
	0.66	96.19
	0.5	128.25
12.25	2	38.41
	1	76.83
	0.66	115.40
	0.5	153.81
14.3	2	44.76
	1	89.68
	0.66	134.60
	0.5	179.52
16.33	2	51.27
	1	102.54
	0.66	153.81
	0.5	205.24

4.2.1.1 Slug flow-induced three-dimensional amplitude responses

As the incoming slugs enter the cylinder, the cylinder is noticed to experience an outward bending in the perpendicular direction (out-of-plane) due to the effects of gravity and flow momentum. The cylinder attains a new stable curved configuration and oscillates around this newly developed configuration. It could be observed that the results exhibit a combination of coexisting two-dimensional out-of-plane and axial oscillations, as well as three-dimensional out-of-plane, in-plane, and axial oscillations, depending on specific f_s/f_n scenarios and flow velocity parameter. When the slug frequency, f_s, is twice the first natural frequency of the cylinder, f_n, the cylinder experiences coexisting out-of-plane and axial oscillations for all the internal velocities considered in this study. Axial oscillation amplitudes are observed to be low but considerable when compared to out-of-plane oscillation amplitudes. Figure 4.2(a-c) shows the maximum RMS amplitude response after removing the mean components in the out-of-plane, in-plane and axial directions. It can be observed from Figure 4.2(a) that the amplitude response in the out-of-plane direction is low compared to other f_s/f_n ratios and constant at lower flow velocities. At higher flow velocities (above $U_r = 12.25$), however, the amplitude is seen to increase considerably with increase in flow velocities. The RMS amplitudes in the axial direction follow similar trends as the out-of-plane direction, with lower internal flow velocities resulting in amplitudes close to zero and increasing notably when U_r reaches 14.3.

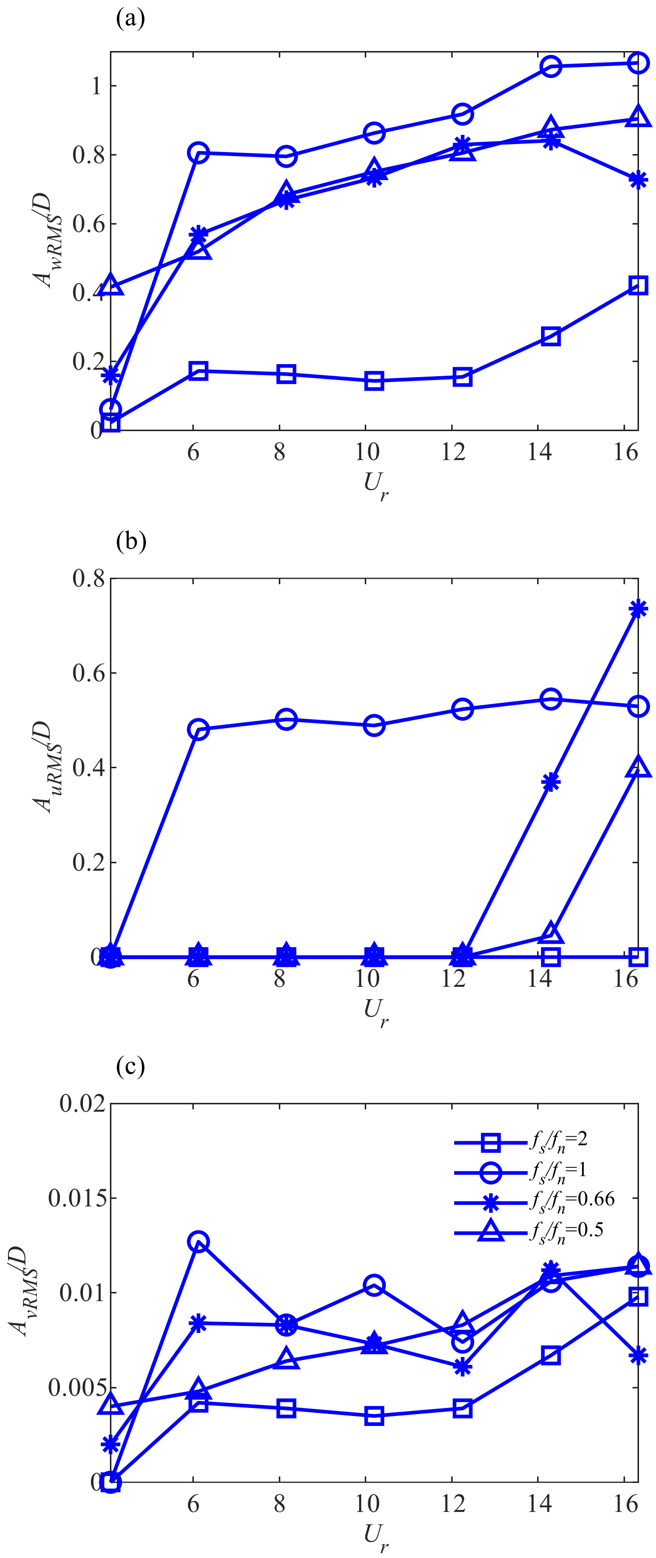

Figure 4.2: Comparison of RMS amplitudes at varying U_r and f_s/f_n ratios. (a) Out-of-plane (b) In-plane (c) Axial oscillation amplitudes.

At f_s/f_n ratios of 0.66 and 0.5, similar to the previous scenario, two-dimensional out-of-plane and axial oscillations occur within the U_r range of 4.08 to 12.25. Beyond this range, at higher flow velocities ($U_r = 14.3$ and 16.33), three-dimensional large amplitude oscillations become evident. It can be observed from Figure 4.2(a-c) that RMS amplitudes in the out-of-plane direction are considerably higher than the previous f_s/f_n ratio ($f_s/f_n = 2$) and are observed to increase with increase in U_r. It should also be mentioned that f_s/f_n ratios of 0.66 and 0.5 generate out-of-plane amplitudes closer to each other at all internal flow velocities as seen in Figure 4.2(a). In-plane RMS amplitudes responses show low amplitude oscillations at lower U_r and increase significantly after U_r reaches 14.3, with $f_s/f_n = 0.66$ ratio inducing higher amplitude response than $f_s/f_n = 0.5$. Axial RMS amplitudes are noticed to follow a zig-zag trend with amplitudes closer to each other when $f_s/f_n = 0.66$. When $f_s/f_n = 0.5$, axial RMS response is seen to increase linearly with increase in internal flow velocities. It can also be observed that the RMS response in the in-plane and axial directions are higher than the previous f_s/f_n discussed.

The highest RMS amplitude response among the four f_s/f_n ratios considered is observed when the incoming slug frequency is equal to the first natural frequency of the cylinder ($f_s/f_n = 1$). When $f_s/f_n = 1$, coexisting three-dimensional oscillations are observed at every U_r except $U_r = 4.08$, wherein in-line oscillations are absent in this case. It can be observed from Figure 4.2(a-c) that RMS amplitudes in all three directions and at all internal flow velocities are higher than those of all other f_s/f_n ratios considered in this study. Out-of-plane amplitude response are noticed to increase with increase in internal flow velocities whereas in-plane maximum RMS responses are largely similar to each other when U_r reaches 6.12 and a slight increase is noticed at higher U_r. Axial oscillations, similar to the previous ratios, follow a zig-zag pattern where maximum amplitudes alternate at each flow velocities. It should be mentioned that when, $f_s/f_n = 1$, in-line oscillations become more evident and a significant increase in amplitude response at every flow velocity is observed compared to other f_s/f_n ratios considered. It could be inferred from Figure 4.2(a-c) that $f_s/f_n = 1$ ratio induce large amplitude oscillations in all three directions and at every flow velocity considered in comparison to other f_s/f_n ratios investigated in this study. The occurrence of chaotic large amplitude oscillations when the incoming slug frequency, f_s, is close or equal to the first natural frequency of the cylinder, f_n, has been previously observed by (Hara, 1973). Subsequently, it can be noticed that $f_s/f_n = 2$ ratio generates the lowest RMS amplitude response among the considered f_s/f_n ratios. f_s/f_n ratios below 1 can be categorised as intermediate responses, producing vibration amplitudes between the f_s/f_n ratios of 1 and 2.

Furthermore, Figure 4.3(a-l) displays contour plots of space-time varying three-dimensional responses by removing the mean components at different f_s/f_n ratios and U_r. Some essential features are noticed. Because of gravity and flow-momentum effects, mean displacements during cylinder oscillations are observed in all three-directions when $f_s/f_n = 2$. Mean displacements are noticed to be the largest in this case due to lower mass and momentum fluctuations, leading to oscillations in the newly attained curved configuration. However, mean displacements tend to become nullified at higher oscillation amplitudes during other f_s/f_n ratios. The increase in oscillation amplitudes in all three directions as U_r increases can be observed in Figure 4.3 for each of the four f_s/f_n ratios. When f_s/f_n = 2, in Figure 4.3(a), (e) and (i), a second mode dominant response at low U_r ($U_r = 4.08\ to\ 12.25$) can be observed in all three directions and a shift to first mode dominant response is observed when $U_r = 16.63$ in the out-of-plane and in-plane directions. In otherf_s/f_n ratios, a first mode dominant response can be noticed in the out-of-plane and in-plane directions, indicating that cases with high oscillation amplitudes generate a predominant first mode response in the corresponding directions of oscillation. Axial responses, however, follow a second mode dominant response in all the above cases. Additionally, the influence of in-plane oscillations at higher flow velocities discussed in Figure 4.2 can be noticed in Figure 4.3(c-h).

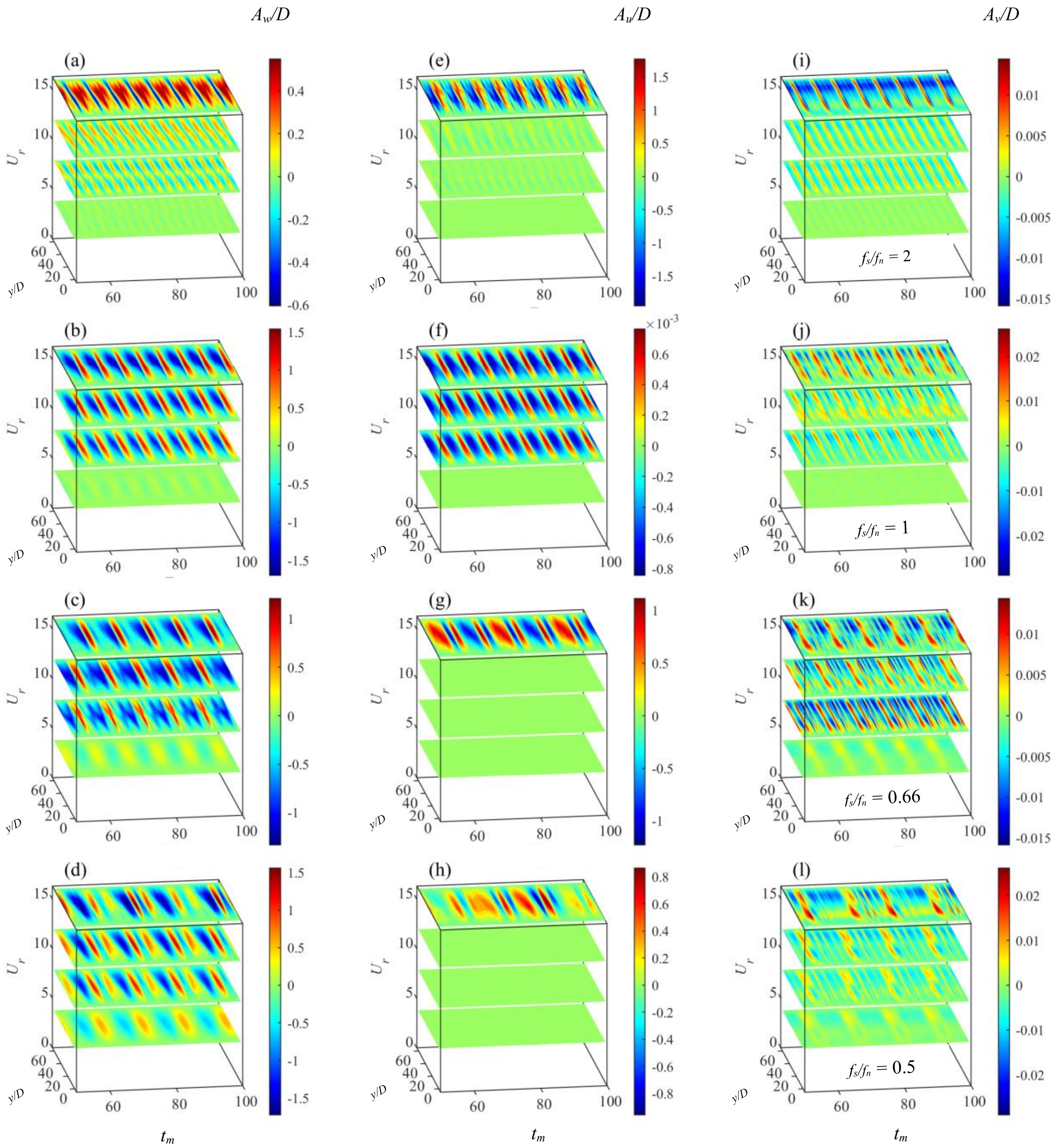

Figure 4.3: Space-time varying contour plots after removing mean components (a-d) out-of-plane, (e-h) in-plane, (i-l) axial, for different f_s/f_n ratios.

In addition, Figure 4.4(a-f) compares in-plane time-history amplitude comparisons between f_s/f_n ratios when $U_r = 14.33$ and 16.33. The figure highlights the delayed response observed in the in-plane directions when $U_r = 14.33$ and 16.33 as opposed to an immediate vibration response in the out-of-plane and axial directions. Oscillations in the in-plane direction is noticed to start several t_m after oscillations in the out-of-plane and axial directions. This phenomenon is attributed to the nonlinear couplings within the developed model as seen in

Section 3.3.1 in the previous chapter. It is also worth noting that the in-plane oscillations starts marginally earlier when $U_r = 16.33$ compared to U_r being 14.3, as the amplitude increases in both the $f_s/f_n = 0.66$ and 0.5 cases. When $f_s/f_n = 1$, oscillations are observed to start almost simultaneously in both U_r, as the amplitudes are similar in both scenarios. Co-existing three-dimensional out-of-plane, in-plane and axial displacements observed during the ratio $f_s/f_n = 1$ and at high flow velocities can be associated to the effect of mean displacements and high amplitude oscillations in the out-of-plane direction, leading to oscillations in the other two directions due to the nonlinear couplings present in the equation. This three-dimensional vibration phenomenon due to mean displacements and large amplitudes in the out-of-plane direction has been previously expressed by Zanganeh and Srinil (2016).

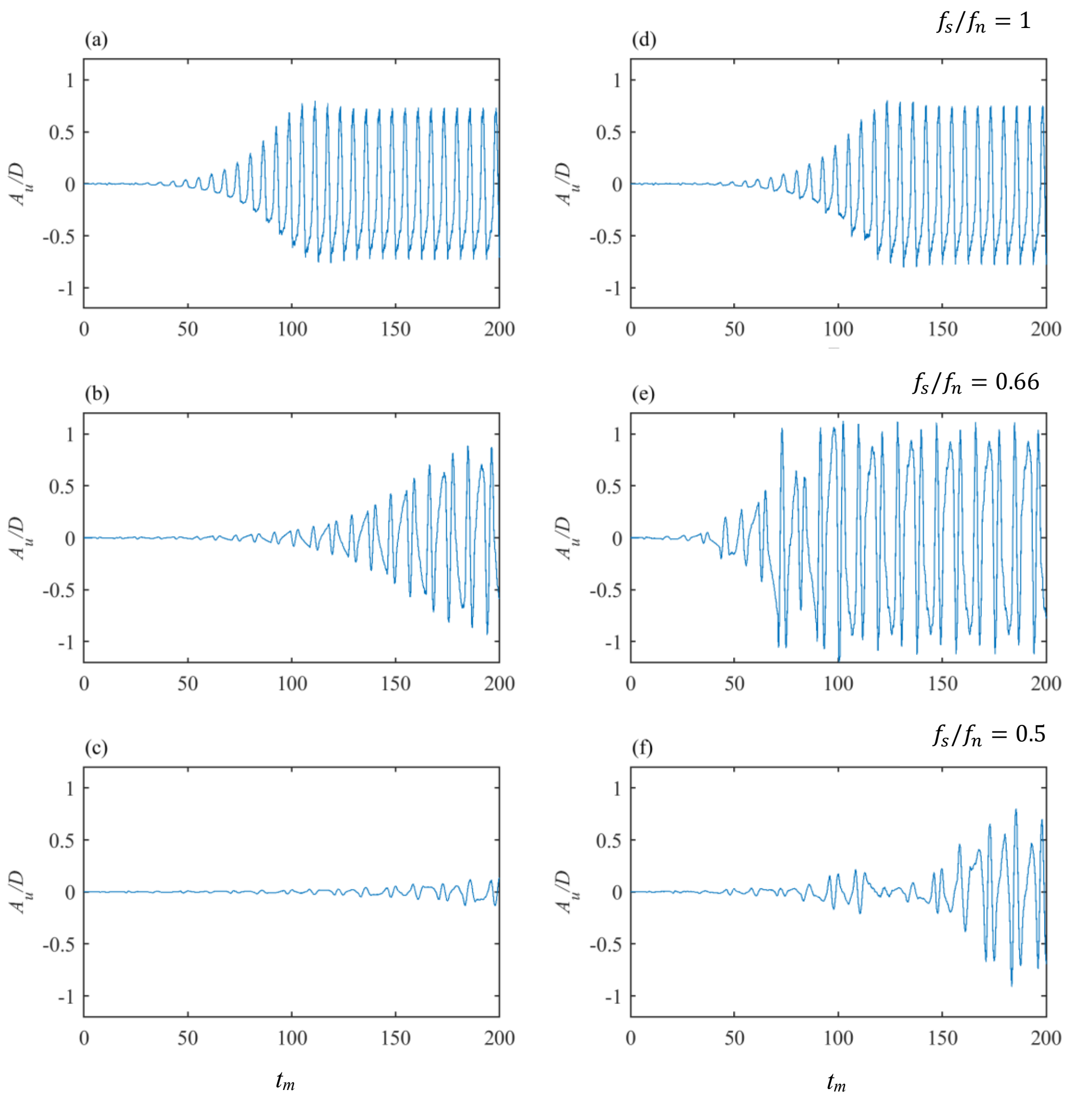

Figure 4.4: In-plane time-history amplitude plots when $U_r = 14.3$ (a-c) and 16.33 (d-f) for varying f_s/f_n ratios.

4.2.1.2 Harmonic and sub-harmonic oscillation frequencies

Figure 4.5(a-h) presents frequency domain FFT plots of the slug-induced cylinder displacements associated with f_s/f_n ratio cases. The power spectral densities shown in the plots are normalised with respect to the corresponding slug frequencies for each case. At low $U_r = 4.08$ (Figure 4.5(a-e)), out-of-plane and axial oscillations show multi-harmonic responses with dominant oscillation frequency close to the second mode natural frequency when $f_s/f_n = 2$. At lower f_s/f_n ratios (1, 0.66 and 0.5) out-of-plane oscillations demonstrate a single-peak frequency response, whereas axial oscillations display multi-harmonic frequency responses. It should also be noted that a 1:2 resonance is observed in all the above cases where axial oscillations have oscillation frequencies twice that of out-of-plane frequencies.

When $U_r = 8.16$ (Figure 4.5(b-f)), out-of-plane frequency response reveal multi-harmonic frequencies at f_s/f_n ratios of 2, 0.66 and 0.5 and single harmonic peak when the ratio is 1. Axial oscillations, however, exhibit high frequency modulations at ratios 0.66 and 0.5, and frequencies with fewer components at ratios 2 and 1. It should be mentioned that a 1:3 frequency response is noticed at ratio 0.66 where the dominant oscillation axial frequency is three times that of out-of-plane frequency and 1:2 response is observed in all other cases. Additionally, out-of-plane oscillations reveal dominant oscillation frequencies equal to the slugging frequency at ratios 2, 1 and 0.66 while the dominant oscillation frequency switches to the first natural frequency of the cylinder when the ratio is 0.5.

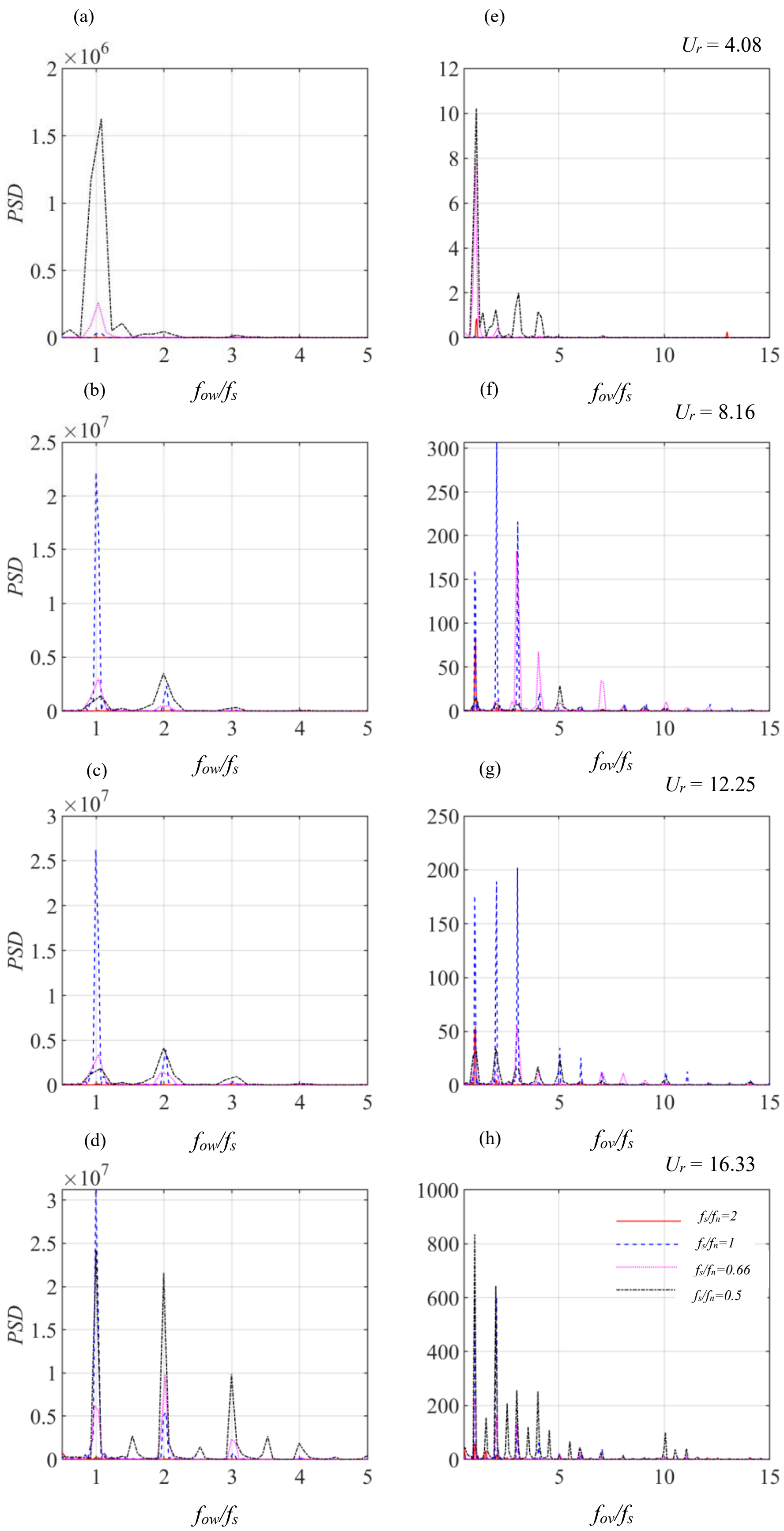

Figure 4.5: Out-of-plane (a-d) and axial (e-h) frequency response at varying f_s/f_n ratios and U_r.

Furthermore, subharmonic frequencies are observed at $U_r = 12.25$ (Figure 4.5(c-g)) when $f_s/f_n = 2$. Out-of-plane frequency equal to F_n is noticed in this case along with higher harmonics in multiples of the slug excitation frequency. Similar to the previous case of $U_r = 8.16$, dynamic response at this velocity exhibit multi-harmonic frequencies and high frequency modulations in the out-of-plane and axial directions respectively at f_s/f_n ratios 1, 0.66 and 0.5. At $U_r = 16.33$ (Figure 4.5(d-h)), similar trends of multi-harmonics and frequency modulation are observed in the out-of-plane and axial directions, respectively, when the ratios are 1, 0.66 and 0.5. In comparison, low frequency contents are observed when the ratio is 2. Additionally, sub-harmonic oscillation frequencies are identified in the out-of-plane and axial directions when f_s/f_n ratio becomes 0.5 as seen in Figure 4.5(d-h).

Figure 4.6(a-c) presents frequency response FFT plots observed in the in-plane direction in cases for cases featuring prominent in-plane oscillations. It can be noticed that when $f_s/f_n = 1$, in-plane oscillations experience multi-harmonic frequency response with lesser frequency contents compared to the axial direction. However, at $U_r = 16.33$, subharmonic frequencies are observed when f_s/f_n ratios are 0.66 and 0.5. The sub-harmonic frequencies noticed in all three directions at higher flow velocities where the amplitude of displacements is large can be attributed to the geometric nonlinearities considered in the three-dimensional SIV model. Moreover, in all the cases discussed above axial oscillations illustrate higher number of frequencies contents present in the oscillations compared to frequencies present in the other two-directions of motion. Furthermore, it is also worth mentioning that the dominant oscillation frequency in the out-of-plane and in-plane directions equals the slugging frequency in all the cases, with the exception occurring only when $f_s/f_n = 0.5$ and at high flow velocities ($U_r \geq 8.16$).

Axial oscillations also reveal 1:2 response in all the cases discussed above indicating a second mode dominant response for all f_s/f_n ratios. $f_s/f_n = 2$ produce lower frequency contents in comparison to other f_s/f_n ratio implying that large oscillation amplitudes when $f_s/f_n = 1$, 0.66 and 0.5 lead to higher harmonic and subharmonic frequencies. Overall, it can be summarised that as U_r increases harmonic peaks in all three directions increases and axial oscillations reveal high frequency contents with lower amplitudes in comparison to out-of-plane and in-plane responses in all the cases discussed above. The presence of high frequency contents with lower amplitude responses, particularly noticeable in the axial direction can lead to an increased likelihood of cyclic stresses and fatigue related issues. It is crucial to account for the factors during the design phase of a cylinder conveying two-phase gas-liquid slug flows.

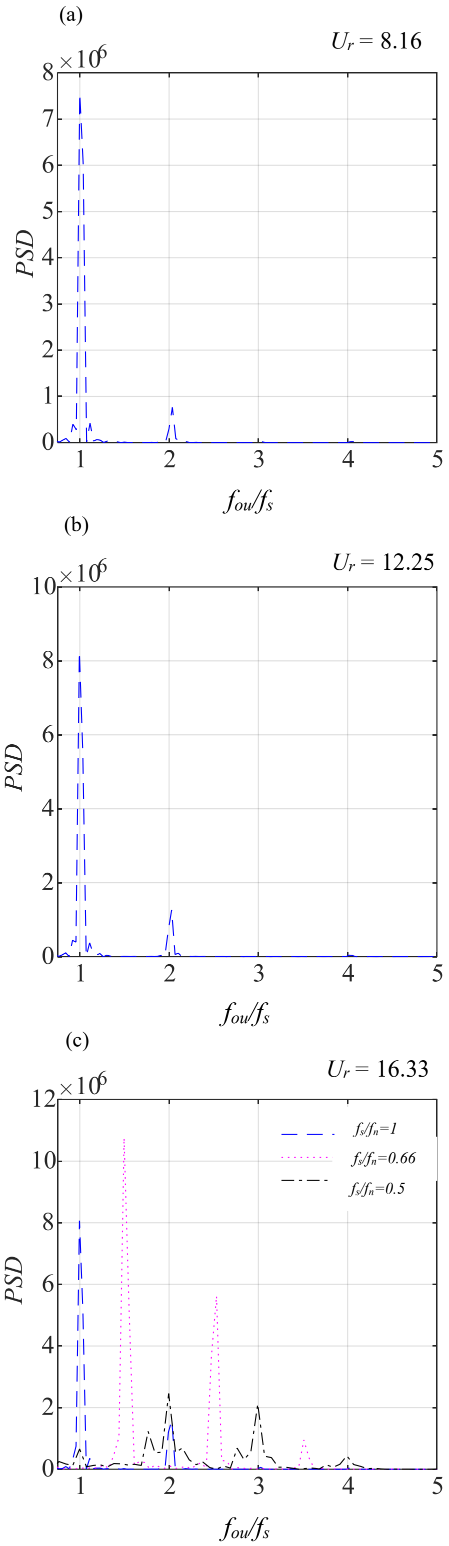

Figure 4.6: In-plane frequency response at varying f_s/f_n ratios and U_r.

4.2.2 Influence of U_r on the vibration mechanisms of a horizontal fluid-conveying cylinder when L_U is held constant

In addition to analysing the effect of various f_s/f_n ratios, this study explores additional crucial parameters associated with slug flow. Since the previous parameter study varied the L_U parameter in each case, cylinder dynamic response when L_U is held constant is studied here. Table 4.2 outlines the slug flow parameters considered in this parameter study. The effect of U_r is considered, with U_r being the only varying parameter in this case, varied from 4.08 to 24.5, as shown in Table 4.2 The slug frequency, f_s, however varies with U_r due to their previously mentioned relation. The L_U parameter is chosen such that, when U_r reaches 12.25, f_s/f_n becomes 1 through the stated relation, $f_s = V_t/L_U$. The H_{LS} and H_{LF} parameter similar to the previous cases, are set to 1 and 0, respectively. Likewise, the L_S and L_F parameter are half of L_U in all the cases considered below.

Table 4.2: Slug flow parameters considered in the case of constant L_U/D.

U_r	L_U/D	f_s/f_n
4.08	76.83	0.33
6.12	76.83	0.5
8.16	76.83	0.66
10.2	76.83	0.83
12.25	76.83	1
14.3	76.83	1.16
16.33	76.83	1.33
18.37	76.83	1.5
20.41	76.83	1.66
22.46	76.83	1.83
24.5	76.83	2

4.2.2.1 Three-dimensional oscillation amplitudes and parametric resonance

For a fixed L_U, with the internal flow velocity U_r as the only varying parameter, Figure 4.7(a-c) illustrates maximum RMS amplitudes in the out-of-plane, axial and in-plane directions versus f_s/f_{n_1} ratios where f_{n1} is the natural frequency of the cylinder containing internal mass. The internal fluid mass with density 1025 Kg/m^3 is calculated and added to the mass of the empty cylinder and the corresponding natural frequency, f_{n1}, is obtained (Song et al., 2011). Simultaneous out-of-plane and axial oscillations are observed at low U_r ($U_r = 4.08$ to 10.2), while three-dimensional oscillations observed are at higher flow velocities ($U_r \geq 12.25$). It could be observed that the maximum RMS amplitudes in the out-of-plane and in-plane directions increase with increase in U_r initially and alternates after U_r reaches 16.33 or $f_s/f_{n_1} = 2$. In Figure 4.7(a) and (c), we observe evidence indicating parametric resonance, as the largest amplitude peaks align with f_s/f_{n_1} ratios of 2 and 3 in the out-of-plane direction and 2 and 3.25 in the in-plane direction. This phenomenon has been experimentally observed and reported by Hara (1973) for a horizontal cylinder subjected to two-phase slug flows. Parametric resonance occurs when the natural frequency of the cylinder fluctuates during oscillation, resonance is induced when the excitation frequency is twice the natural frequency of the oscillating cylinder. This phenomenon is triggered by the presence of slug flow and consequently the model's capability to capture variations in internal mass. Nevertheless, axial oscillation amplitudes are observed to increase significantly and linearly with an increase in U_r as seen in Figure 4.7(b). Moreover, large amplitude oscillations, high frequency contents and switching of dominant oscillation frequency from f_s to f_n noticed in the previous section when f_s/f_n = 0.5 and 0.66 can be associated with parametric resonance as mentioned in Hara (1973).

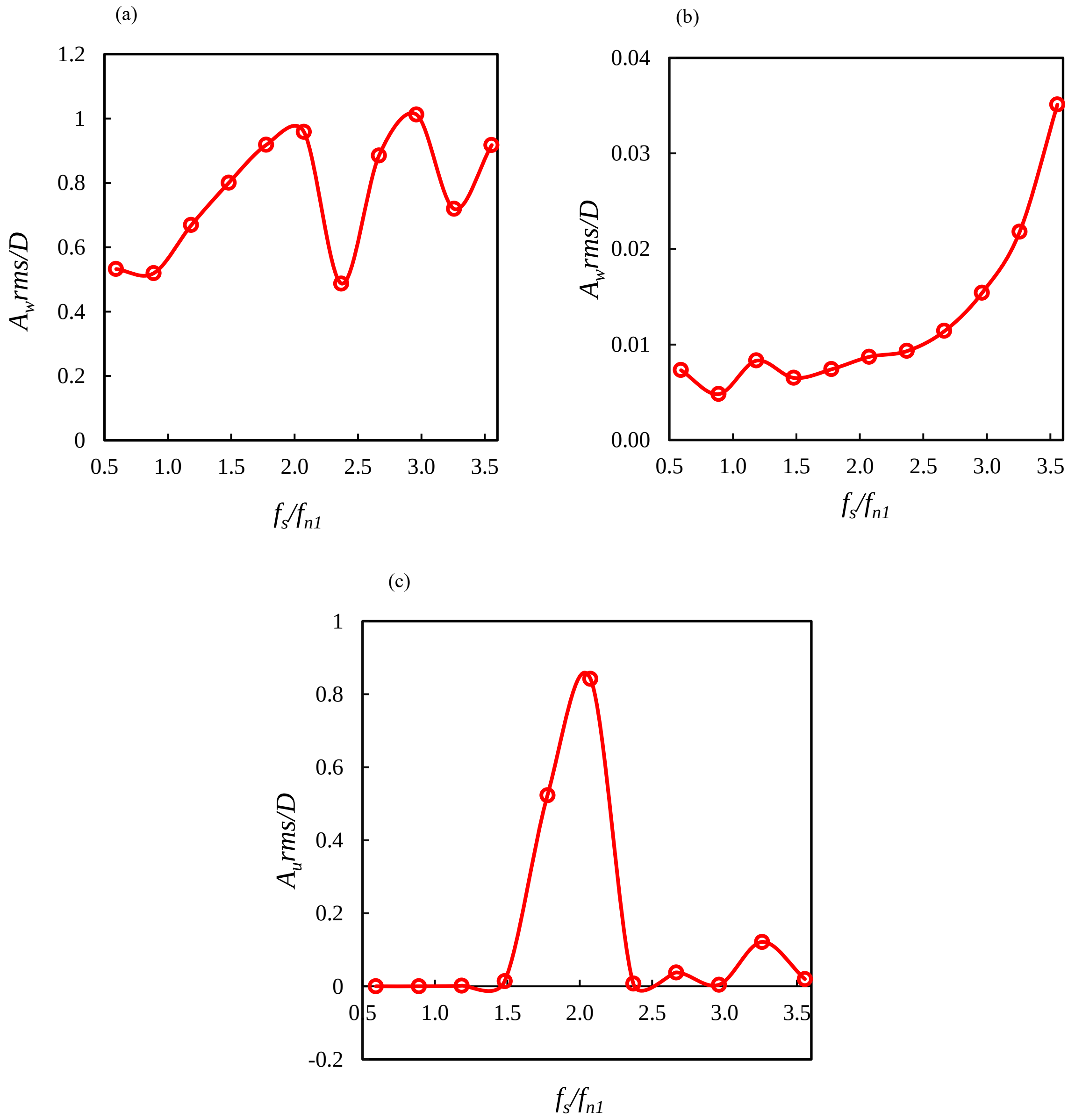

Figure 4.7: Maximum RMS out-of-plane (a), axial (b) and in-plane (c) amplitude response versus f_s/f_{n1}.

Figure 4.8(a-c) depicts 3-D contour plots illustrating three-dimensional oscillations after removing the mean components with varying U_r and fixed L_U. A predominantly first mode dominant response is evident in the U_r range of 4.08 to 14.3 in both out-of-plane and in-plane oscillations. However, at U_r =16.33 a shift to a second mode dominated response occurs in both directions. This transition in dominant mode could explain the low amplitude oscillations observed in Figure 4.7(a) and (b) when $f_s/f_{n1} = 2.37$. Notably, the prescence of second mode is prominent in both out-of-plane and in-plane directions when U_r is equal to or above 16.33. Conversely, axial oscillations, however, predominantly exhibit a second mode response across all U_r cases considered. Observations of similar oscillation amplitude trends previously discussed, indicating parametric resonance can also be noticed using the colour bars associated with each contour. Furthermore, the presence of large in-plane oscillations when $U_r \geq 12.25$ and the increasing trends of axial amplitudes with U_r are evident in Figure 4.8(c-h) and (i-l).

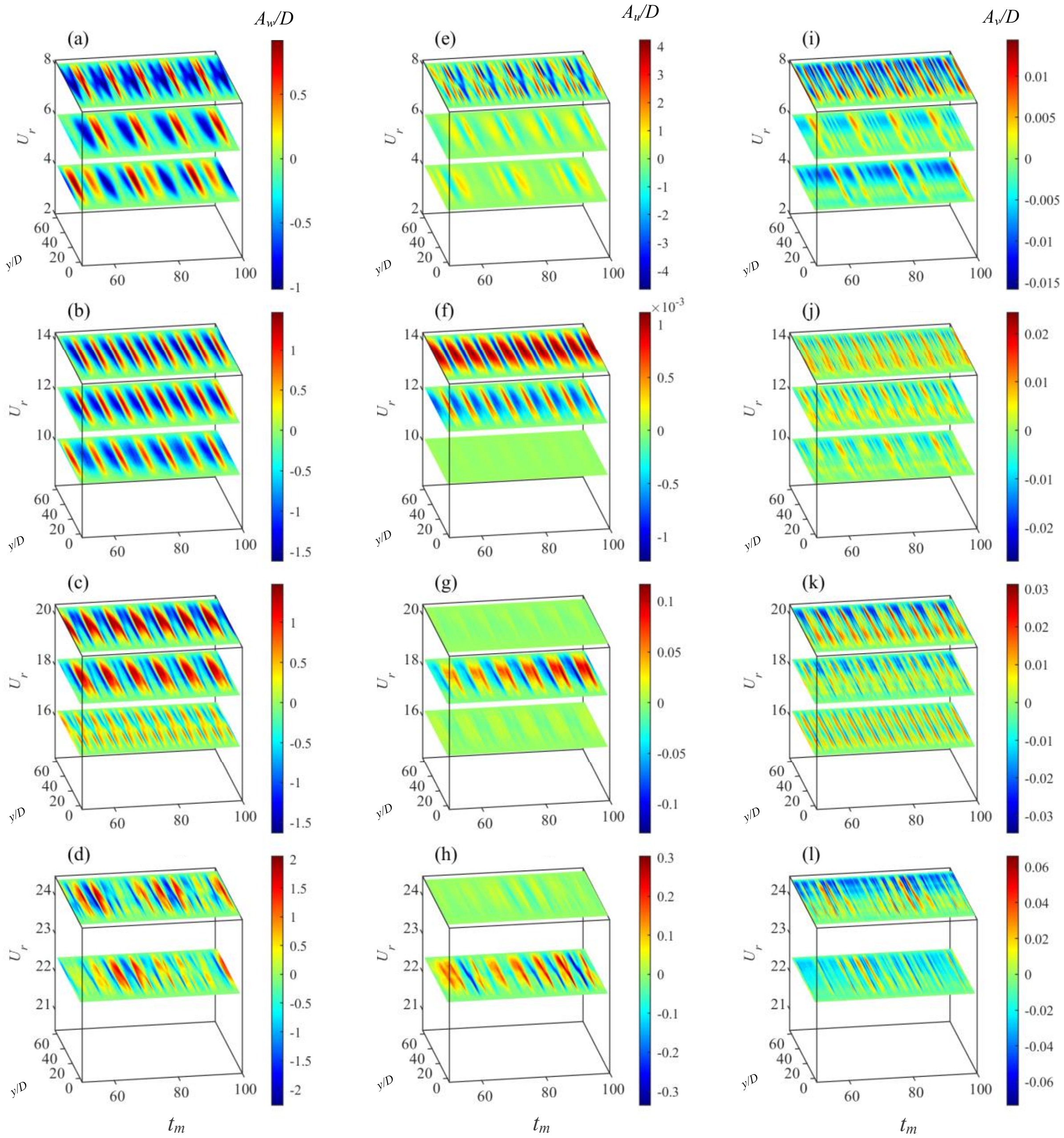

Figure 4.8: Space-time varying 3-D contour plots excluding mean components (a) out-of-plane, (b) in-plane, (c) axial, for a fixed L_U and varying U_r.

4.2.2.2 Oscillation frequencies and multi-harmonic response

Figure 4.9(a-l) presents FFT plots in all three-directions of oscillations at varying U_r. During low internal flow velocities ($U_r = 4.08$ to 12.25), the frequency responses exhibit multi-harmonic patterns with low amplitudes in both out-of-plane and axial directions, with the axial response containing a larger frequency spectrum. Notably, when f_s/f_n ratios become or are around 0.5, the dominant oscillation frequencies shift towards f_n, as mentioned in Section 4.2.1.2. At $U_r = 14$ and 16.33, higher harmonic responses are evident across all three directions of oscillation, albeit with differences in frequency content distribution. Out-of-plane and in-plane response generate lesser frequency contents and axial frequencies exhibit higher frequency peaks compared to previous U_r cases. Consistent with observations made in Section 4.2.1.2, when f_s/f_n ratio approaches 1, out-of-plane and in-plane responses produce frequency contents with single-peaks. This phenomenon has been previously documented by Bowen and Srinil (2020), who observed a unimodal response during scenarios involving large amplitudes of oscillation. Furthermore, sub-harmonic oscillation frequencies emerge for $U_r \geq 18.37$. As discussed in Section 4.2.1.2, sub-harmonic influences become more pronounced at higher internal flow velocities, such as $U_r = 22.46$ and 24.5, resulting in chaotic responses characterised by low-amplitude high-frequency modulations. In addition, sub-harmonics could also be a consequence of parametric resonance observed in Figure 4.7(a-c). Nevertheless, this emphasises a trend where an increase in U_r leads to a rise in the number of low-amplitude frequency components, especially notable at higher flow velocities. It is also worth mentioning that the dominant oscillation frequencies, except for f_s/f_n ratios close to 0.5, increase with increase in U_r. These frequencies are observed to be equal to f_S, further confirming the relation $f_S = V_t/L_U$.

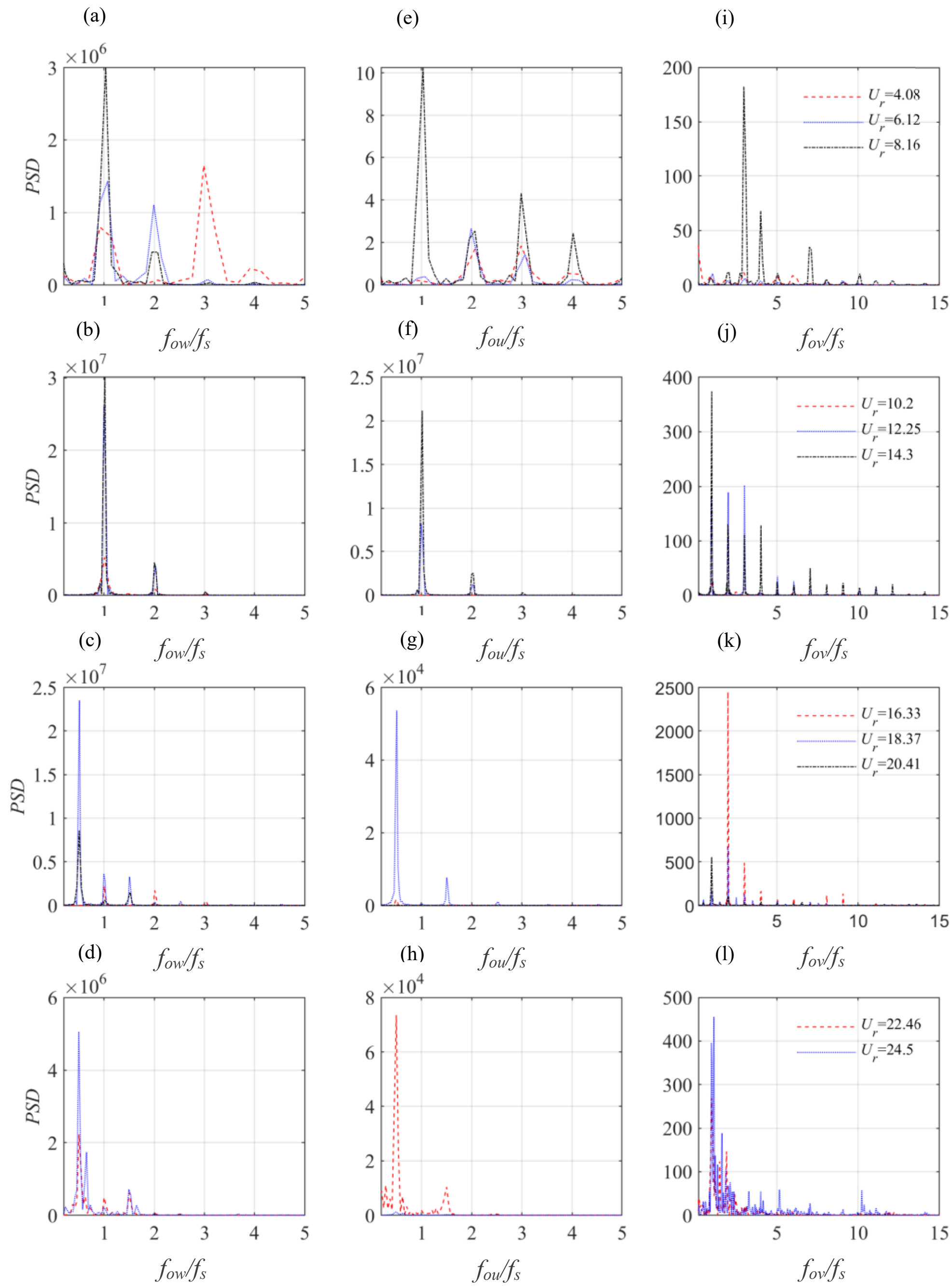

Figure 4.9: FFT frequency domain plots in the case of fixed L_U and varying U_r. (a-d) out-of-plane, (e-h) in-plane and (i-l) axial oscillations.

4.2.3 Effect of varying mass quotient, M, on the vibration dynamics of a horizontal fluid-conveying cylinder.

Furthermore, the effect of varying mass quotient, M, defined as the ratio of internal fluid mass to the mass of empty pipe, is investigated at four different internal flow velocities. Table 4.3 describes the parameters considered during the variation of M. Four cases of M are considered, such that the M ratio varies as a function of the internal fluid density. The mass of the empty pipe and the internal cross-sectional area are treated as fixed values as shown in Table 3. The slug flow parameters H_{LS}, H_{LF}, L_S and L_F remain consistent in the current investigation and are identical to the values used in the previous case study. Moreover, it should be highlighted that the M value employed in the previous two parameter studies is identical to the M value utilised in the validation process.

Table 4.3: Slug flow parameters utilised in the case of varying M.

U_r	Density (Kg/m^3)	L_U/D	M	f_s/f_n
4.08, 8.16, 12.25, 16.33	465	76.83	1	1.03
	930	76.83	2	2.06
	1390	76.83	3	3.09
	1855	76.83	4	4.12

4.2.3.1 Oscillation amplitude response

Figure 4.10 illustrates maximum RMS amplitudes across varying combinations of M and U_r. Two-dimensional out-of-plane and axial responses can be observed at low M ratio ($M = 1$) while at higher M ratios ($M \geq 3$) three-dimensional out-of-plane, in-line and axial oscillations become prevalent. At each flow velocities it can be noticed that the amplitude increases with increase in M in the out-of-plane and axial directions, with $M = 4$ case producing the highest response in both directions. This could be attributed to the greater momentum flux between gas and liquid induced by the increase in fluid density, resulting in increased internal fluid forces on the cylinder as highlighted in previous chapter. In the in-plane direction, however, oscillations are minimal at lower U_r and increases significantly at higher U_r for M ratios 2, 3 and 4. The RMS amplitudes in all three-directions of motion are observed to increase with increase in U_r at each M ratio cases, further highlighting the impact of U_r on the vibration response of a horizontal flexible cylinder. This increase in oscillation amplitudes can also be seen using the color bars in Figure 4.11, which illustrates space-time varying contour plots of three-dimensional oscillations in the case of varying M and U_r. From Figure 4.11 a first mode dominant response in the out-of-plane and in-plane directions is evident in the cases where high oscillation amplitudes are large. It can be seen in both Figure 4.10 and 4.11 that at M ratio of 1 and 2, the amplitude of oscillations in all three directions decreases when $U_r = 16.33$. This decrease in amplitudes can be attributed to the shift in dominant mode from mode 1 to mode 2, as discussed earlier in Section 4.2.2.1. This shift is seen due to the use of similar values for L_U, H_{LS} and H_{LF} values used in this section. However, the dominant mode shift to 1st mode response when M becomes 3 and 4, further highlighting that high oscillation amplitudes result in 1st mode dominant response.

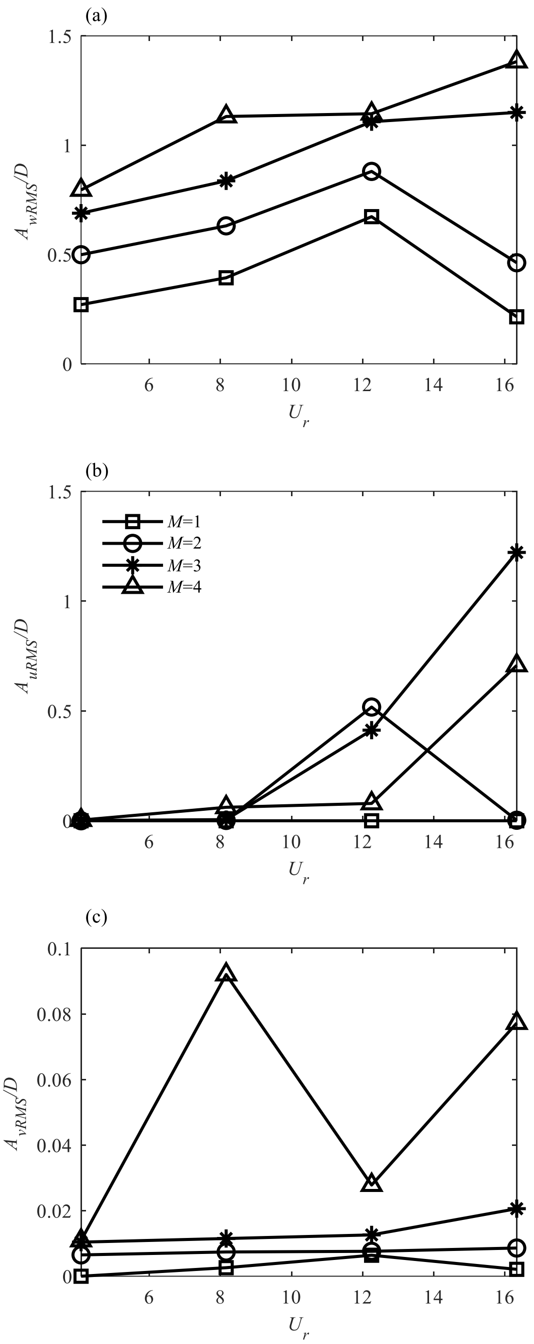

Figure 4.10: Comparison of RMS amplitudes at varying U_r and M ratios. (a) Out-of-plane (b) In-plane (c) Axial oscillation amplitudes.

The effect of high M ratios could be further outlined by comparing Figure 4.10(a-c) with Figure 4.2(a-c). It should be mentioned that the ratio $M = 2$ case is similar to the M ratios used in the f_s/f_n parameter study. Considerable increase in RMS amplitudes could be observed in all three-directions and at all U_r when $M = 3$ and 4, compared to RMS amplitudes in Figure 4.2(a-c). It is also worth mentioning that the U_r range considered in this study is based on reallife slug translational velocity scenarios calculated using the *iSLUG* model (Zanganeh et al., 2021). In summary, oscillation amplitudes in all three-directions are observed to increase with increase in M and U_r. Large amplitude responses in the out-of-plane, in-plane and axial oscillations are observed at high internal flow velocities ($U_r \geq 14.3$) and during high M ratios ($M \geq 3$). In cases where high oscillation amplitudes occur, a 1st mode dominant response is observed in the out-of-plane and in-plane direction. Such high amplitude vibrations in all three directions of motions, specifically axial oscillations, could lead to fatigue damages over time and must be considered during the initial design stage of a gas-liquid slug flow conveying horizontal cylinder.

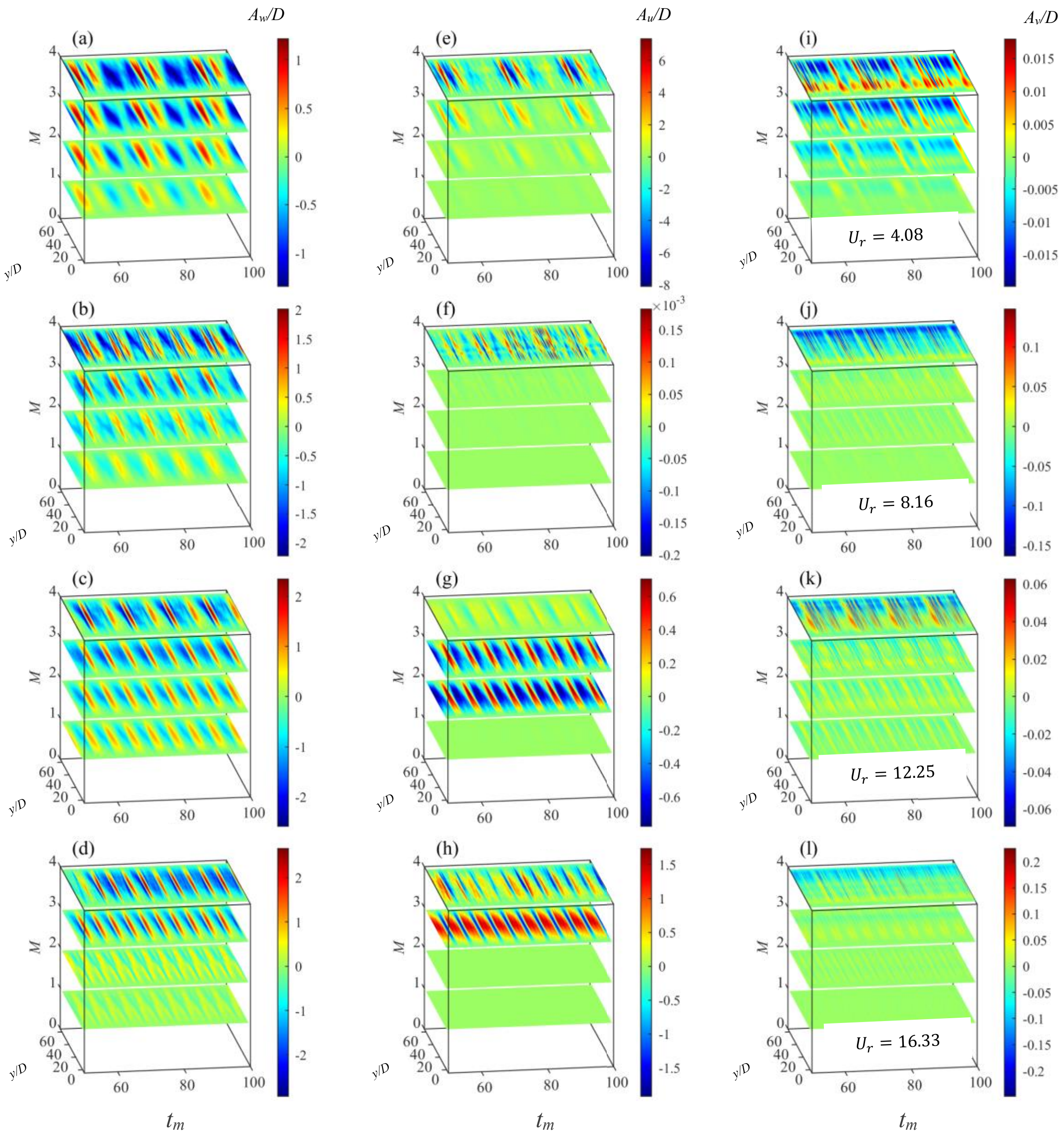

Figure 4.11: Space-time varying contour plots including mean and oscillating components (a-d) out-of-plane, (e-h) in-plane, (i-l) axial, for different M ratios.

4.2.3.2 Slug flow-induced frequencies

In the case of varying $M = 1, 2, 3,$ and 4, Figure 4.12(a-h) displays FFT plots of out-of-plane and axial oscillation time-histories obtained for four different translational velocities. When $U_r = 4.08$ (Figure 4.12(a) and (e)), it becomes apparent that as the M increases, the cylinder tends to respond with higher harmonics in both out-of-plane and axial directions, with highest frequency contents noticed when $M = 4$. Additionally, the presence of second mode dominant response becomes prominent in the axial direction when M reaches 3 and 4. It is also noteworthy that when $M = 4$, the dominant oscillation frequency shifts from f_s, observed in the previous cases, to f_n. As seen previously, this shift in dominant oscillation frequency can be attributed to the f_s/f_n ratio in this case, which is observed to be close to 0.5. Similar trends of increasing harmonic peaks with an increase in M are observed at $U_r = 8.16$,12.25, and 16.33 (Figure 4.12(b-h)) where the dominant oscillation frequencies align with the slug excitation frequency corresponding to each case.

However, when $U_r = 12.25$ and 16.33, particularly at large M ratios ($M = 3$ and 4), several subharmonic peaks with low amplitudes are noticeable. Frequency contents in the axial direction are noticed to be the highest with high frequency low amplitude-modulations and several sub-harmonic frequencies present when $U_r = 16.33$ and $M = 4$ as shown in Figure 4.12(h). In-plane oscillations follow similar trends of higher harmonic peaks when $M = 4$ and also generates several low amplitude sub-harmonic frequencies at $U_r = 16.33$ as shown in Figure 4.13(a-b). Consistent with the previous parameter study, axial oscillations in these cases generate more harmonic peaks compared to out-of-plane and in-plane response. In summary, as oscillation amplitudes increase with rising U_r and M, multi-harmonic response with significant number of peaks occur, indicating the participation of higher vibration modes in these extreme cases. Such phenomena may lead to significant stresses and fatigue damages over time in all three-directions of oscillation.

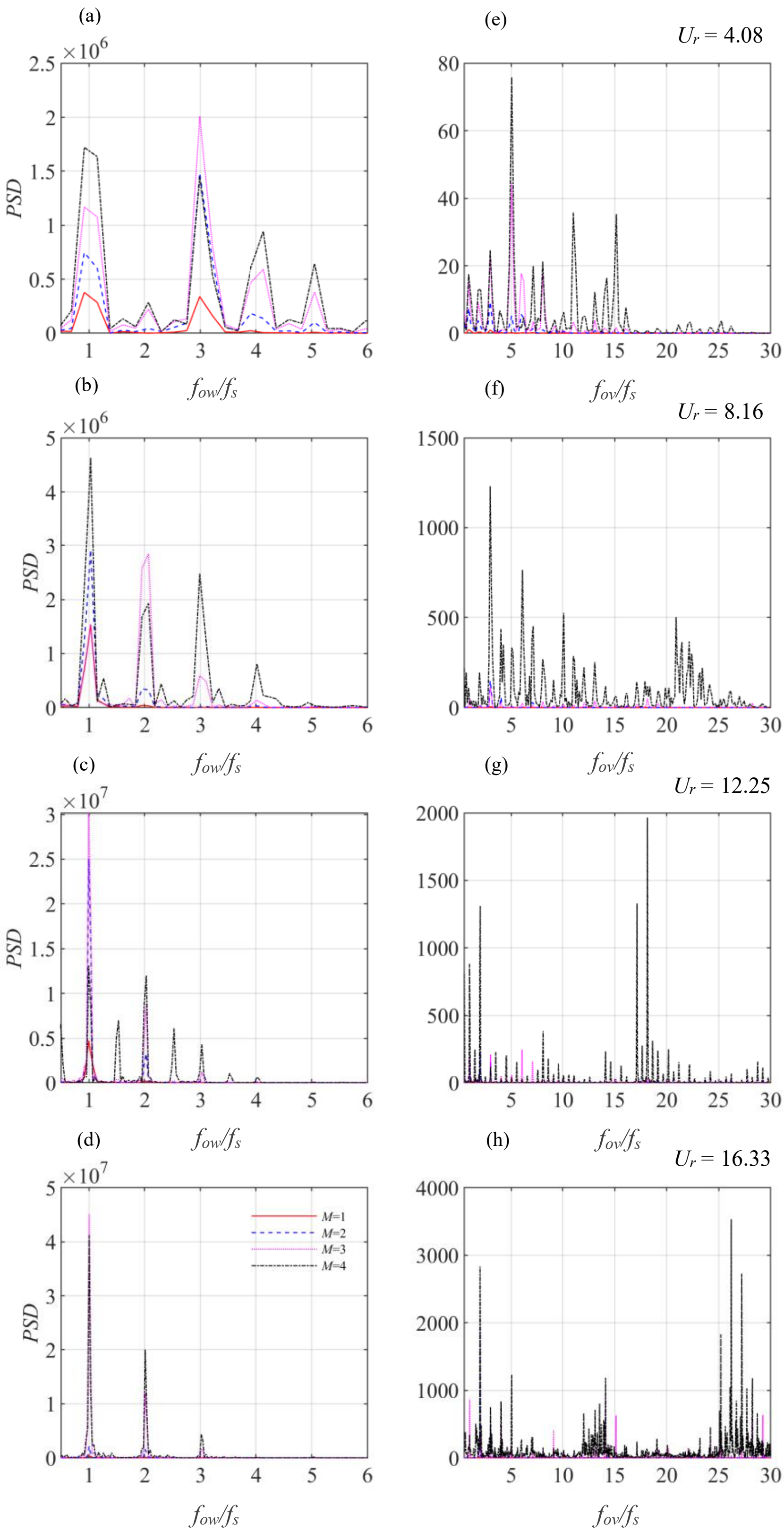

Figure 4.12: Out-of-plane (a-d) and axial (e-h) frequency response at varying M ratios and U_r.

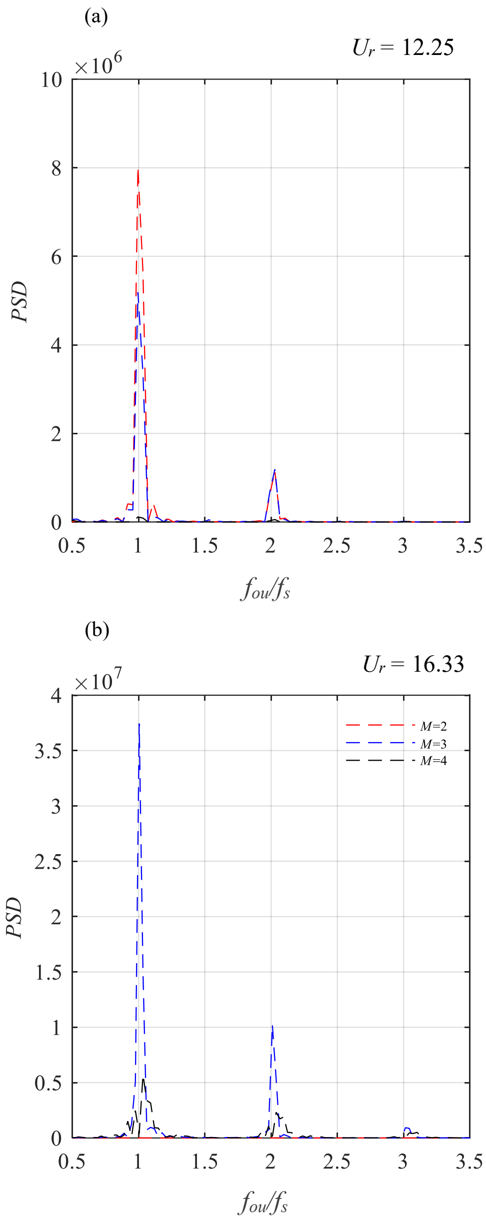

Figure 4.13: In-plane frequency response at varying M ratios and U_r.

4.3 Conclusions

In this chapter, slug flow-induced vibration responses of a horizontal flexible cylinder is investigated taking into account the geometric nonlinearities. The horizontal cylinder is assumed to be surrounded by air, and a fixed-pinned boundary condition is applied. The model was solved through a finite-difference scheme, and the corresponding numerical results were analysed in both time and frequency domains, as well as through modal analysis. A steady-state internal slug flow was modelled as a rectangular pulse train model, where slug properties are assumed to be fully developed and undisturbed by pipe oscillations. Model comparisons are made with experimental results of a horizontal cylinder subjected to two-phase slug flows. Time-history plots of out-of-plane oscillations demonstrate the model's capability to accurately capture amplitude and frequencies compared to experimental results. A parametric study is further conducted to analyse the effect of key slug flow parameters on the nonlinear dynamic response of the horizontal cylinder. Three-dimensional large amplitude responses were observed when the incoming slugging frequency is equal to the structure's natural frequency ($f_s/f_n = 1$) and during high U_r when $f_s/f_n = 0.66$ and 0.5. Oscillation amplitudes are found to increase with an increase in U_r in the out-of-plane and in-plane directions for all f_s/f_n ratios while a zig-zag alternating trend is noticed in the axial direction. Parametric resonance was observed in the out-plane and in-plane directions, with the largest amplitude response observed when the slugging frequency was equal to twice the natural frequency of the cylinder containing internal mass. Axial oscillations, on the other hand, exhibited a linear increase in oscillation amplitudes with rapid escalation in amplitudes at high internal flow velocities. Additionally, the largest amplitude response in all three-directions among all the cases considered were noticed when the mass quotient parameter was the highest value ($M = 4$). An increase in M allows for greater mass-momentum fluctions inside the cylinder, resulting in increased oscillation amplitudes. Frequency response FFT plots exhibit multi-harmonic responses, with sub-harmonic frequencies observed in cases where the cylinder experiences large oscillation amplitudes. Axial oscillation frequency response result in large number of frequency contents compared to out-of-plane and in-plane response. Frequency contents in all three-directions increase with increase in U_r and M ratios, with high frequency modulations were observed when $M = 4$.

Chapter 5

Three-dimensional Vibration Characteristics of Flexible Cylinders Subjected to Combined VIV and SIV

In deepwater oil and gas production, hydrocarbon flows inside the subsea riser may occur in multiple phases, among which slug flows are known as an undesired flow pattern due to their complex nature involving fluctuating mass, velocities and pressure changes. Moreover, the subsea riser is also susceptible to forces due to external currents. This could result in challenging operation conditions due to the simultaneous effects of combined VIV and SIV. In this chapter, the dynamic responses of a submerged flexible cylinder subject to combined VIV and SIV are investigated. The nonlinear semi-empirical model introduced in Chapter 3, which incorporates coupled cross-flow, in-line and axial structural oscillations, along with equations involving centrifugal and Coriolis forces is herein considered for the prediction and analysis of combined VIV and SIV effects. Forces due to VIV are governed by two coupled wake oscillators describing the variations of lift and drag coefficients. This highly nonlinear model is solved using a finite difference approach in space and time. A frequency domain and modal analysis is performed to analyse the three-dimensional oscillation responses. Model validations are carried out through maximum amplitude and dominant modes comparisons with published experimental results. A detailed parametric study is performed to investigate the effects various combined VIV-SIV scenarios on the dynamic response of a flexible cylinder. Numerical results highlight the significant influence of SIV during the combined VIV-SIV scenario through comparisons of RMS amplitudes, mean displacements, harmonic and sub-harmonic frequencies and modal contributions.

5.1 Model Validation

Prior to investigating the combined effects of VIV and SIV, the model presented in Chapter 3 is validated in the case of VIV through numerical and experimental comparisons utilising laboratory tests studied by Song et al., (2011). A long flexible cylinder with properties E = 201 GPa, L = 28.04 m, OD = 0.016 m, ID = 0.015 m, ρ= 7930 kg/m^3 is considered, with pre-tension T = 700 N and subjected to uniform external flow velocities V_e, ranging from 0.2 to 0.5 m/s. The submerged cylinder in the experiment test is horizontal and the simulation assumes the same orientation. Internal gas-liquid two-phase flow is neglected in this case. The highly nonlinear equations are numerically solved in MATLAB with a dimensionless time step of t_m = 0.001, and the cylinder is discretised spatially into 100 equal spacings. This discretisation in time and space allows for convergence of steady-state results. To validate the model, maximum cross-flow and in-line oscillation amplitudes are compared with the experimental results. Figure 5.1(a, b, c) displays maximum cross-flow and in-line amplitudes for external flow velocities ranging from 0.2 m/s - 0.5 m/s for pretension 600 N, 700 N and 800 N. Consistent with experiment results, numerical predictions follow similar trends of zig-zag progressions of cross-flow and in-line amplitudes with increase in current velocity for all three pretension values. Additionally, model predictions capture similar trends of larger cross-flow oscillation amplitudes compared to in-line amplitudes with simulation amplitudes being reasonably closer to the experimental results. Such variations are also highlighted by Zanganeh and Srinil (2016). Furthermore Figure 5.1(d, e, f) illustrates the comparison between numerical and experimental results of obtained dominant modes for external flow velocity ranging from 0.2 – 0.6 m/s and for pretension 600 N, 700 N and 800 N. It can be observed from Figure 5.2(d, e, f) that the numerical simulation follows similar trends of modal participation, with increasing dominant mode numbers as external flow velocity increases following the Strouhal rule for all three pretension values. In addition, it can be observed from Figure 5(e) that at current velocities 0.2 m/s, 0.25 m/s, 0.4 m/s and 0.45 m/s, numerical predictions precisely match the experimental results, displaying exact dominant mode numbers while other velocities exhibit reasonable similarities in dominant mode numbers. Overall, it can be concluded from the figures that the predicted VIV results provide quantitative and qualitative similarities with experimental results.

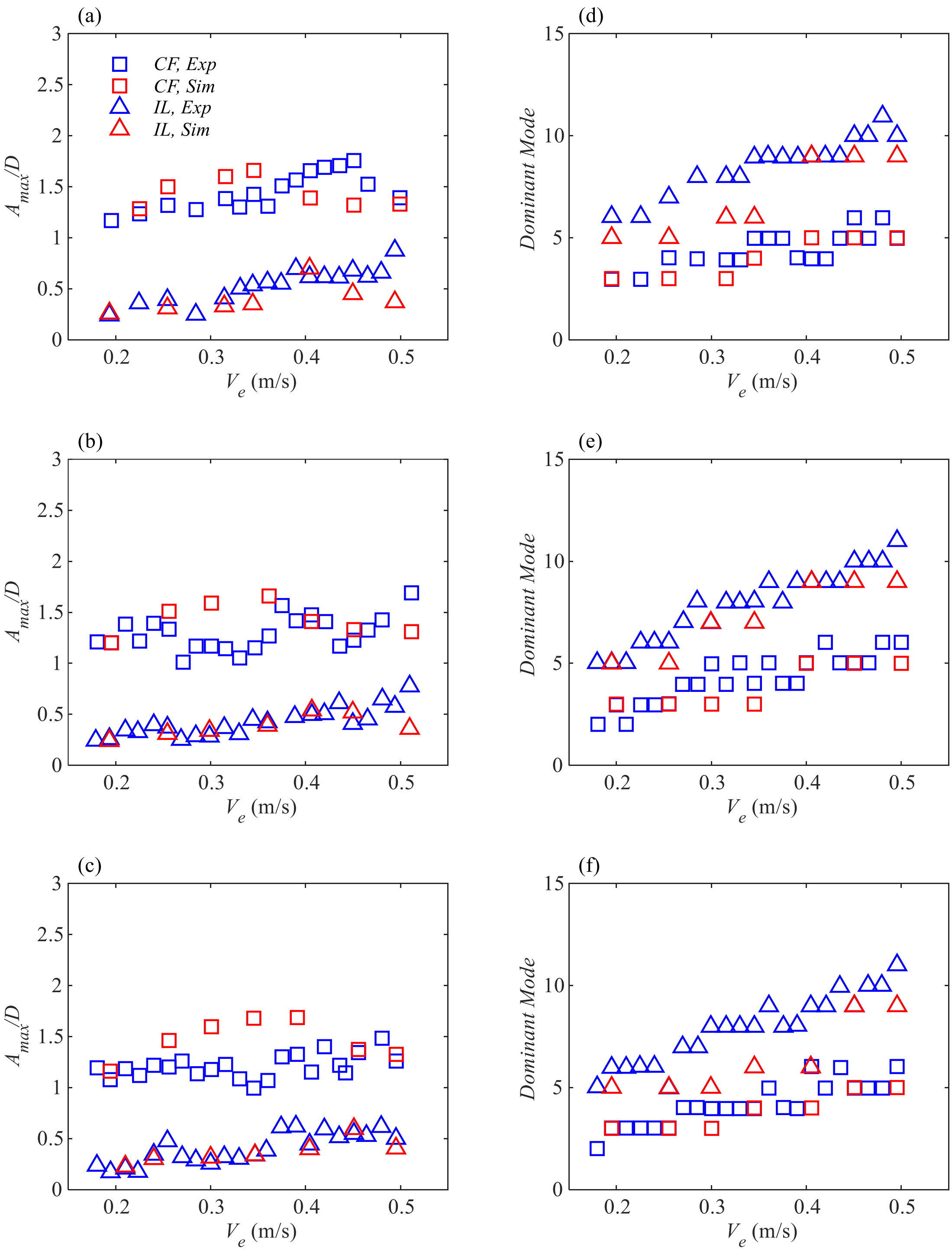

Figure 5.1: Comparison between numerical and experimental results of maximum cross-flow and inline amplitudes (a, b, c) and dominant modes at varying V_e (d, e, f) for T_0 = 600 N (a, d), 700 N (b, e), 800 N (c, f).

5.2 Numerical Results and Discussion

5.2.1 Dynamic responses under various VIV-only and VIV-SIV scenarios

In this section, the long flexible cylinder used for validation is employed to conduct a parametric study to investigate the combined effects of external-internal excitations on the dynamic response of the flexible cylinder system shown in Figure 3.1. The flexible cylinder has an aspect ratio (L/D) of 1750, with damping coefficient ζ assumed to be 0.01. The external flow is assumed to spatially uniform, and five dimensionless external current velocities, V_r = 11.68, 17.52, 23.36, 29.2 and 35.04, with pre-tension 700 N are considered for this study, where $V_r = V_e/(f_n * D)$ is the reduced velocity. Two cases of combined VIV-SIV effects are examined: case 1, where the slugging frequency (f_s) equals the vortex-shedding frequency (f_{vs}), and case 2, where the slugging frequency (f_s) equals the VIV cross-flow dominant mode frequency (f_{dm}). These cases are considered for all five external current velocities to capture maximum features of combined VIV-SIV phenomena. In this study, the associated internal slug flow properties are calculated using the *iSLUG* tool (Zanganeh et al., 2021). Additionally, numerical simulations of VIV-only are carried out to compare and identify key SIV effects on the dynamic response of the cylinder during combined VIV-SIV excitations. Table 5.1 and Table 5.2 describes key external and internal flow properties considered in each of the two VIV-SIV cases mentioned above. The frequency of vortex shedding is calculated by assuming a Strouhal number of 0.17 (Zanganeh and Srinil, 2016). In this study L_U is held constant for all the cases considered, such that L_S and L_F are considered to be half of L_U. Similarly, H_{LS} and H_{LF} values are set to 1 and 0 respectively, for all the cases considered to maximise SIV features. The slug frequencies associated with each case can be estimated using the relation $f_s = V_t/L_U$.

Table 5.1: External and internal flow parameters considered in the case of VIV-SIV: $f_s = f_{vs}$.

V_r	U_r	L_U/D	H_{LS}	H_{LF}	f_{vs}
11.68	15.8	50	1	0	2.12
17.52	23.7	50	1	0	3.18
23.36	31.6	50	1	0	4.25
29.2	39.5	50	1	0	5.31
35.04	47.4	50	1	0	6.37

Table 5.2: External and internal flow parameters considered in the case of VIV-SIV: $f_s = f_{dm}$.

V_r	U_r	L_U/D	H_{LS}	H_{LF}	f_{dm}
11.68	24.17	50	1	0	3.26
17.52	24.17	50	1	0	3.26
23.36	24.17	50	1	0	3.26
29.2	41.27	50	1	0	5.55
35.04	41.27	50	1	0	5.55

Figure 5.2 depicts the maximum amplitude response with mean deflections (Figure 5.2(a-c)) and maximum RMS responses by removing the mean components (Figure 5.2(d-f)) for varying external flow velocities (V_r). As mentioned in Chapters 3 and 4, when internal flow enters cylinder, a large mean deflection in the cross-flow (perpendicular to external flow direction) direction due to gravity effects is noticed as shown in Figure 5.2(a). Compared to the mean deflection caused by forces due to VIV-only, combined VIV-SIV cases show amplified large

mean displacements in the cross-flow direction due the effect of internal mass and gravity effects. However, the mean deflections are observed to decrease as V_r increases. This may be due to the increase in mean deflection amplitudes in the in-line direction with increase in V_r as seen in Figure 5.2(b), which can lead to reduced mean deflection amplitudes in the cross-flow direction. Mean deflections in the in-line and axial directions are observed to increase linearly with increase in V_r for all the three VIV-only and VIV-SIV cases. At lower V_r ($V_r = 11.68$ and 17.52), VIV-only cases are noticed to generate higher mean displacements in the in-line direction compared VIV-SIV cases. However, at higher V_r ($V_r = 23.36 - 35.04$), VIV-SIV cases exhibit slightly higher mean displacements in the in-line direction. This increase in mean displacements at higher V_r can be attributed to the mean drag magnifications caused by high oscillation amplitudes in the cross-flow direction, leading to an increase in in-line mean displacements due to nonlinear couplings. In the axial direction, however, VIV-SIV cases illustrate higher mean displacements compared to VIV-only cases for all V_r considered as shown in Figure 5.2(c).

Maximum RMS responses in the cross-flow and in-line directions shown in Figure 5.2(d, e) follows a zigzag feature with V_r as observed during validation. VIV-only and VIV-SIV cases show comparable maximum RMS amplitudes, though some variances are noticed at several V_r. At lower V_r (V_r = 11.68 – 23.36), VIV-only case appears to dominate the response in the cross-flow direction with slightly higher amplitudes. However, at higher V_r (V_r = 29.2 and 35.04), both VIV-SIV cases generate similar amplitudes, which are higher than those of VIV- only case. Contrastingly, in the in-line direction, VIV-SIV cases dominate the response with significantly higher amplitudes in four of the five V_r values considered as shown in Figure 5.2(e). This can be attributed to the large amplitude mean deflection observed in the cross-flow direction upon the introduction of internal flow, leading to increased amplitudes in the in-line direction due to nonlinear coupling terms in the developed model (Zanganeh and Srinil, 2016). Axial RMS responses demonstrate a linearly increasing trend with V_r in the VIV-only case. In contrast, both VIV-SIV cases exhibit a zig-zag trend with comparable RMS amplitudes, albeit significantly larger RMS amplitudes are noticed when compared to VIV-only cases as shown in Figure 5.2(f). Additionally, it should be mentioned that the cross-flow responses in all the cases considered are higher in comparison to in-line and axial oscillations. Overall, combined VIV-SIV phenomena seem to dominate the vibration response in the in-line and axial directions, exhibiting significantly higher RMS amplitudes compared to VIV-only cases. In the cross-flow direction, however, both VIV-SIV and VIV-only cases show comparable RMS amplitudes, with slightly higher values observed at higher V_r.

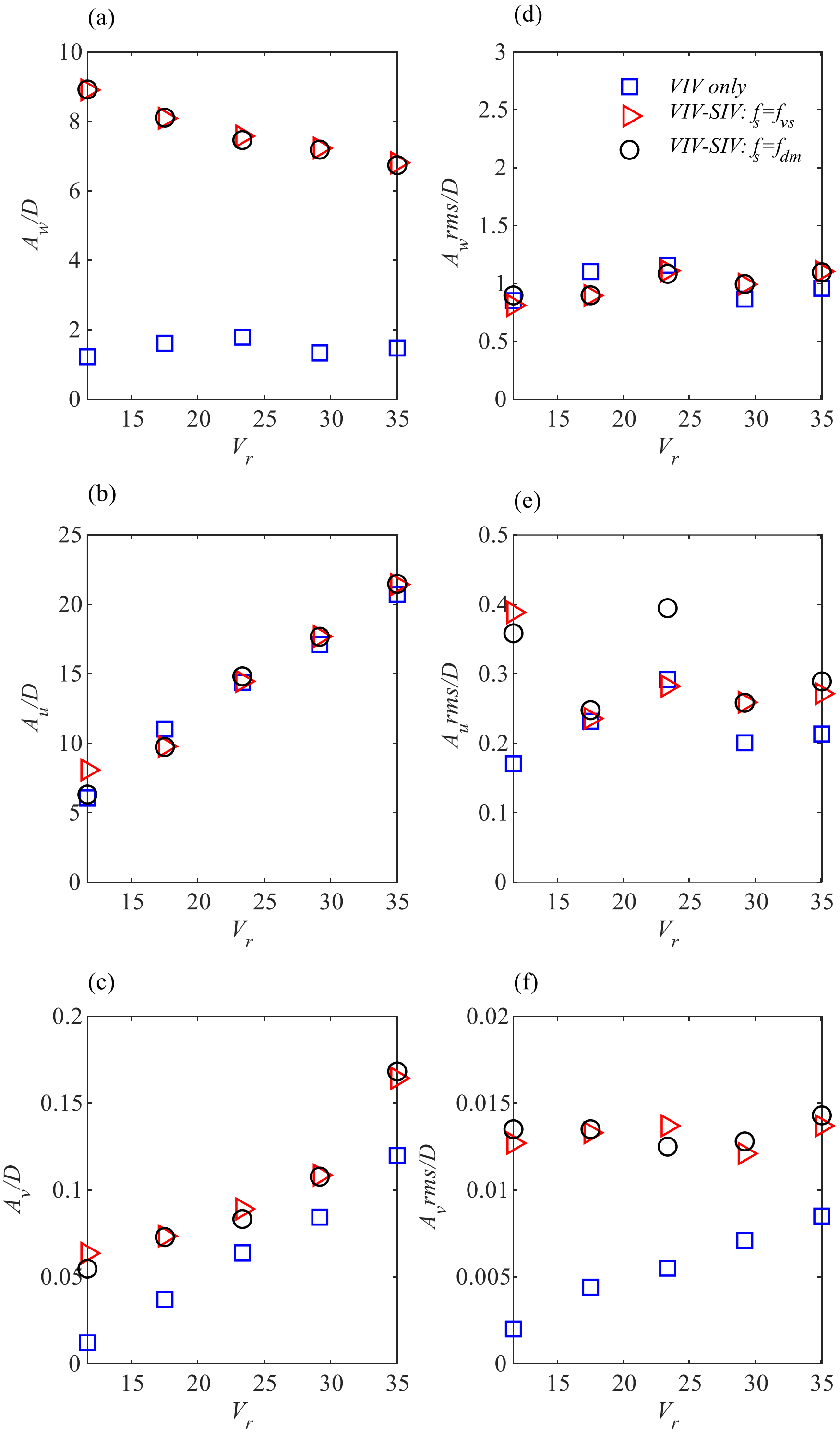

Figure 5.2: Comparison of maximum (a-c) and RMS (b-f) amplitudes of cross-flow (a, d), in-line (b, e) and axial (c, f) in the case of VIV-only (blue squares), VIV-SIV: $f_s = f_{vs}$ (red triangle) and VIV-SIV: $f_s = f_{dm}$ (black circles).

Expanding on the discussion mentioned earlier, Figure 5.3(a-e) illustrates the time-history plots of in-line mid-point amplitudes at varying V_r for both VIV-only and VIV-SIV cases. Noticeable differences in amplitudes between VIV-only and VIV-SIV are observed when $V_r = 11.68$ and 17.52, but these disparities decrease as V_r increases to 23.36, with the amplitudes becoming more closely aligned. At V_r = 29.2 and 35.04, VIV-SIV cases exhibit higher mean displacement amplitudes compared to VIV-only case. It is also worth noting that at $V_r = 29.2$ and 35.04, VIV-SIV experiences steady harmonic oscillations, while at $V_r = 11.68$ and 17.52, the oscillations are slight unsteady and chaotic. Furthermore, it is evident that the mean displacement amplitudes in the in-line direction are considerably higher than those observed in the cross-flow direction. These amplified amplitudes due to SIV, particularly in the in-line and cross-flow directions, could result in increased bending stresses over time and should be taken into account during the design phase to prevent fatigue failures.

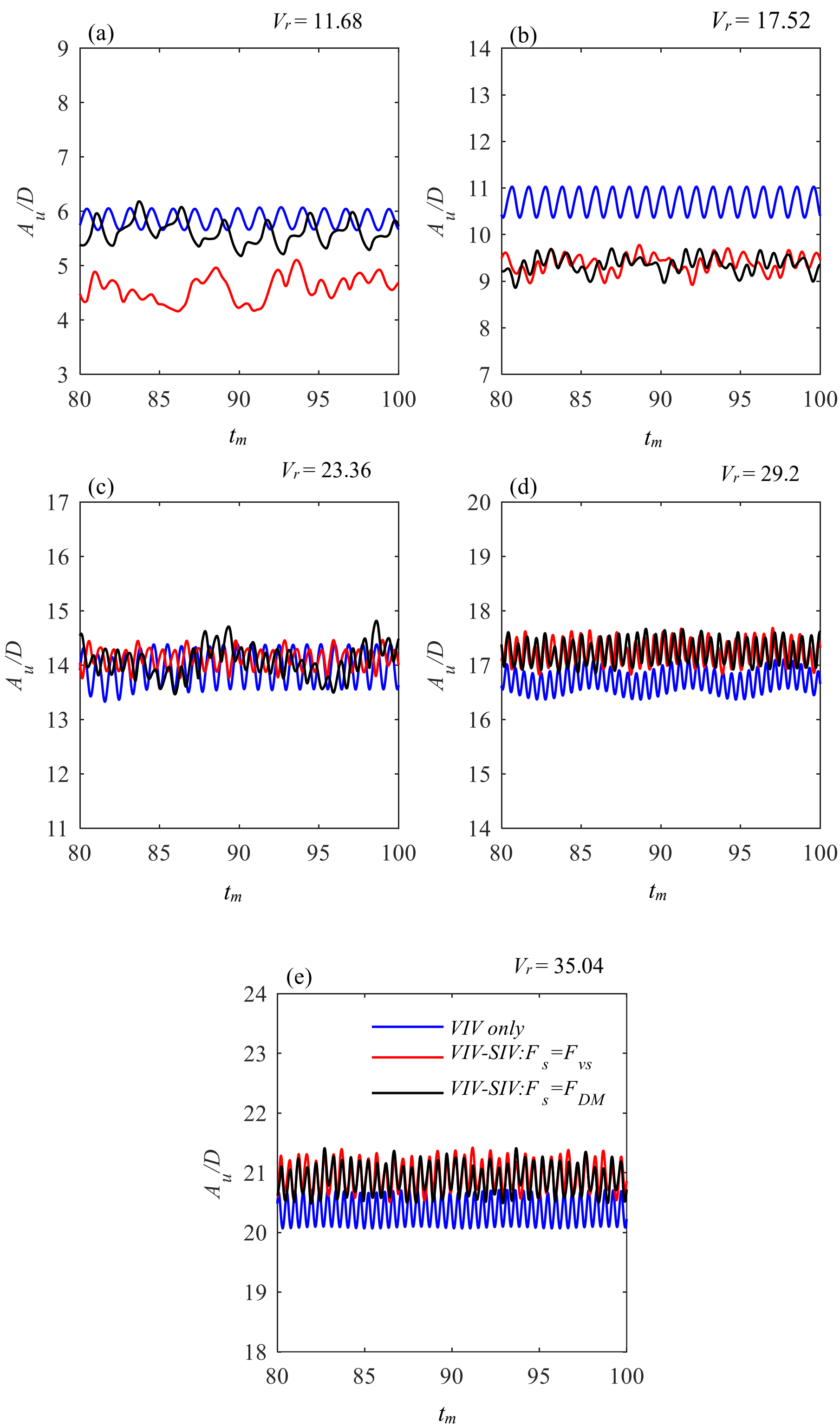

Figure 5.3: Time-history plots of observed mean displacements in the in-line direction at varying external flow velocities for VIV-only and VIV-SIV cases.

5.2.1.1 VIV-SIV induced modal contributions

Figure 5.4(a-l) presents 3-D contour plots of three-dimensional cross-flow (a-d), in-line (e-h) and axial (i-l) after removing the mean components at varying V_r for VIV-only and VIV-SIV cases in the space-time domain. The figure highlights the notable increase in oscillation amplitudes, particularly in the in-line and axial directions, in both VIV-SIV cases across all V_r considered. Furthermore, this figure also illustrates that the frequencies in the in-line and axial directions are almost as twice that of in the cross-flow direction for both VIV-only and VIV-SIV cases. These higher oscillation frequencies in the in-line and axial directions could lead to increased vibration modes in these directions. The spatio-temporal plots of structural vibrations at $V_r = 29.2$ and 35.04 evidently confirm this observation. Similar features were previously observed by Zanganeh and Srinil (2016) in the case of cylinder oscillations due to VIV-only. Moreover, a travelling wave response is captured in the in-line and axial directions across all V_r considered in both VIV-only and VIV-SIV scenarios. Additionally, it is observed that maximum oscillation amplitudes in the axial direction occurs near the two ends of the cylinder and midsection of the cylinder has minimum longitudinal displacements. These displacements are further enhanced during VIV-SIV cases as shown in Figure 5.5(i-l).

Further comparisons are made by conducting a modal analysis based on the approach by Lie and Kassen (2006) and used by Song et al., (2011) and Zanganeh and Srinil (2016) for the analysis of VIV in flexible cylinders. In the combined VIV-SIV cases, it can be observed that both VIV-SIV cases exhibit a higher dominant mode response (4th mode dominant) in the cross-flow direction compared to VIV-only response (3rd mode dominant) at lower external flow velocities ($V_r = 17.52$ and 23.36), as shown in Figure 5.4(a, b). However, at higher V_r ($V_r = 29.2$ and 35.04), it is observed that the dominant mode response in the VIV-only case increases to fifth mode dominant response, while the VIV-SIV cases does not exhibit a difference from the VIV-only case. In-line oscillations exhibit similar trends, with the dominant mode increasing to 7th mode in the VIV-SIV cases compared to 5th mode in the VIV-only case at lower flow velocities ($V_r = 17.52$ and 23.36). At higher flow velocities ($V_r = 29.2$ and 35.04), the dominant mode increases to 9th mode in the VIV-only case and remains the same in the VIV-SIV cases.

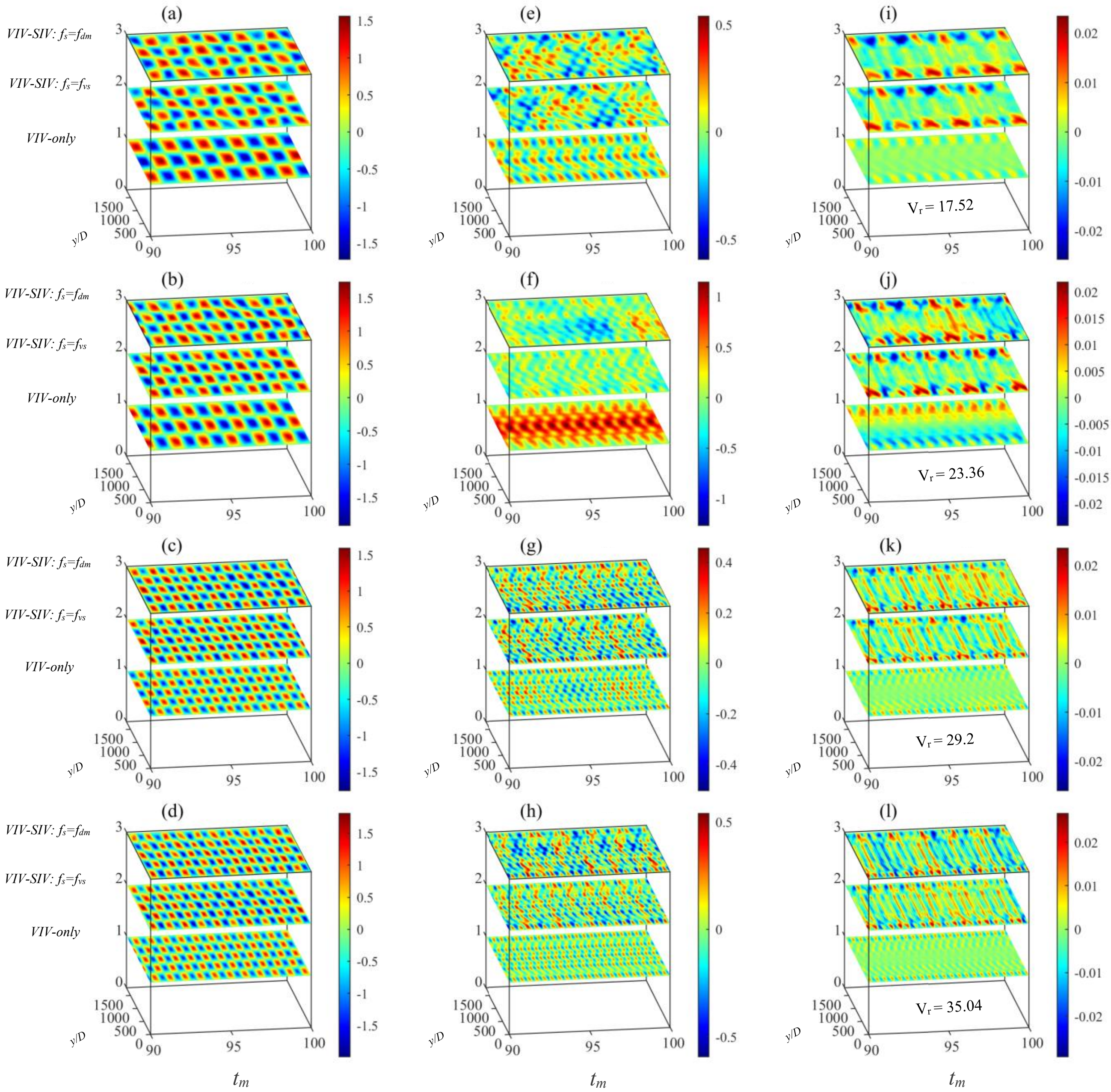

Figure 5.4: 3-D contour plots of three-dimensional cross-flow (a-d), in-line (e-h) and axial (i-l) oscillations with removed mean values at varying external flow velocities for VIV-only and VIV-SIV cases.

In the axial direction however, the dominant mode shifts to a lower 3rd mode dominant response in the VIV-SIV cases from 4th mode dominant in the VIV-only case at lower flow velocities ($V_r = 17.52$ and 23.36). This trend of decreasing dominant mode is also observed at higher flow velocities ($V_r = 29.2$ and 35.04), where the dominant mode shifts to a lower 4th mode response VIV-SIV cases from 8th mode response in the VIV-only case. It is also worth mentioning that a dominant mode switch with time from 5th mode to 3rd was observed in the cross-flow direction at $V_r = 23.36$ in the VIV-only case. This dominant mode switch with time has been previously observed by Violette et al., (2010). However, the VIV-SIV cases does not exhibit a switch in dominant modes with time for all the cases considered in this study. This can be due to the increase in overall mass of the cylinder, leading to excessive bending in the cross-flow direction and changes in natural frequencies, unlike the VIV-only case. Associated with the response in Figure 5.4, modal distributions are shown in the case of VIV- only, VIV-SIV: $f_s = f_{vs}$ and VIV-SIV: $f_s = f_{dm}$ for all three cross-flow (Figure 5.5(a-e)), in-line (Figure 5.5(f-j)) and axial (Figure 5.5(k-o)) directions at varying V_r. In each figure the horizontal axis is the mode number, and the vertical axis represent power of the vibration modes normalised by the power of the first dominant mode in all three directions. Consistent with observations from VIV experiments conducted by Vandiver et al., (2009) and Lie and Kassen (2006), Figure 5.5 show that cross-flow oscillations are single mode oscillations, whereas in the in-line and axial directions, the cylinder experiences multi-mode VIV. This holds true predominantly for both the VIV-SIV cases in the cross-flow direction, except at $V_r = 11.68$, where VIV-SIV cases exhibit a multi-mode response. The shift in dominant modes in the cross-flow direction, as discussed previously, can be seen noticed in Figure 5.5(a-e). For both VIV- only and VIV-SIV scenarios, modal contributions are noticed to increase with an increase in V_r in the in-line and axial directions. However, multi-mode behaviour in these directions appears to be enhanced during VIV-SIV scenarios. In VIV-only scenarios, cylinder responses in the in-line direction primarily excite symmetric (1, 3, 5....) or odd mode numbers, while axial motions excite even mode numbers. However, in VIV-SIV cases, both even and odd mode numbers are excited in the in-line and axial directions, with a higher number of secondary modes excited compared to the VIV-only scenarios in several cases. The shift in dominant modes and increased secondary mode numbers in the combined VIV-SIV cases can be attributed to the change in eigen frequencies, predominantly influenced by the increase in overall mass of the system.

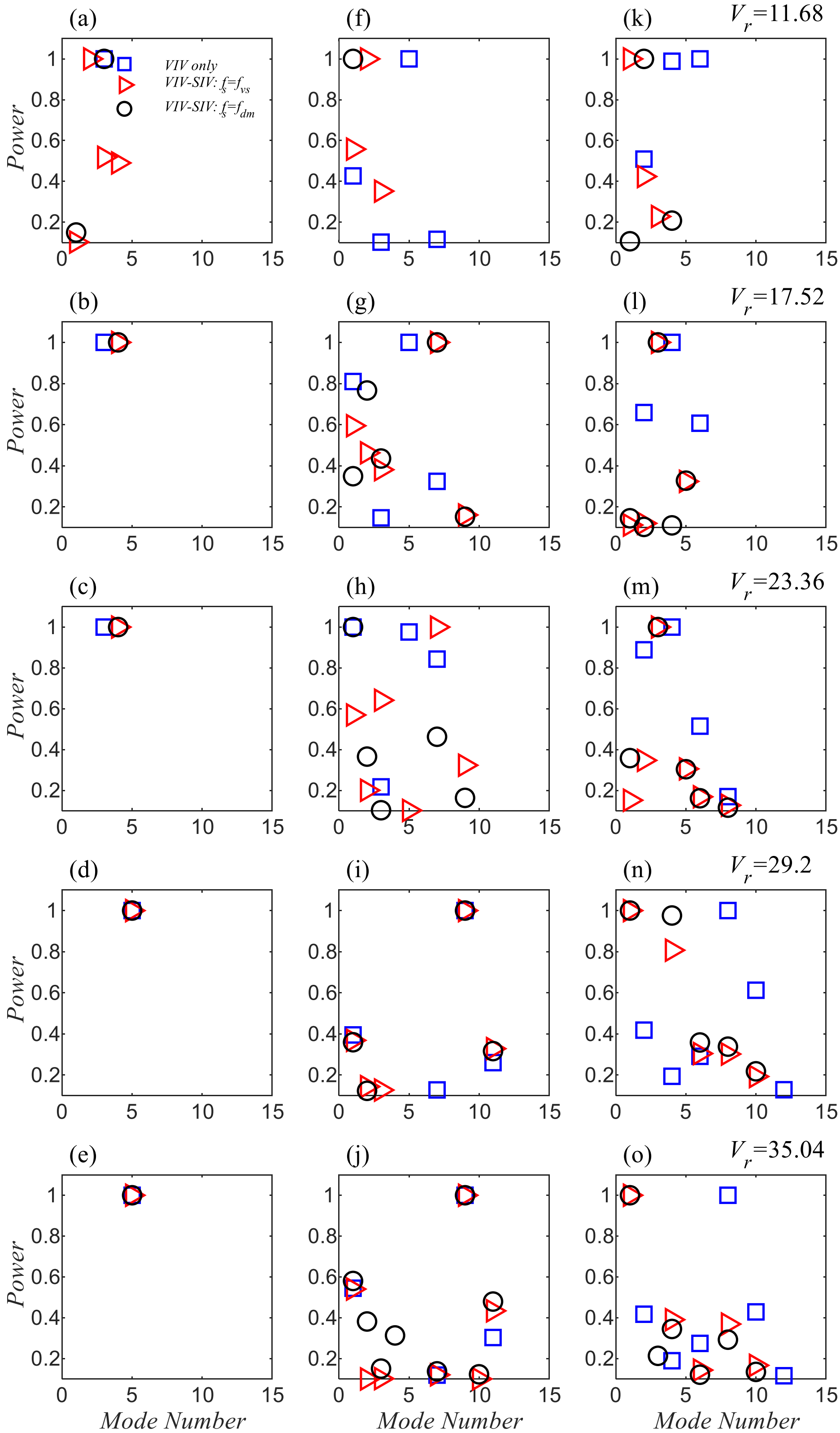

Figure 5.5: Modal distributions in cross-flow (a-e), in-line (f-j) and axial (k-o) directions at varying V_r for VIV-only (blue squares), VIV-SIV: $f_s = f_{vs}$ (red triangle) and VIV-SIV: $f_s = f_{dm}$ (black circles).

5.2.1.2 Frequency domain analysis and sub-harmonics

Figure 5.6(a-c) shows the comparisons of dominant oscillation frequencies (f_o) for the three scenarios at various V_r. Generally, it is observed that f_o for the considered cases increase linearly with V_r and follows the Stouhal rule for all three cross-flow, in-line and axial oscillations. However, comparison of f_o varies at different V_r. It is observed that at lower V_r (V_r = 11.68 – 23.36), VIV-SIV cases evidently exhibit higher f_o in the cross-flow and in-line directions than the VIV-only case, whereas at higher V_r (V_r = 29.2 and 35.04), VIV-only case shows higher f_o as seen in Figure 5.6(a, b). In the axial direction (Figure 5.6(c)), however, VIV-SIV scenarios are observed to produce lower f_o compared to VIV-only cases for all V_r considered with the difference in f_o between VIV-only and VIV-SIV scenarios becoming considerably lesser at higher V_r (V_r = 29.2 and 35.04). Additionally, it is worth noting that the in-line dominant f_o across all V_r considered is twice that of the dominant f_o observed in the cross-flow direction in the VIV-only and VIV-SIV scenarios. In the axial direction, the dominant f_o at V_r = 11.68 – 23.36 are equal to cross-flow dominant f_o and at V_r = 29.2 and 35.04, the dominant f_o is twice that of cross-flow f_o in the VIV-SIV scenarios. However, VIV-only scenarios exhibit axial dominant f_o twice that of cross-flow f_o across all current velocities considered. The variations in f_o could be associated with slug-induced changes in the structural stiffness, leading to mode-switching and multi-mode behaviour in the cylinder responses. These differences in f_o could explain the increase in dominant modes during VIV-SIV scenarios at lower V_r in the cross-flow and in-line directions, as well as the shifting of dominant modes to a lower mode number for all V_r considered in the axial direction.

Figure 5.7(a-o) presents frequency domain FFT plots of three-dimensional cylinder displacements associated with VIV-only and VIV-SIV scenarios. The oscillation frequencies plotted against the power spectral densities are normalised against the vortex-shedding frequencies (f_{vs}) of the corresponding case. The results presented in Section 5.2.1.1 indicated that the frequencies in the in-line and axial directions are almost twice that of the cross-flow direction. VIV-only results of this study confirm this 2:1 frequency response across all V_r considered, arising due to the nonlinear forcing terms in Eqs. (3.17 – 3.19) in Chapter 3 as shown in Figure 5.6 and 5.7 (Zanganeh and Srinil, 2016). However, VIV-SIV scenarios exhibit some interesting varying features.

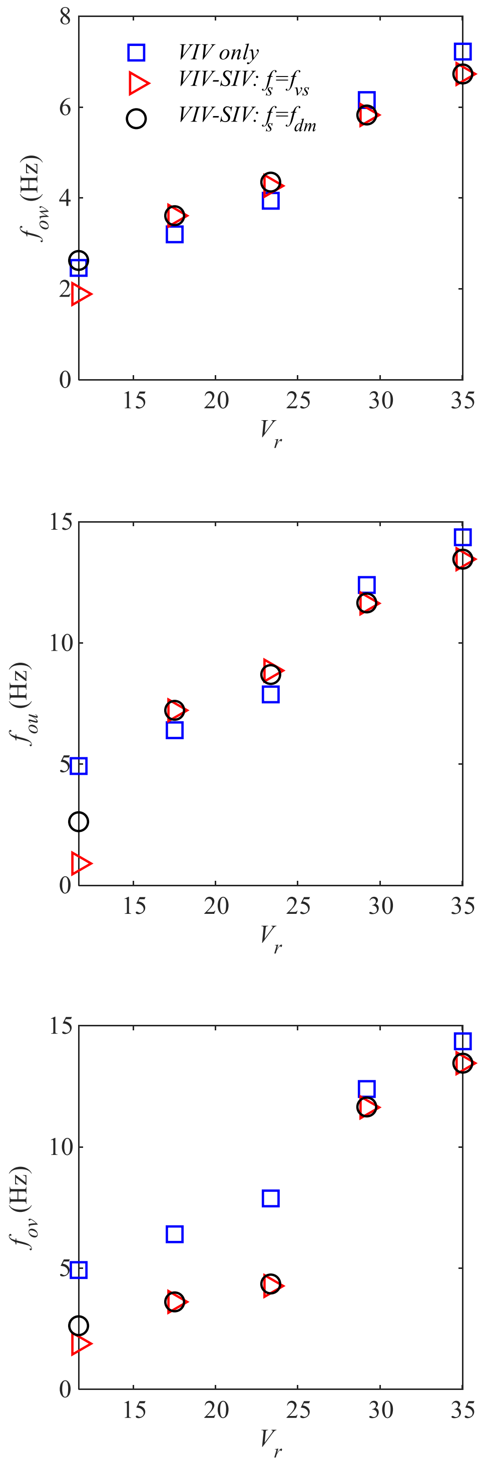

Figure 5.6: Comparison of dominant oscillation frequencies for cross-flow (a), in-line (b) and axial (c) oscillations at varying V_r in case of VIV-only (blue squares), VIV-SIV: $f_s = f_{vs}$ (red triangle) and VIV-SIV: $f_s = f_{dm}$ (black circles).

Frequency domain analysis at lower flow velocities (V_r = 11.68 and 17.52) show high frequency modulated response with the presence of sub-harmonic frequencies in all three directions of oscillations, in contrast to VIV-only scenario where the structure oscillates at one dominating frequency, as shown in Figure 5.7(a, b, f, g, k and l). At $V_r = 23.36$, VIV-SIV scenarios illustrate single-peak dominated frequency in the cross-flow direction, whereas in-line and axial oscillations reveal low-amplitude multi-harmonic frequency contents. Additionally, V_r = 29.2 and 35.04 follow similar trends of high harmonic contents present in the in-line and axial directions and single-peak dominating frequency in the cross-flow direction. This is in contrast to the observations made during VIV-only scenarios at V_r = 23.36 – 35.04, where a single-peak frequency is observed in all three-directions of oscillations. As presented in Chapter 4, slug flows are able to excite riser responses with high frequency modulations and sub-harmonics. These observations hold true with the combined internal-external excitation scenarios where high frequency modulation and harmonic contents are observed. It is also worth mentioning that the excited dominant oscillation frequencies in the case of VIV-only and VIV-SIV scenarios are close to the vortex shedding frequency of the structure, in contrast to the dominant frequencies excited at slugging frequency observed in Chapter 4. This shows that the cylinder oscillation frequencies are dominated by VIV induced forces in the combined VIV-SIV cases, which has been previously observed by Bowen and Srinil (2022).When slug flows are introduced in the system, it is seen that high harmonic frequency contents with sub-harmonic frequencies are excited during structure oscillations at low V_r in all three-directions, and as V_r increases, cross-flow oscillations shows single-peak frequencies while in-line and axial show high harmonic frequency contents. It also worth noting that both VIV-SIV scenarios considered excites oscillation frequencies closer to each other. These findings show the importance of considering three-dimensional oscillations in the case of combined VIV-SIV scenarios, as the observed harmonic and sub-harmonic frequencies, particularly in the in-line and axial directions, could lead to fatigue damages of the cylinder over time (Mukundan et al., 2009).

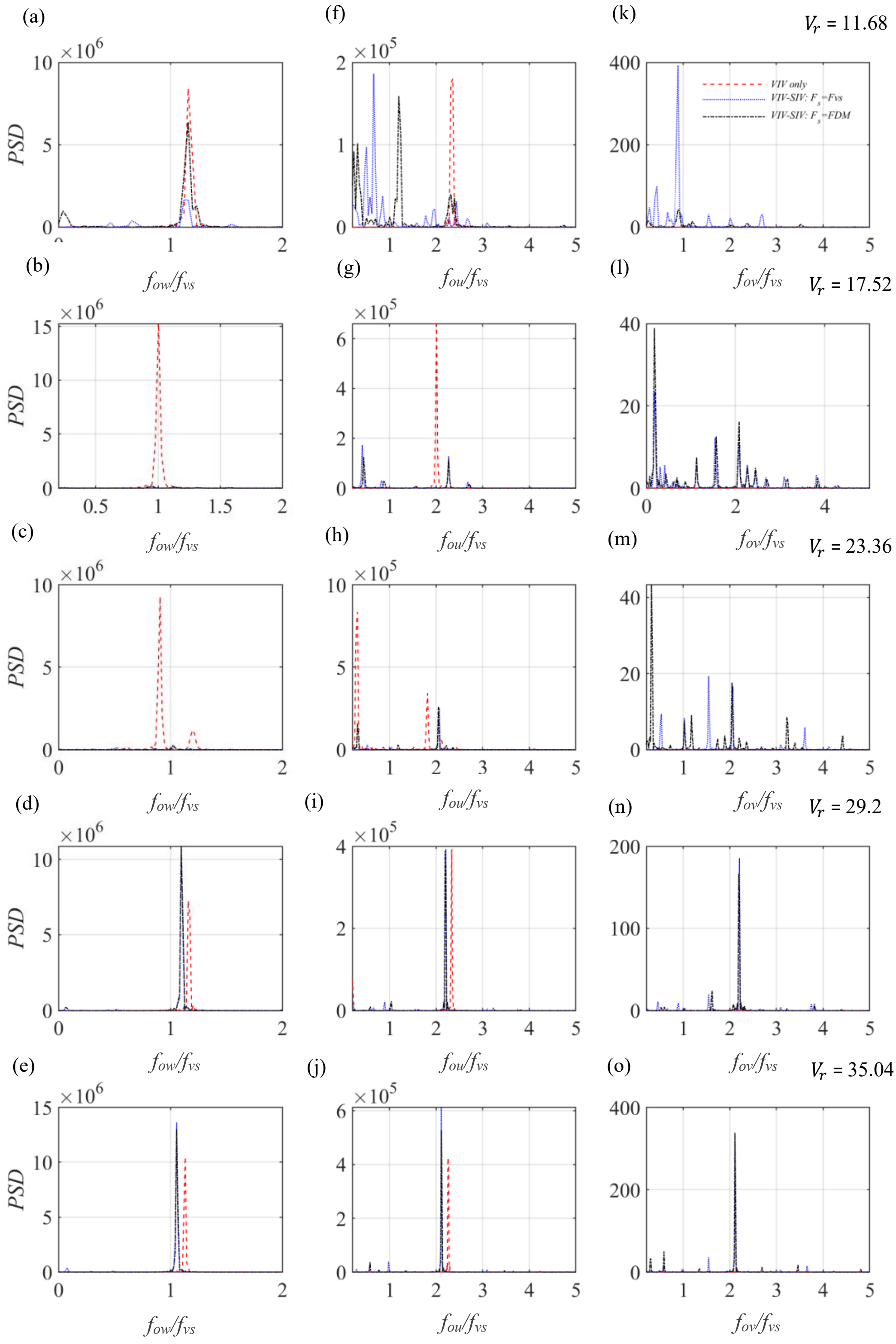

Figure 5.7: Cross-flow (a-e), in-line (f-j) and axial (k-o) oscillation frequencies associated with Figure 5.6.

5.2.2 Influence of U_r on the dynamic response of combined VIV-SIV scenarios

In addition to analysing different VIV-SIV scenarios, this section investigates the effect of varying internal translational flow velocities. Four U_r values are chosen ranging from 0 to 139.44 in equal spacings, where U_r is the dimensionless internal flow velocity, two external flow velocities $V_r = 11.68$ and $V_r = 35.04$ are considered. The slug flow parameters of L_U, H_{LS} and H_{LF} are maintained at consistent values identical to those utilised in the previous section. Additionally, it is worth mentioning that the slugging frequency associated with these cases are not equal to the vortex shedding frequencies or the frequency of the cross-flow VIV dominant mode. Figure 5.8(a-f) presents comparison of RMS oscillation amplitudes in cross-flow (Figure 5.8(a, d)), in-line (Figure 5.8(b, e)) and axial (Figure 5.8(c, f)) directions against varying U_r for two external flow velocities, $V_r = 11.68$ (Figure 5.8(a-c)) and 35.04 (Figure 5.8(d-f)). $U_r = 0$ in this figure represents VIV-only simulation where internal slug flows are absent. It can be observed from the figure that as U_r increases from 0 (VIV-only) to 46.48 (VIV-SIV), a slight increase in RMS amplitudes is observed in the cross-flow and in-line directions when $V_r = 11.68$. Axial oscillation response, however, shows a considerable increase in oscillation amplitudes when SIV is introduced into the system at $V_r = 11.68$. With further increase in U_r, oscillation amplitudes remain consistent with minimal differences in RMS amplitudes. In the case of $V_r = 35.04$, a considerable increase in RMS amplitudes is noticed in all three directions of oscillation when U_r increases from 0 to 46.48. Further increase in U_r result in consistent RMS amplitudes in all three directions of oscillations, similar to $V_r = 11.68$ case. However, a significant increase in RMS amplitudes is observed in the cross-flow and in-line directions across all U_r considered at $V_r = 35.04$ compared to $V_r = 11.68$. In the axial direction, however, comparable RMS amplitudes are noticed between $V_r = 11.68$ and 35.04. These results indicate that the combined external-internal excitations are more pronounced at higher V_r, highlighted by a significant increase in oscillation amplitudes from VIV-only to VIV-SIV as V_r increases. Furthermore, comparing RMS amplitudes results of the cases presented in this section with VIV-SIV scenarios ($f_s = f_{vs}$ and $f_s = f_{dm}$) outlined in the previous section (Figure 5.1), it is observed that at higher V_r ($V_r = 35.04$) RMS amplitudes are similar to each other in all three-directions of motion. However, at $V_r = 11.68$, cross-flow and in-line amplitudes are noticeably higher in the VIV-SIV: $f_s = f_{vs}$ and $f_s = f_{dm}$ scenarios compared to results presented in this section. For instance, cross-flow RMS in the case of varying U_r is 0.87, whereas VIV-SIV ($f_s = f_{dm}$) is 0.89. Similarly, in the in-line direction

RMS amplitudes of varying U_r is 0.18, whereas both VIV-SIV ($f_s = f_{vs}$ and $f_s = f_{dm}$) produce 0.38.

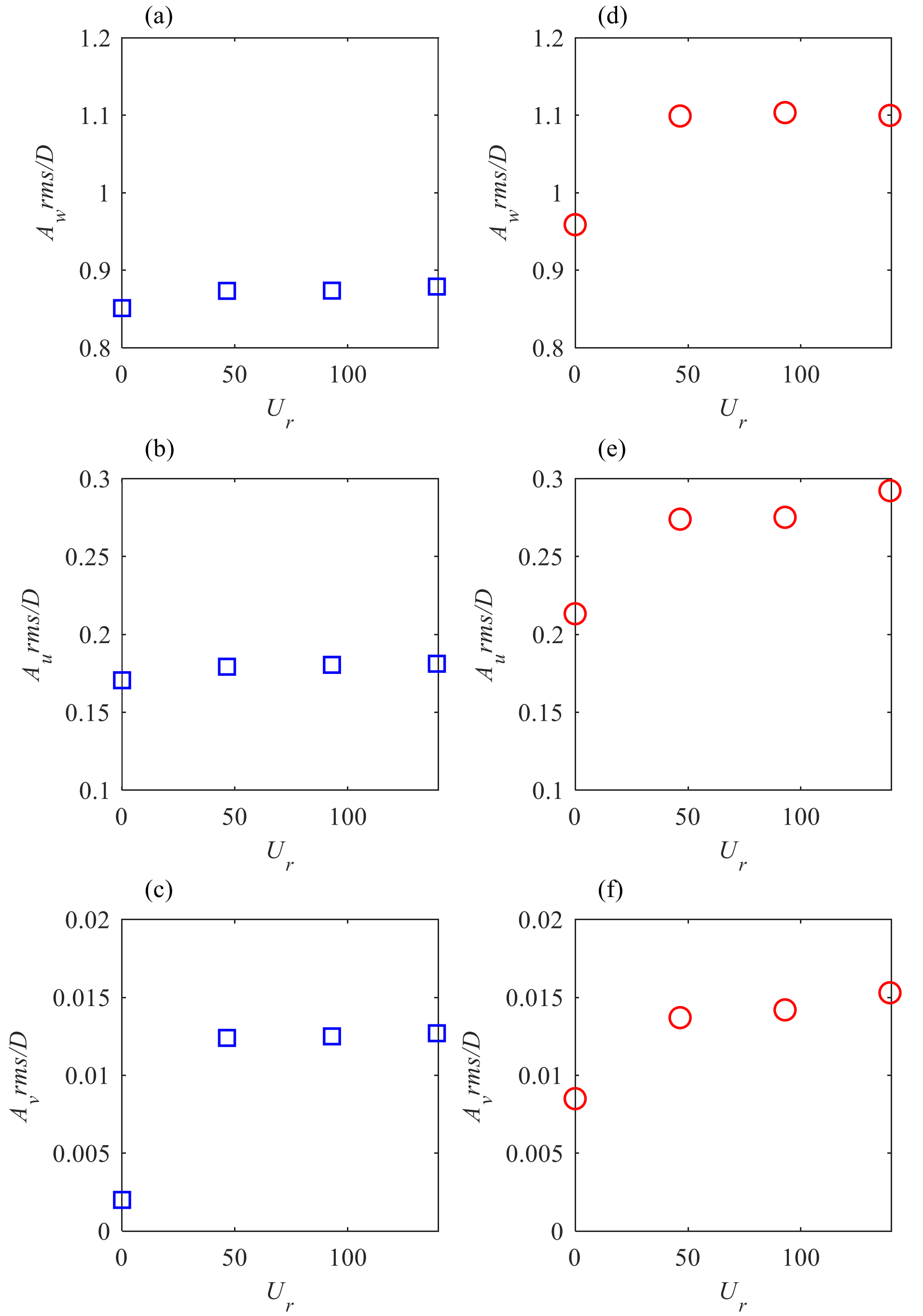

Figure 5.8: RMS oscillation amplitudes of cross-flow (a, d), in-line (b, e) and axial (c, f) motions at varying U_r for V_r = 11.68 (a-c) and 35.04 (d-f).

Figure 5.9(a-f) displays FFT plots of three-dimensional cross-flow, in-line and axial oscillations at varying U_r for V_r = 11.68 and 35.04. Frequency domain and modal analysis of the structural displacements presented in Figure 5.8 reveal that for all U_r considered, the oscillation frequencies are predominantly influenced by forces excited due to VIV. These oscillation frequencies exhibit single-peak dominance in the cross-flow direction and contain sub-harmonic components in the in-line and axial directions. However, the number of harmonic peaks observed in the in-line and axial directions are considerably fewer compared to VIV-SIV scenarios discussed in the previous section. Additionally, variations in dominant modes, similar to the VIV- SIV: $f_s = f_{vs}$ and $f_s = f_{dm}$ scenarios previously seen in Figure 5.5 are observed. At V_r = 11.68, the cylinder oscillates with dominant modes of 3 and 5 in the cross-flow and in-line directions, respectively, which align with the dominant mode in the VIV-only case (see Figure 5.5(a, f)). In the axial direction, the dominant mode shifts from 6 to 2 (Figure 5.5(k)) compared to the VIV-only case. Similarly, at $V_r = 35.04$, the dominant mode in the cross-flow and in-line oscillations align with the VIV-only case, while axial dominant modes shift from 8 to 4 (Figure 5.5(o)) compared to the VIV-only case. Moreover, multi-mode responses, similar to the VIV-SIV cases discussed in the previous section, exhibit higher number of secondary modes compared to the VIV-only case. It should also be mentioned that the frequency and modal responses discussed remain consistent across all U_r considered. These results demonstrate that when the incoming slug frequencies are not closely aligned with the vortex shedding or VIV dominant mode frequencies, the influence of slug flow on the cylinder responses become less significant, characterised by low frequency components.

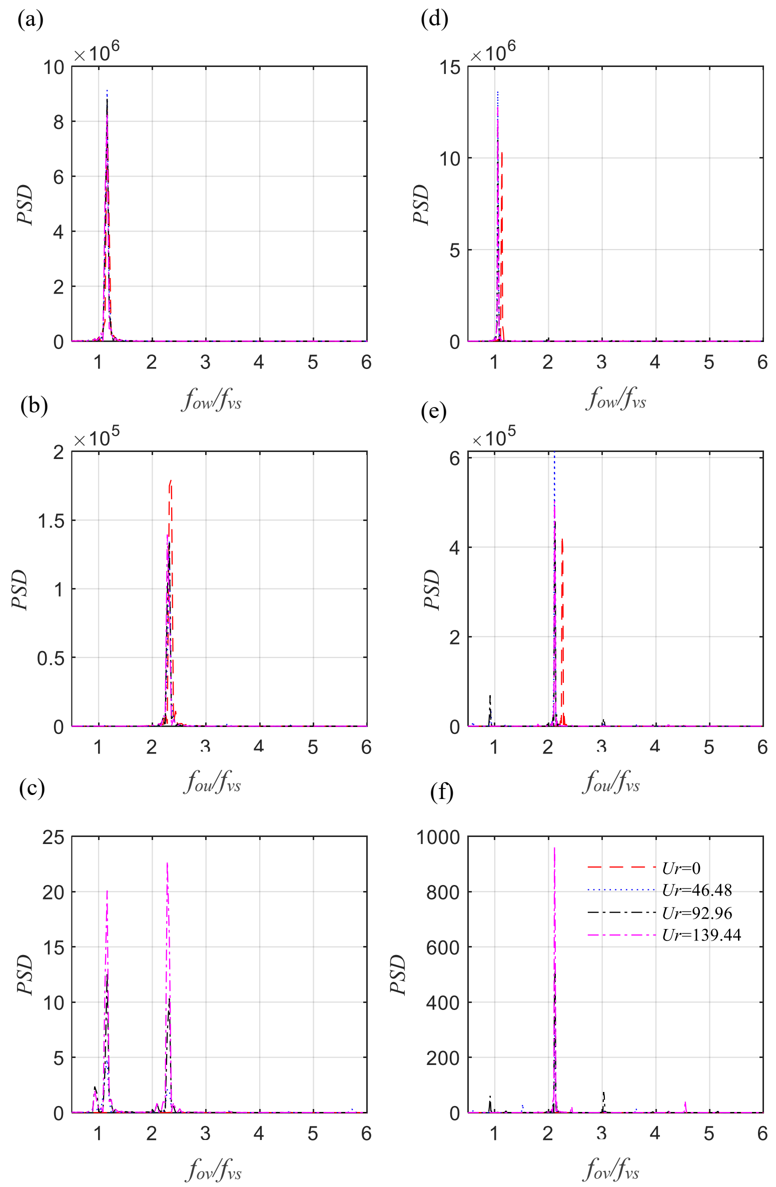

Figure 5. 9: FFT plots of three-dimensional cross-flow (a, d), in-line (b, e), axial (c, f) oscillations at varying U_r for V_r = 11.68 (a-c) and 35.04 (d-f).

5.2.3. Effect of mass quotient (M) on the vibration characteristics of combined internal-external excitations

Further to analysing various combined internal-external excitations scenarios, the effect of varying dimensionless mass quotient (M) on the vibration response of a flexible cylinder is investigated in this section. The slug flow parameters considered in the case of VIV-SIV: $f_s = f_{vs}$ (Table 5.1) are utilised in this scenario. For this study, four M values (M = 0.23, 0.45, 0.68 and 0.91), which are functions of varying internal fluid densities, are considered for two external flow velocities (V_r = 11.68 and 35.04). It is worth mentioning that M = 0.45 represents the M value considered in the previous sections, corresponding to a fluid density of 1025 kg/m^3. $M = 0.23$ represents half the internal fluid density of $M = 0.45$, while $M = 0.68$ and 0.91 represent three and four times the fluid density at $M = 0.23$, respectively. Figure 5.10 depicts space-time contour plots of three-dimensional cross-flow, in-line and axial displacements for varying M when $V_r = 11.68$. It can be observed from the figure that the dominant mode in the cross-flow direction shifts from 3 at $M = 0.23$ and 0.45 to 4 at $M = 0.68$ and 0.91. Dominant modes in the in-line direction increase to 3 at $M = 0.68$ and 0.91 from 2 at $M = 0.23$ and 0.45. In the axial direction, similar increase in dominant modes from 2 to 3 is observed at the corresponding M values.

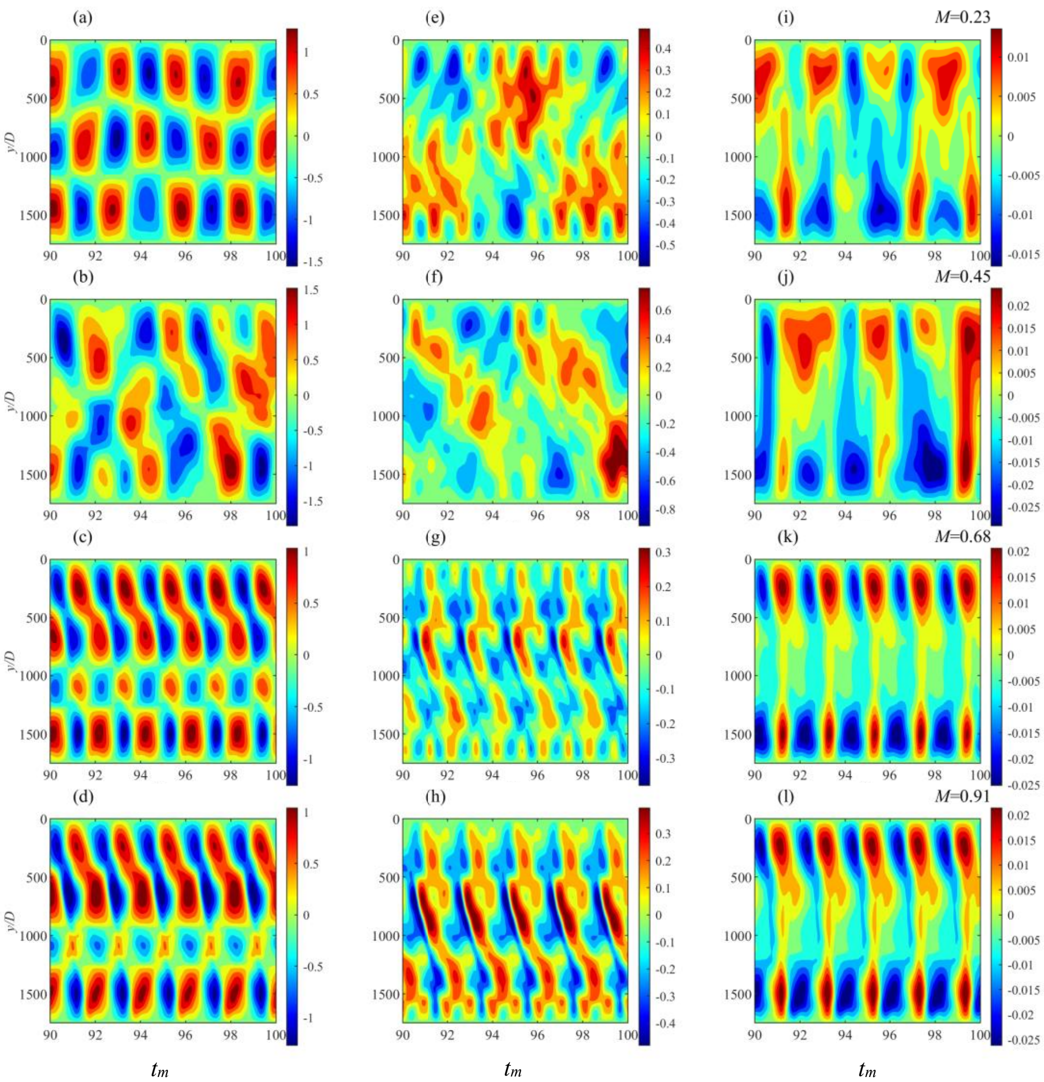

Figure 5.10: Space-time varying contour plots of three-dimensional cross-flow (a-d), in-line (e-h) and axial (i-l) oscillations with removed mean values at varying $M = 0.23$ (a, e, i), $M = 0.45$ (b, f, j), $M = 0.68$ (c, g, k) and $M = 0.91$ (d, h, l) when $V_r = 11.68$.

Additionally, a travelling wave pattern is noticed at higher M ($M = 0.68$ and 0.91) in all three-directions of oscillations (Figure 5.10(c, d, g, h, k and l)) as opposed to a standing wave pattern observed at low M (M = 0.23 and 0.45) values. Furthermore, analysis of RMS amplitudes at $V_r = 11.68$ show that cross-flow amplitudes decrease with increase in M and increases when M reaches 0.91 as depicted in Figure 5.11(a). In-line RMS response (Figure 5.11(b) follows a zig-zag trend, where oscillations alternatively increase and decrease with

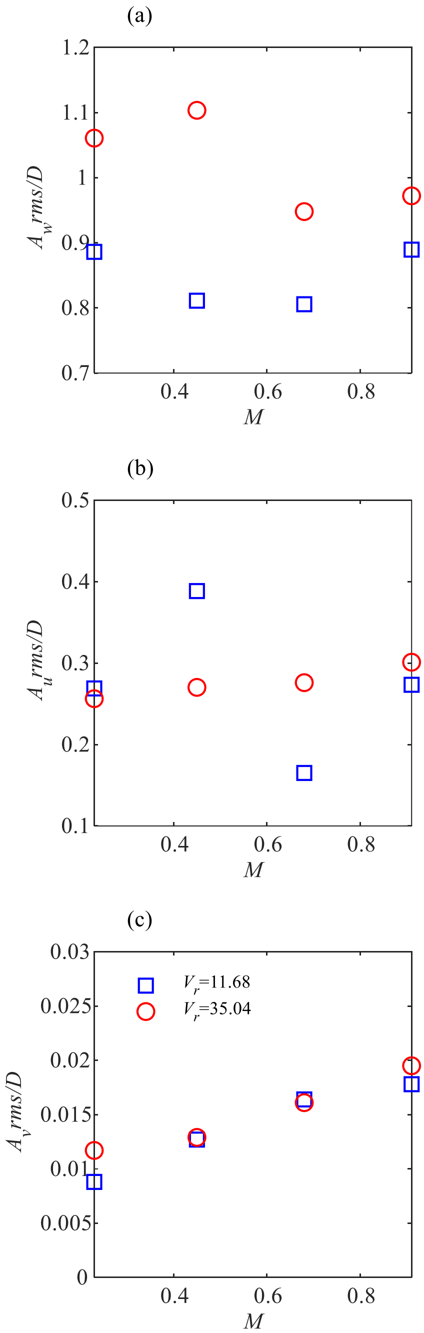

Figure 5.11: Maximum cross-flow (a), in-line (b) and axial (c) RMS oscillation amplitudes against varying M at V_r = 11.68 and 35.04.

every increase in M. The decrease in RMS amplitudes at M = 0.68 could be attributed to the observed shift in the dominant mode when M reaches 0.68. Axial oscillations, however, are observed to increase with M values, with M = 0.91 exhibiting almost twice the amplitude compared to M = 0.23 as shown in Figure 5.11(c). At higher current velocity (V_r = 35.04), cross-flow RMS amplitudes (Figure 5.11(a)) follow an alternating increase-decrease pattern, similar to in-line RMS response at V_r = 11.68. The noticeable decrease when M reaches 0.68 could again be attributed to the shift in dominant modes from 5 at M = 0.23 and 0.45 to

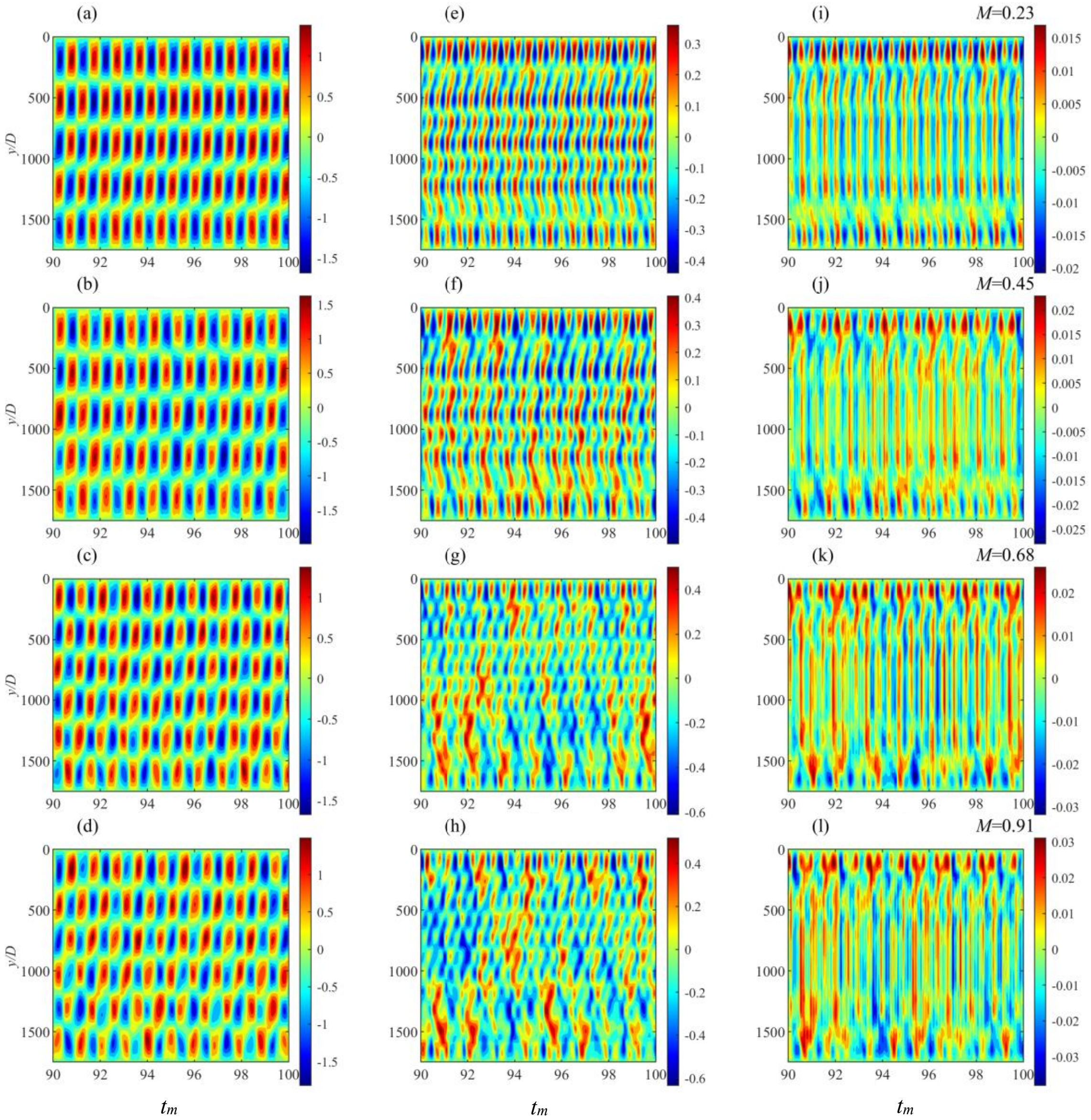

Figure 5.12: Space-time varying contour plots of three-dimensional cross-flow (a-d), in-line (e-h) and axial (i-l) oscillations with removed mean values at varying M = 0.23 (a, e, i), M = 0.45 (b, f, j), M = 0.68 (c, g, k) and M = 0.91 (d, h, l) when V_r = 35.04.

6 at M = 0.68 and 0.91 as observed in Figure 5.12(a-d), which depicts space-time contour plots of cross-flow (a-d), in-line (e-h) and axial (i-l) oscillations for varying M at V_r = 35.04. In-line and axial RMS response, however, follows a steady increase with increase in M, with axial amplitudes comparable to RMS amplitudes at V_r = 11.68 across all M considered as shown in Figure 5.11(b-c). The dominant mode response in in-line and axial directions at $M = 0.23$ and 0.45 are 9 and 4 respectively, which resembles the dominant modes observed in the VIV-SIV scenarios outlined in Section 5.2.1 at this current velocity. However, as M increases, a shift to higher dominant modes is observed. For instance, the dominant modes in the in-line and axial direction at M = 0.68 and 0.91, shifts to 11 and 5 respectively, as opposed to 9 and 5 observed at M = 0.23 and 0.45.

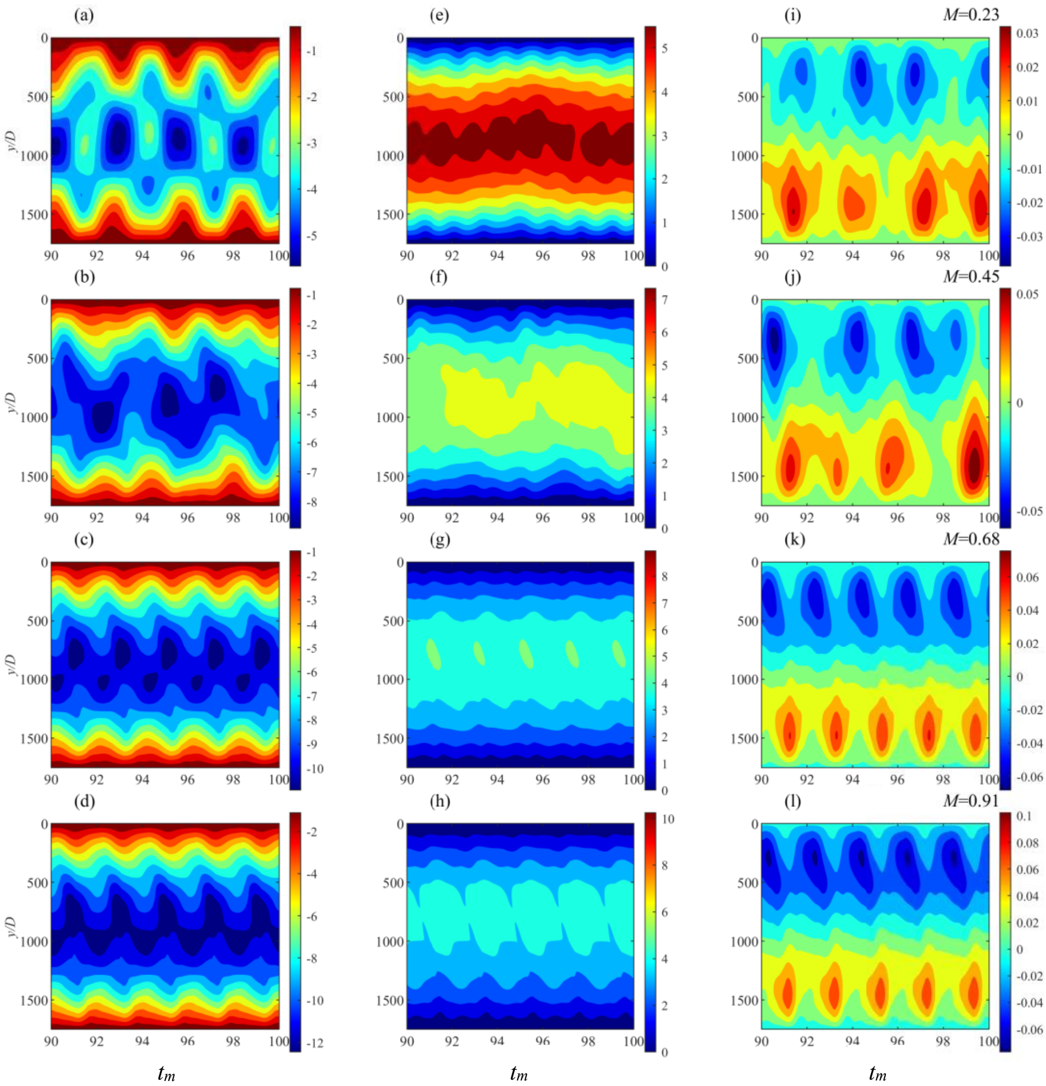

Figure 5.13: Space-time varying contour plots of three-dimensional cross-flow (a-d), in-line (e-h) and axial (i-l) oscillations with mean values at varying M = 0.23 (a, e, i), M = 0.45 (b, f, j), M = 0.68 (c, g, k) and M = 0.91 (d, h, l) when V_r = 11.68.

Furthermore, mean deflections are observed to increase with increase in M in the cross-flow, in-line and axial directions at both V_r considered. Figure 5.13(a-l) displays space-time varying contour plots with mean components in all three-directions of motion for varying M at $V_r = 11.68$. It is evident from the colour bars associated with each figure that mean deflection amplitudes increase with increase in M in all three-directions of oscillation. For example, the mean deflection in the cross-flow, in-line and axial directions increases from 5.66, 6.03 and 0.03 when M = 0.23 to 12.4567, 11.27 and 0.12 at $M = 0.91$ respectively. The highest mean deflection is observed in the cross-flow direction which is expected due to the effects of gravity in the direction perpendicular to external flow. Similarly, Figure 5.14(a-l) shows the space-time varying contour plots with mean components in all three-directions of oscillation for varying M at V_r = 35.04. The mean deflections in the cross-flow direction at V_r = 35.04 are observed to increase with increase in M. However, comparing colour bars in Figure 5.13(a-d) with Figure 5.14(a-d), it can be seen that the mean displacements in the cross-flow direction are lower than the mean displacements observed at V_r = 11.68 for all M. Subsequently, in-line and axial mean displacements at V_r = 35.04 are observed to be comparable with each other as M increases as shown in Figure 5.14(e-h) and (i-l) respectively. The decrease in mean displacement amplitudes at higher V_r can be attributed to the increase in VIV induced large mean displacements and oscillation amplitudes in the in-line, axial and cross-flow directions, thereby reducing the influence of internal slug flow. However, comparing these mean displacement amplitudes with the VIV-only mean displacement amplitudes (Figure 5.2(a-c)), it is observed that the influence of SIV at higher M generates larger mean displacement values. Consequently, this could lead to higher bending stresses on the cylinder, impacting its lifespan, and therefore should be considered during the design phase of a cylinder subjected to combined VIV and SIV.

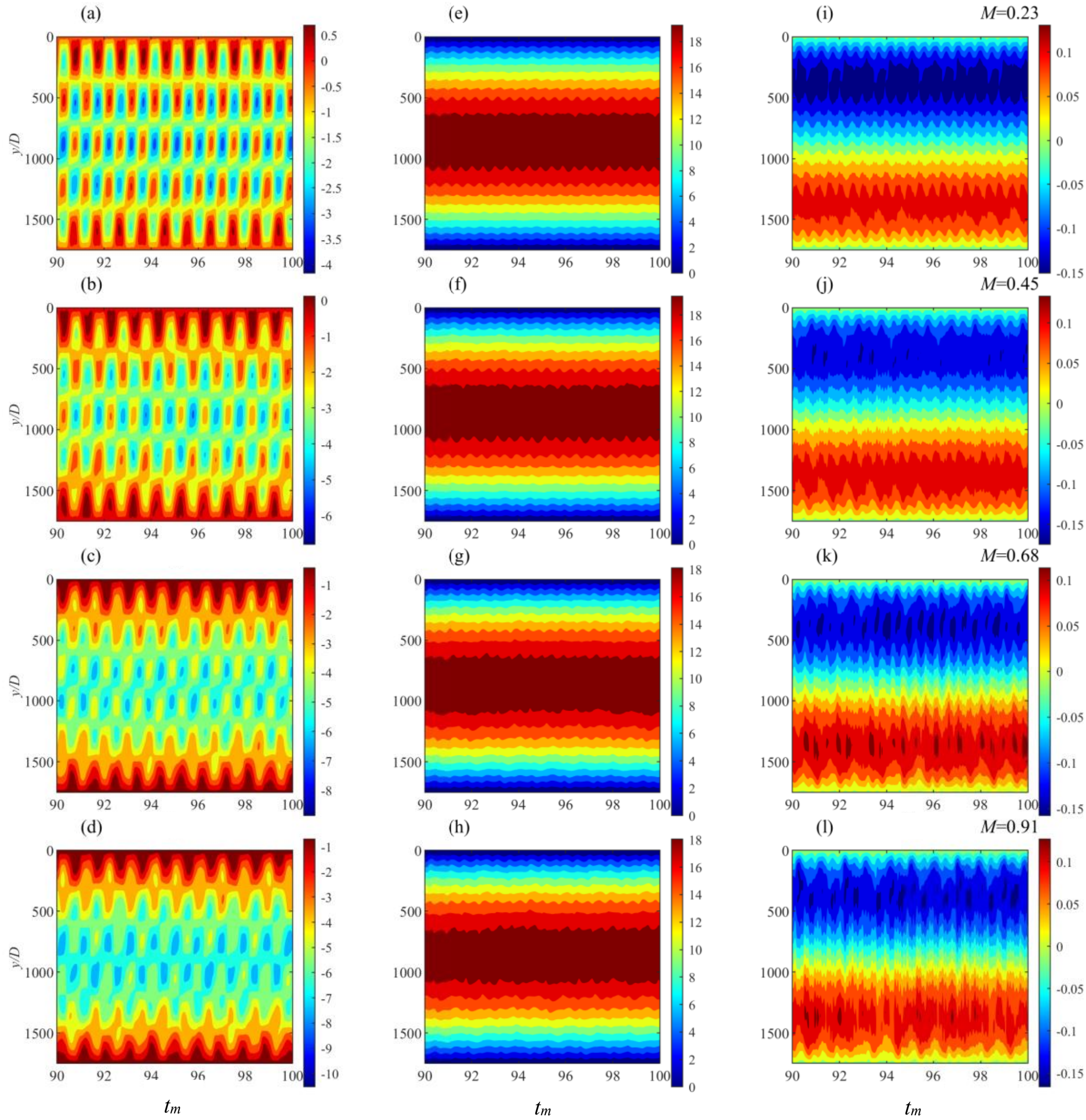

Figure 5.14: Space-time varying contour plots of three-dimensional cross-flow (a-d), in-line (e-h) and axial (i-l) oscillations with mean values at varying M = 0.23 (a, e, i), M = 0.45 (b, f, j), M = 0.68 (c, g, k) and M = 0.91 (d, h, l) when V_r = 35.04.

Furthermore, Figure 5.15 (a-f) displays oscillation frequencies associated with three-dimensional cross-flow, in-line and axial oscillations for varying M at V_r = 11.68 and 35.04. The oscillation frequencies plotted against the power spectral densities are normalised against the vortex-shedding frequencies (f_{vs}) of the corresponding case. Similar to observation made from Figure 5.7, oscillation frequencies in the combined VIV-SIV scenario generate high frequency components in the in-line and axial directions. However, the influence of increased fluid densities in the system exhibits alterations in the dominant oscillation frequencies and the associated harmonic response. At V_r = 11.68, cross-flow oscillations show a single-peak frequency close to the vortex-shedding frequency, while in-line and axial oscillations exhibit multi-subharmonic response when $M = 0.23$ and 0.45. Several low oscillation frequencies (near zero) are excited in the in-line and axial directions, with their harmonic response ranging up to two times the cross-flow dominant frequency, as shown in Figure 5.15(b-c). However, as M increases (M = 0.68 and 0.91), the low sub-harmonic frequencies are no longer excited, instead harmonic responses as a function of the dominant oscillation frequencies become prevalent in the in-line and axial directions. In the cross-flow direction, in contrast to single-peak oscillation frequencies at lower fluid densities, several low amplitude harmonic peaks are observed. At V_r = 35.04, several sub-harmonic and harmonic frequencies are observed in all three-directions of oscillations with the in-line and axial dominant frequencies being twice the cross-flow dominant frequency when M = 0.23 and 0.45. However, low (near zero) oscillation frequencies are not present at this current velocity. As M increases, the magnitude of these sub-harmonic and harmonic peaks increases with frequency modulations (side-bands) observed in the cross-flow direction. Additionally, the number of harmonic peaks is observed to increase in the axial direction at higher M as shown in Figure 5.15(f). This feature has been previously observed in Section 4.2.3 in Chapter 4.

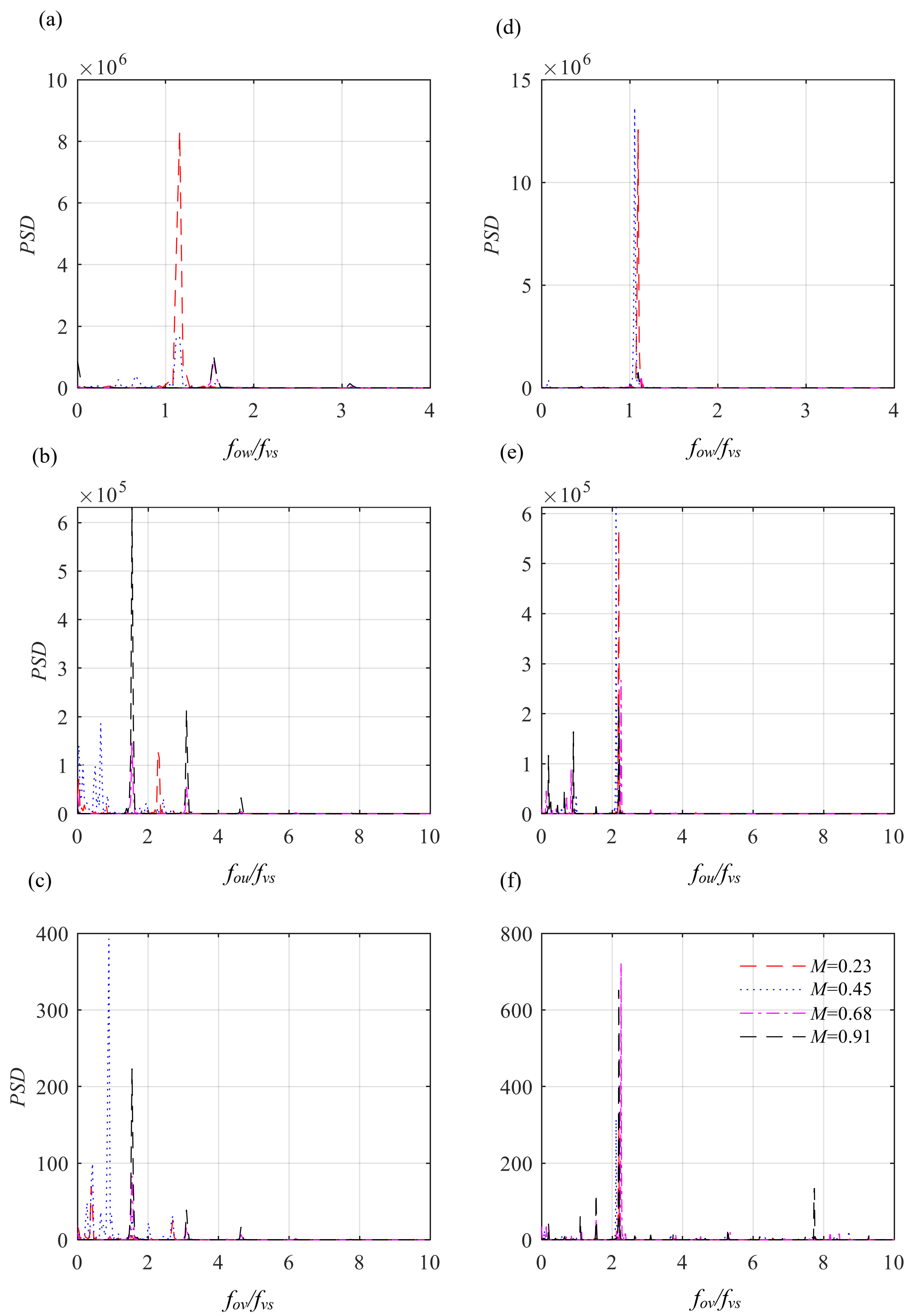

Figure 5.15: Frequency domain analysis of structure oscillations in the cross-flow (a, d), in-line (b, e) and axial (c, f) directions for varying M at V_r = 11.68 (a-c) and 35.04 (d-f).

5.2.4. Slug flow-induced parametric resonance

This section investigates the occurrence of parametric resonance in the combined VIV-SIV scenario, in continuation to the observations made in Section 4.2.2 in Chapter 4. The maximum RMS amplitude in Chapter 4 was observed to be when the incoming slug frequency was twice the natural frequency of the cylinder with internal mass. For this purpose, in the combined VIV-SIV scenario the internal slug frequency is set to twice the obtained natural frequency of the cylinder with internal mass (f_{n1}) (Song et al., (2011)). Five external flow velocities are considered in this section with U_r chosen to be equal to 46.48 (Section 5.2.2) and the corresponding L_U is obtained using the relation $f_s = V_t/L_U$. L_S and L_F are set to be equal halves of L_U and H_{LS} and H_{LF} are set to 1 and 0, similar to the previous sections. It should be mentioned that U_r and L_U are held constant across all external flow velocities considered, such that, $f_s = 2 * f_{n1}$. Figure 5.16(a-f) presents a comparison of the maximum mean displacement and RMS amplitudes for varying external velocities across all combined VIV-SIV and VIV-only cases considered in this study. It can be observed from Figure 5.16(a) that the mean displacement amplitudes in the cross-flow direction are slightly enhanced in the $f_s = 2f_{n1}$ case compared to other VIV-SIV cases across all external flow velocities. Similarly, at $V_r = 11.68$ and 17.52, in-line mean displacements are observed to be notably higher than other VIV-SIV cases, however, at higher current velocities, mean displacement amplitudes are noticed to be closer to each other (Figure 5.16(b)). Similarly, axial mean displacements are observed to be comparable with other VIV-SIV scenarios across all V_r considered (Figure 5.16(c)). However, the occurrence of parametric resonance can be evidently observed through the comparisons of RMS amplitudes. Figure 5.16(d) displays maximum RMS amplitudes across all VIV-only and VIV-SIV scenarios for varying V_r. Cross-flow RMS amplitudes are observed to be significantly higher than other VIV-SIV scenarios at $V_r = 11.68 – 23.36$. The RMS amplitudes are noticed to be almost twice the amplitude of other VIV-SIV cases at V_r = 11.68 and 17.52. However, as V_r increases cross-flow RMS are observed to decrease and when V_r reaches 29.2 and 35.04, the amplitudes are comparable with other VIV-SIV cases. Additionally, significantly large RMS amplitudes are observed in the in-line direction compared to other combined scenarios across all V_r as shown in Figure 5.16(e). RMS amplitudes are noticed to be more than twice the amplitudes of other combined cases at lower V_r ($V_r = 11.68$ and 17.52) and decreases at higher V_r (V_r = 23.36 – 35.04), still being considerably higher than the combined VIV-SIV cases for these current velocities.

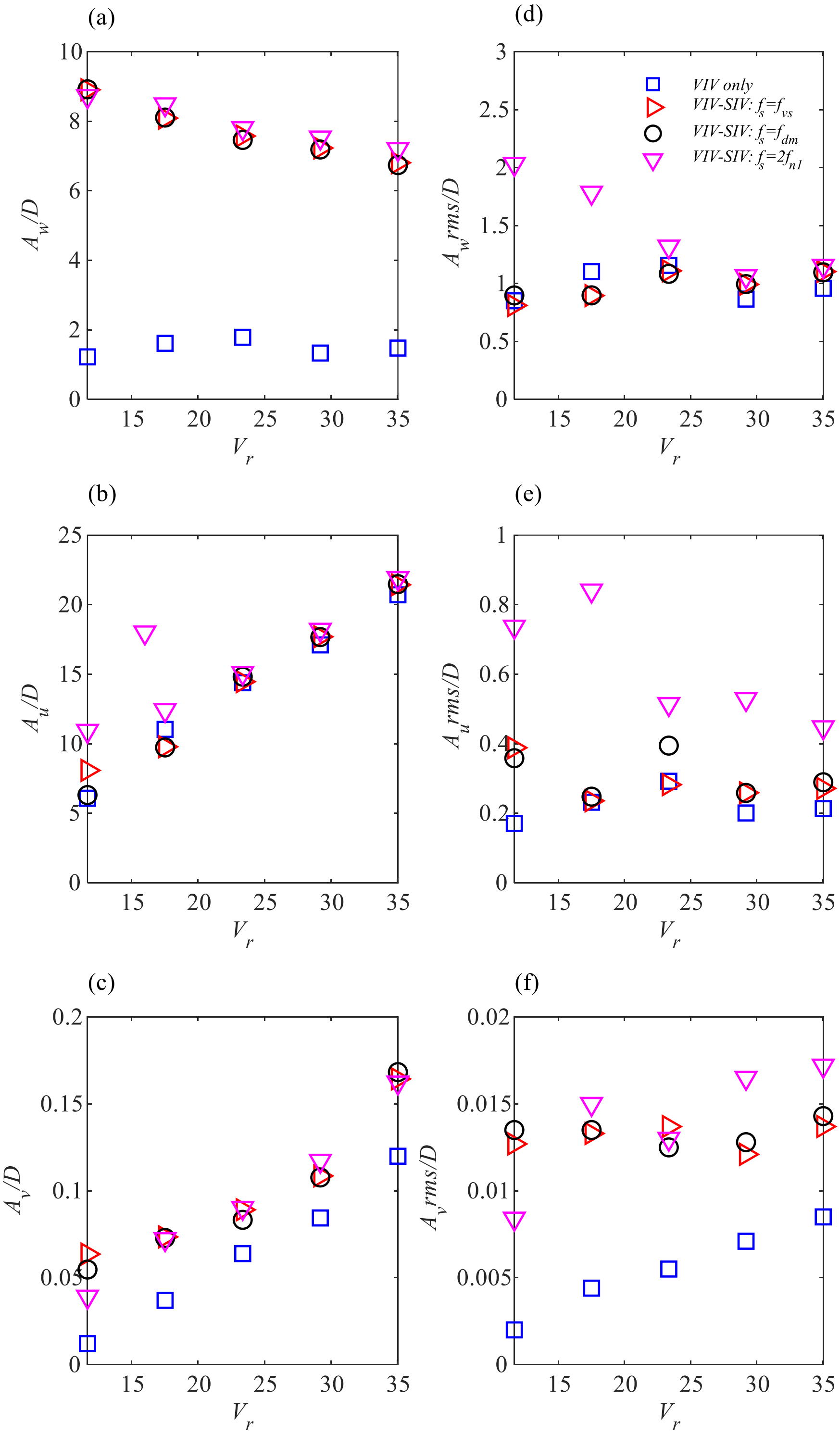

Figure 5.16: Comparison of maximum (a-c) and RMS (b-f) amplitudes of cross-flow (a, d), in-line (b, e) and axial (c, f) in the case of VIV-only (blue squares), VIV-SIV: $f_s = f_{vs}$ (red triangle) and VIV-SIV: $f_s = f_{dm}$ (black circles) and VIV-SIV: $f_s = 2f_{n1}$ (magenta downward triangle).

In contrast, axial oscillations show comparable RMS amplitudes with previous cases at lower V_r (V_r = 11.68 – 23.36) and becomes considerably higher at higher V_r (V_r = 29.2 and 35.04) as shown in Figure 5.16(f). These significantly large oscillation amplitudes observed when $f_s = 2f_{n1}$, confirm that the structure experiences parametric resonance in the combined VIV-SIV scenario. Furthermore, the decrease in RMS amplitudes at higher V_r in both cross-flow and in-line directions indicates that the structure oscillations are primarily dominated by forces due to VIV during high current velocities, with the influence of slug induced vibrations becoming minimal. Figure 5.17(a-o) depicts space-time varying contour plots of three-dimensional cross-flow, in-line and axial oscillations without mean components at varying external current velocities. Large amplitude oscillations in the cross-flow and in-line directions can be observed from the colour bars associated with Figure 5.17(a-j). Cross-flow oscillation response at V_r = 11.68 and 17.52 are observed to be dominated by a 1st mode response (Figure 5.17(a, b)), in contrast to a 3rd mode dominated response in the previous VIV-SIV scenarios (see Figure 5.5(a, b)). Similarly, in-line and axial oscillation responses are noticed to be dominated by a 1st and 2nd mode response at V_r = 11.68 and 3rd and 2nd mode response at V_r = 17.52 respectively. These dominant modes in the in-line and axial directions are also lower compared to the dominant modes observed in Figure 5.5(f, g, k and l). The 1st mode response in the cross-flow direction and the lower modes excited in the in-line and axial direction shows that at lower V_r (V_r = 11.68 and 17.52), the cylinder response is dominated by slug induced parametric forces in the combined VIV-SIV scenario, when f_s is close to or equal to twice the natural frequency of the fluid-conveying cylinder. At higher V_r (V_r = 23.36 – 35.04), cross-flow oscillations are observed to be 4th mode (V_r = 23.36) (Figure 5.17(c)) and 5th mode (V_r = 29.2 and 35.04) (Figure 5.17(d-e)) dominant similar to responses from VIV-SIV: $f_s = f_{vs}$ and VIV-SIV: $f_s = f_{dm}$ scenarios (see Figure 5.5(c-e)). The dominant modes being similar to each other is reflected in Figure 5.16(d), where oscillation amplitudes at these current velocities becomes comparable with each other. In the in-line direction however, dominant modes are observed to be 4, 2 and 1 at V_r = 23.36, 29.2 and 35.04 respectively. In the axial direction, the dominant mode is 1 at V_r = 23.36 – 35.04. These dominant modes in in-line and axial directions are lower compared to previous combinations of VIV-SIV scenarios, indicating a strong influence of slug induced forces at higher V_r in the in-line and axial directions. This dominance is also reflected in Figure 5.16(e) and (f) where oscillation amplitudes in the in-line and axial directions are significantly higher than other VIV-SIV scenarios.

Furthermore, some interesting features are observed in the frequency domain analysis of the above mentioned 3-D oscillations. Figure 5.18(a-o) presents FFT plots of the three-dimensional cross-flow, in-line and axial oscillations in the case of in the case of $f_s = 2f_{n1}$

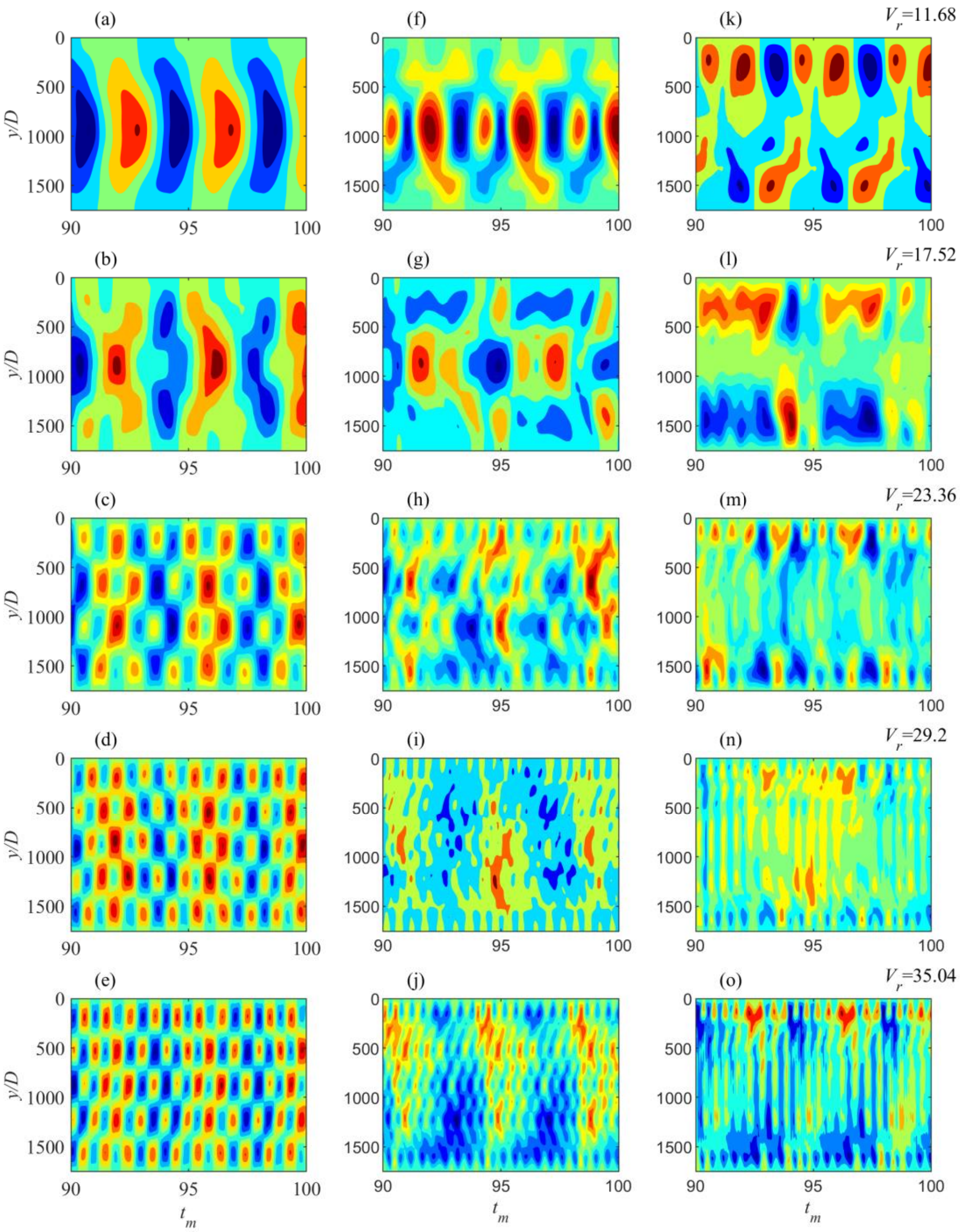

Figure 5.17: Space-time varying contour plots of three-dimensional cross-flow (a-e), in-line (f-j) and axial (k-o) oscillations without mean components in the case of $f_s = 2f_{n1}$ for varying V_r.

for varying V_r normalised over the slugging frequency corresponding to each case. It can be observed from the Figure 5.18(a-c) that the dominant oscillation frequency in the cross-flow direction is close to the slugging frequency at $V_r = 11.68$ – 23.36. This is in contrast to the observations made in the previous VIV-SIV scenarios (Figure 5.7), where the dominant oscillation frequencies were observed to be close to the vortex shedding frequencies of corresponding V_r. This shows the significant influence of slug induced forces when slugging frequency is equal to twice the natural frequency of the fluid-conveying cylinder. At $V_r = 11.68$, cross-flow, in-line and axial oscillations exhibit harmonic responses with dominant frequencies equal to twice the cross-flow dominant frequency. However, at V_r = 17.52, cross-flow responses exhibit harmonic frequency components with in-line and axial responses exhibiting several sub-harmonic frequencies, where harmonic frequencies are a multiple of half the cross-flow dominant oscillation frequency as shown in Figure 5.18(b, g and l). At $V_r = 23.36$, (Figure 5.18(c, h and m)) the dominant oscillation frequency in all three-directions of motions aligns closely with the slug frequency, however, oscillation frequencies near vortex shedding frequency becomes more pronounced compared to $V_r =$ 17.52. In the in-line and axial directions, a greater number of sub-harmonic frequency components are observed to be excited compared to V_r = 17.52. As external current velocity increases (V_r = 29.2 and 39.04), several sub-harmonic frequencies and frequency modulations with side bands are excited in all three directions of oscillations as seen in Figure 5.18(d, i, n, e, j and o). In the cross-flow direction at V_r = 29.2 and 35.04 (Figure 5.18(d) and (e)), the dominant oscillation frequency is observed to be close to the vortex-shedding frequency with side band frequencies in equal spacings. However, oscillation frequencies close to the slugging frequency are also excited at these current velocities. In the in-line direction, several sub harmonic frequencies with side bands are observed with dominant oscillation frequencies close to the slugging frequency. Dominant oscillation frequencies close to slugging frequency in the in-line direction across all V_r shows the significant influence of SIV on the structure response at this direction of oscillation. Similarly, axial responses exhibit several sub-harmonic frequencies with side bands of equal spacings, however, the dominant oscillation frequencies in this case are close to twice the cross-flow dominant frequency. The observed frequency modulations along with several sub-harmonic frequencies observed are a consequence of considering geometric nonlinearities and could lead to fatigue damages over time for a cylinder exposed to combined external and internal excitations. Overall, it can be summarised that when the incoming slug frequency is close to or equal to twice the natural frequency of the cylinder with internal mass, the structure experiences three-dimensional large amplitude oscillations (parametric resonance) with sub-harmonic frequency modulations and alterations in excited dominant mode. Additionally, at higher V_r, VIV induced forces are noticed to partially dominant than slug induced forces with reduced oscillation amplitudes and dominant oscillation frequencies excited close to the vortex shedding frequency. It should also be mentioned that modal contributions in this VIV-SIV scenario are similar to those previously discussed in Section 5.2.1.1.

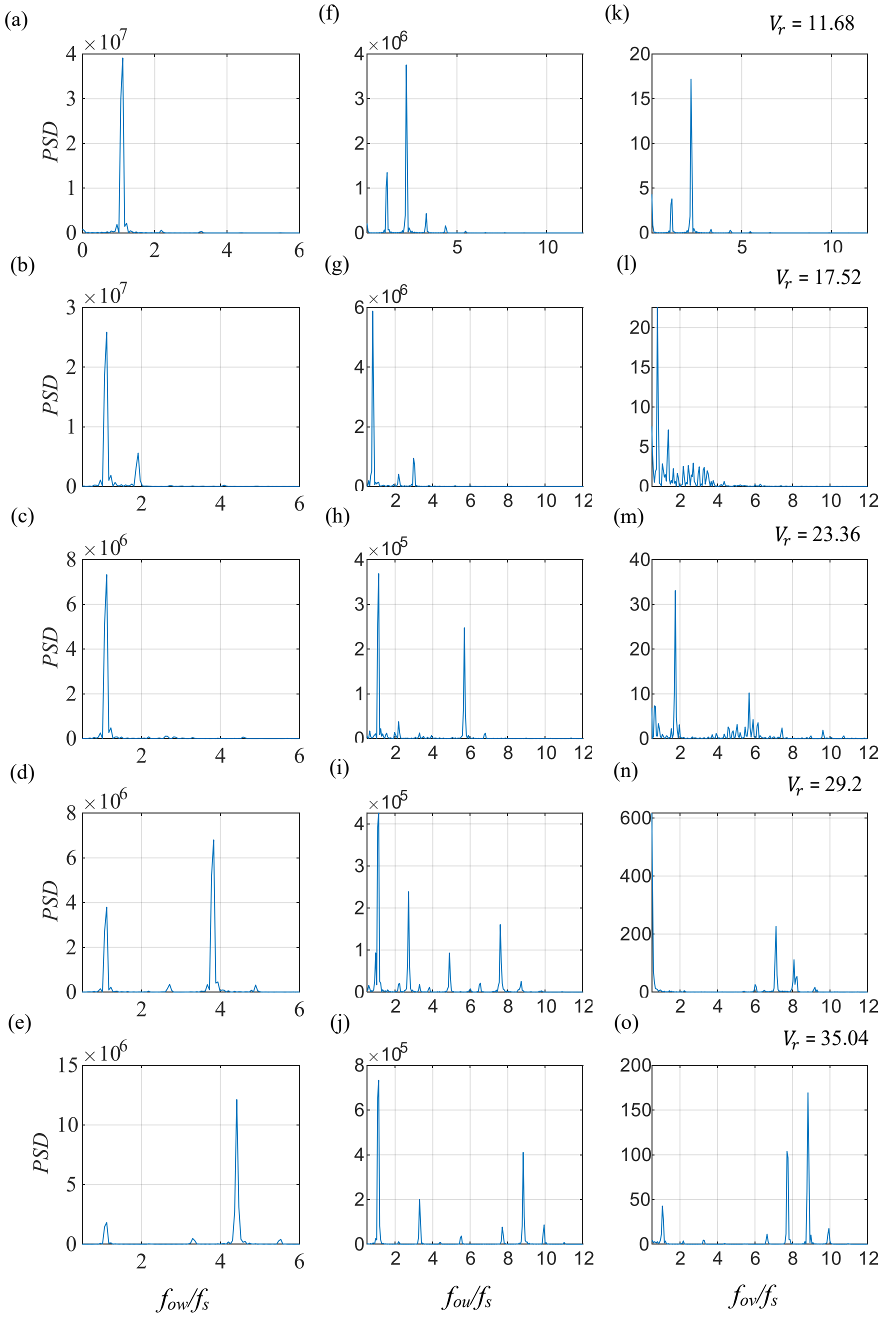

Figure 5.18: Frequency domain analysis of three-dimensional cross-flow (a-e), in-line (f-j) and axial (k-o) oscillations in the case of $f_s = 2f_{n1}$ for varying V_r.

5.3 Conclusions

In this chapter, the three-dimensional dynamic response of a submerged horizontal flexible cylinder subjected to combined external (VIV) and internal (SIV) forces is investigated. The developed semi-empirical model takes into account the geometric nonlinearities and fully nonlinear fluid-forcing terms have been employed. Coupled cross-flow, in-line and axial oscillations are incorporated along with centrifugal and Coriolis forces to emulate vibrations due to internal two-phase slug flows. The model is solved via a finite difference scheme and is capable of capturing mass variations in the internal flow. The results from model validation for VIV with experimental results showed that the model predictions exhibited quantitative and qualitative similarities to the experimental results. This study further explored the dynamic effects of various VIV-SIV scenarios on the cylinder responses through a parametric study. Compared to VIV-only numerical results, combined VIV-SIV scenarios showed increased mean displacement amplitudes in all three-directions of oscillations. In particular, cross-flow oscillations were observed to generate the largest mean displacement due to cylinder bending upon the introduction of internal two-phase slug flows. RMS amplitude responses followed a zig-zag trend with increase in external current velocity (V_r) in all three-directions, where a significant increase in the in-line and axial oscillations was observed compared to VIV-only case. Furthermore, higher dominant modes in the cross-flow and in-line directions were excited at lower current velocity in the combined scenario, whereas comparable modes between VIV-only and VIV-SIV scenarios are excited at higher current velocity. Alternatively, axial dominant modes compared to the VIV-only case were observed to decrease across all V_r considered in the combined scenario. Frequency domain analysis exhibited frequency responses with increased frequency components and sub-harmonics particularly in the in-line and axial directions in the combined VIV-SIV scenarios. Three-dimensional mean displacements were observed to increase with increase in M for lower V_r (V_r = 11.68). However, during high V_r mean displacements in the in-line and axial direction were comparable with increase in M, while cross-flow mean displacements increased. Moreover, the highest oscillation amplitudes among all VIV-SIV scenarios considered in this study was observed when the incoming slug frequency was close to twice the natural frequency of the cylinder with internal mass (parametric resonance). This phenomenon produced variations in excited dominant modes with high frequency modulations (side-bands) and subharmonic frequencies excited in all three-directions of oscillation. Additionally, the dominant oscillation frequencies at lower V_r were observed to be close to the slugging frequency in contrast to the vortex shedding frequency observed in the other VIV-SIV scenarios. The presented semi-empirical model with reduced simplifications could provide practical predictions of combined VIV-SIV in offshore risers during the early stages of the design process.

Chapter 6

Conclusions and Future Work

In this thesis, a novel fully nonlinear three-dimensional phenomenological model capable of predicting vibrations of a straight flexible cylinder due SIV and VIV together and separately is developed and presented. The developed model takes into account both geometric and hydrodynamic nonlinearities and captures mass variations in the slug flow regime. The semi-empirical model consists of nonlinear structural equations of coupled out-of-plane, in-plane and axial oscillations combined with equations involving centrifugal and Coriolis forces to capture vibrations induced by two-phase slug flows. New dimensionless functions are derived from the dimensional model to analyse the effect of key flow characteristics and improve the overall understanding of the FSI phenomena. Internal slug flows are modelled as a steady space-time varying internal flow, with slug units of identical lengths travelling along the pipe. In addition, slug flows are assumed to be fully developed and undisturbed by pipe oscillations. A numerical space-time finite difference approach is adopted in this study to solve and analyse the highly nonlinear equations present in the model. The model combines forces due to VIV using a phenomenological wake oscillator model, which simulates oscillatory lift and drag forces induced by VIV. The 3-D SIV model has been validated through comparing model results with experimental and numerical results from literature related to SIV and VIV of flexible straight cylinders. A parametric study is performed to analyse the effect of key slug characteristics such as slug length, thin-film liquid length, slug liquid and thin film holdup, slug unit length, translational velocity and internal fluid mass on the nonlinear dynamic response of submerged and free-hanging flexible cylinders. Numerical investigation on the combined SIV and VIV have also been performed by varying internal and external flow properties. The main outcomes and contributions of the present thesis are summarised as follows.

6.1 Slug flow-induced vibrations in a submerged straight vertical cylinder

- The 3-D dimensionless numerical model has been utilised to investigate slug flow-induced vibrations of submerged vertical straight cylinders. A parametric study was performed to analyse the effect of key slug features on the coupling response of the cylinder.
- At lower slug translational velocities, the RMS amplitudes induced by slug flow in both out-of-plane and in-plane directions were observed to increase up to 350% with increase in flow velocities. In contrast, at higher translational flow velocities, the RMS amplitudes were observed to be constant with increase in internal flow velocities.
- At high mass quotient cases, mean displacements and large amplitude oscillations in the out-of-plane and in-plane directions induces external hydrodynamic forces on the submerged cylinder. These forces lead to simultaneous three-dimensional out-of-plane, in-plane and axial oscillations due to nonlinear coupling terms in the presented model.
- The longest slug unit generate large amplitude-modulation response which can lead to increased fatigue damages over time.
- Compared to internal single-phase flows, two-phase slug flows induced oscillations at lower flow velocities generated significantly large oscillations, up to 4 times, in both out-of-plane and in-plane structural motions. However, at higher flow velocities, the maximum amplitudes are found to be closer to each other.
- The vibration response of the submerged cylinder becomes a coupling response excited by combined SIV and VIV at high mass quotient cases. In the absence of any external flow, VIV happens due to the structural oscillations in the stationary external fluid. In other words, when the structure oscillates due to internal SIV, the hydrodynamic forcing terms in equations simulate the VIV caused by the relative motion of the structure to the external fluid. While the model accounts for these VIV oscillations, the coupling response of VIV and SIV occurs only during high mass quotient cases, where the oscillation amplitudes are high. In all other instances, where SIV amplitudes are not high enough, the vibration response is exclusively attributed to forces induced by the slug flow.
- Changes in the two-phase slug flow oscillation frequencies were found to be negligible when compared to the single-phase oscillation frequencies for all the internal translational velocities considered. However, the dominant modes and oscillation frequencies vary according to distinct slug formations and are found to exhibit a linear relationship with the overall amplitude response.

- A dimensionless parameter U_r' is introduced for the purpose of predicting high oscillation amplitude scenarios corresponding to the cases considered in this study. U_r' values ranging from 2 to 18 were found to generate high amplitude responses while the other values outside this range generate low oscillation amplitudes.

6.2 Slug flow-induced vibrations in a horizontal flexible cylinder

- Slug flow-induced vibration responses of a horizontal flexible cylinder are investigated taking into account the geometric nonlinearities. The horizontal cylinder is assumed to be surrounded by air, and a fixed-pinned boundary condition is applied. The model is compared with experimental results of a horizontal cylinder subjected to two-phase slug flows. Time-history plots of out-of-plane oscillations demonstrate the model's ability to replicate similar trends in both amplitude and frequency response, as observed in the experimental literature.
- The effect of varying slug frequency to cylinder first natural frequency ratios (f_s/f_n) for different internal translational flow velocities were analysed. Additionally, the influence of dimensionless internal flow velocity at constant slug unit lengths and the effect of varying mass quotient on the vibration characteristics of a horizontal cylinder were analysed.
- Three-dimensional large amplitude responses across all flow velocities considered were observed when the incoming slugging frequency is equal to the structure's natural frequency ($f_s/f_n = 1$). At this ratio, high amplitudes with an increase of up to 4 times compared to $fs/fn = 2$ ratio were observed at certain flow velocities. Moreover, three-dimensional large oscillation amplitudes were also observed when f_s/f_n = 0.66 and 0.5, albeit only at high internal flow velocities.
- Oscillation amplitudes were found to increase with an increase in U_r in the out-of-plane and in-plane directions for all f_s/f_n ratios while a zig-zag alternating trend is noticed in the axial direction.
- In the case of varying dimensionless internal flow velocity at constant slug unit lengths, comparison of maximum RMS amplitudes with f_s/f_{n1} ratios, where f_{n1} is the first natural frequency of the cylinder containing internal mass, revealed parametric resonance observed in the out-plane and in-plane directions, with the largest amplitude response observed when the slugging frequency was equal to twice the natural frequency of the cylinder containing internal mass. Axial oscillations, on the other hand, exhibited a linear increase in oscillation amplitudes with rapid escalation in amplitudes at high internal flow velocities.

- The largest amplitude response in all three-directions of oscillations among all the cases considered were observed when the mass quotient parameter was at its highest value, where the increase is almost 4 times compared to the lowest mass quotient parameter considered. An increase in M allows for greater mass-momentum fluctions inside the cylinder, resulting in increased oscillation amplitudes.
- Frequency response FFT plots display multi-harmonic responses, with sub-harmonic frequencies present in the oscillations as a consequence of accounting for geometric nonlinearities in the presented model. Axial oscillation frequency response result in large number of frequency contents compared to out-of-plane and in-plane response. Frequency contents in all three-directions increase with increase in U_r and M ratios, with high frequency modulations were observed at the highest mass quotient value.

6.3 Combined VIV-SIV scenarios in submerged horizontal cylinders

- The dynamic response of a submerged horizontal cylinder subjected to simultaneous VIV-SIV excitation scenarios were investigated through a parametric study. The results from model validation for VIV with experimental results showed that the model predictions exhibited quantitative and qualitative similarities to the experimental results.
- By comparing VIV-only and combined VIV-SIV scenarios, the significant effects of SIV on VIV have been highlighted. Results from the parametric study showed that combined VIV-SIV scenarios exhibited an increase in mean displacement amplitudes in all three-directions of oscillations. In particular, cross-flow oscillations were observed to generate the largest mean displacement, up to 5 times compared to VIV-only, upon the introduction of internal two-phase slug flows due to cylinder bending. RMS amplitude responses followed a zig-zag trend with increase in external current velocity (V_r) in all three-directions, where a significant increase of up to 200% was observed in the in-line and axial oscillations compared to VIV-only case.
- Furthermore, higher dominant modes in the cross-flow and in-line directions were excited at lower current velocity in the combined scenario, whereas comparable modes between VIV-only and VIV-SIV scenarios are excited at higher current velocity. Alternatively, axial dominant modes compared to the VIV-only case were observed to decrease across all V_r considered in the combined scenario.

- In the case of combined VIV-SIV scenarios, frequency domain analysis exhibit oscillation frequencies with increased frequency components and sub-harmonics particularly in the in-line and axial directions.
- Moreover, parametric resonance was observed in the combined scenario, where the highest oscillation amplitudes among all VIV-SIV scenarios considered in this study was observed when the incoming slug frequency was close to twice the natural frequency of the cylinder with internal mass (parametric resonance). Parametric resonance conditions produced an oscillation amplitude increase of up to 2 times in the cross-flow direction and up to 8 times in the in-line direction. This phenomenon produced variations in excited dominant modes with high frequency modulations (side-bands) and subharmonic frequencies excited in all three-directions of oscillation.
- Additionally, the dominant oscillation frequencies at lower current velocities were observed to be close to the slugging frequency in contrast to the vortex shedding frequency observed in the other VIV-SIV scenarios. The presented semi-empirical model with reduced simplifications could provide practical predictions of combined VIV-SIV in offshore risers during the early stages of the design process.

6.4 Recommendations for future research

The results obtained from the novel predictive model provides encouraging results. However, to the authors knowledge, the presented model is the first of its kind and several interesting research directions can be pursued for future exploration on this topic. Following points outlines some of these suggestions.

- In the present thesis, a steady idealised slug unit model has been utilised to analyse the vibration characteristics of flexible cylinders subjected to internal two-phase slug flows. The 3-D model can be further enhanced by accounting unsteadiness of slug flow (e.g. slug units have non-uniform lengths) and its dependence on structural oscillations (e.g. variations in slug unit lengths based on cylinder oscillation dynamics). These enhancements can yield in a more computationally robust tool for fully coupled SIV of flexible cylinders. In addition, vibration dynamics of other multiphase (two-phase/three-phase) flow regimes can be investigated by taking into account the geometric nonlinearities of the structure.
- For numerical analysis of SIV, it is of practical importance to consider different pipe configurations, including straight pipes at varying inclinations, catenary shaped risers, lazy wave risers and pipe with bends, where slug flow characteristics may vary as they are

susceptible to pipe geometry. Further investigations can explore three-dimensional cylinder responses in different current profiles, such as linear and nonlinear sheared flows. Furthermore, for combined external-internal excitation scenario, it is essential to examine the influence of other environmental factors such as wave and floating structure motions.

- Numerical results in this study highlight the significance of in-plane and axial oscillations of a flexible straight cylinder excited by SIV. While some experimental studies have reported the importance of in-plane oscillations due to SIV, axial oscillations are yet to be measured. Therefore, experimental investigations of flexible cylinders measuring simultaneous out-of-plane, in-plane and axial oscillations due to SIV is suggested. Additionally, the significance of geometric nonlinearities can be verified using CFD simulations of flexible cylinders subjected to SIV-only and combined VIV-SIV scenarios by taking into account the structural nonlinearities.

References

Al-Hashimy, Z.I., Al-Kayiem, H.H. and Time, R.W., 2016. Experimental investigation on the vibration induced by slug flow in horizontal pipe. ARPN J. Eng. Appl. Sci. (11), 12134–12139.

Baker, O., 1954. Simultaneous flow of oil and gas. Oil and Gas Journal 53, pp. 185-190.

Barnea, D., Shoham, O., Taitel, Y. and Dukler, A.E., 1980. Flow pattern transition for gas-liquid flow in horizontal and inclined pipes. Comparison of experimental data with theory. International Journal of Multiphase Flow 6, pp. 217-225.

Blevins. (1977). Flow-induced vibration.

Blanco, A., and Casanova, E., 2010. A Preliminary Study on the Interaction Between Slug Flow and Vortex Induced Vibration in Fatigue Life of Submarines Pipelines. Proceedings of the ASME 2010 29th International Conference on Ocean, Offshore and Arctic Engineering. 29th International Conference on Ocean, Offshore and Arctic Engineering: Volume 5, Parts A and B. Shanghai, China. June 6–11, pp. 545-550. ASME.

Bossio V., B. M., Blanco A., A. J., and Casanova M., E. L., 2014. Numerical Modeling of the Dynamical Interaction Between Slug Flow and Vortex Induced Vibration in Horizontal Submarine Pipelines. ASME. J. Offshore Mech. Arct. Eng. November 2014; 136(4): 041803.

Bordalo, S.R.N., Morooka, C.K., Cavalcante, C.C., Matt, C.G. and Franciss, R., 2008, January. Whipping phenomenon caused by the internal flow momentum on the catenary risers of offshore petroleum fields. In International Conference on Offshore Mechanics and Arctic Engineering (Vol. 48180, pp. 315-323).

Bowen, M. and Srinil, N., 2020. Planar dynamics of inclined curved flexible riser carrying slug liquid-gas flows. J. Fluids. Struct. 94, 1–41.

Cargnelutti, M.F., Belfroid, S.P. and Schiferli, W., 2009, January. Two-phase flow-induced forces on bends in small scale tubes. In ASME Pressure Vessels and Piping Conference (Vol. 43673, pp. 369-377).

Cargnelutti, M.F., Belfroid, S.P.C. and Schiferli, W., 2010. Two-phase flow-induced forces on bends in small scale tubes.

Danielson, T.J., 2012. Transient multiphase flow: past, present, and future with flow assurance perspective. Energy & Fuels 26, pp. 4137-4144.

Dai, H.L., Wang, L., Qian, Q. and Ni, Q., 2013. Vortex-induced vibrations of pipes conveying fluid in the subcritical and supercritical regimes. Journal of Fluids and Structures, 39, pp.322-334.

Dai, H.L., Wang, L., Qian, Q. and Ni, Q., 2014. Vortex-induced vibrations of pipes conveying pulsating fluid. Ocean Engineering, 77, pp.12-22.

Dukler, A.E. and Hubbard, M.G., 1975. A Model for Gas-Liquid Slug Flow in Horizontal and Near Horizontal Tubes. Industrial & Engineering Chemistry Fundamentals, 14, 337-347.

Duan, J., Zhou, J., You, Y. and Wang, X., 2021. Time-domain analysis of vortex-induced vibration of a flexible mining riser transporting flow with various velocities and densities. Ocean Engineering, 220, p.108427.

Duan, J., Zhou, J., Wang, X., You, Y. and Bai, X., 2022. Cross-flow vortex-induced vibration of a flexible fluid-conveying riser undergoing external oscillatory flow. Ocean Engineering, 250, p.111030.

Facchinetti, M., Langre, E.d. and Biolley, F., 2004. Coupling of structure and wake oscillators in vortex-induced vibrations. J. Fluid Struct. 19, 123–140.

Fernandes, R.C., Semiat, R. and Dukler, A.E., 1983. Hydrodynamic model for gas-liquid slug flow in vertical tubes. American Institute of Chemical Engineers Journal 29, pp. 981-989.

Gao, Y., Zou, L., Zong, Z., Takagi, S. and Kang, Y., 2019. Numerical prediction of vortex-induced vibrations of a long flexible cylinder in uniform and linear shear flows using a wake oscillator model. Ocean Engineering, 171, pp.157-171.

Gong, Z., 2010. Explosion analysis of the steam pipeline. Guangzhou Chem Ind, 38, pp.181-182.

Govier, G.W. and Omer, M.M., 1962. The horizontal pipeline flow of air-water mixtures. The Canadian Journal of Chemical Engineering 40, pp. 93-104.

Guo, H.Y. and Lou, M., 2008. Effect of internal flow on vortex-induced vibration of risers. Journal of Fluids and Structures, 24(4), pp.496-504.

Haile, S.G., Woschke, E., Tibba, G.S. and Pandey, V., 2022. Internal two-phase flow induced vibrations: A review. Cogent Engineering, 9(1), p.2083472.

Hara, F., 1973. A theory on the two-phase flow induced vibrations in piping systems. In: Transactions of the 2nd International Conference on Structural Mechanics in Reactor Technology, F 5/1, pp. 1–16.

Hara, F., 1977. Two-phase-flow-induced vibrations in a horizontal piping system. Bulletin of JSME.

Hewitt, G.F. and Roberts, D.N., 1969. Studies of two-phase flow patterns by simultaneous x-ray and flast photography. Atomic Energy Research Establishment, Harwell, England (United Kingdom).

Hoogendoorn, C.J. and Buitelaar, A.A., 1961. The effect of gas density and gradual vaporization on gas-liquid flow in horizontal pipes. Chemical Engineering Science 16, pp. 208-221.

Huang, K., Chen, H.-C. and Chen, C.-R., 2010. Flexible catenary riser VIV simulation in uniform current, The Twentieth International Offshore and Polar Engineering Conference. International Society of Offshore and Polar Engineers.

Huang, K., Chen, H.C. and Chen, C.R., 2011. Numerical scheme for riser motion calculation during 3-D VIV simulation. Journal of Fluids and Structures, 27(7), pp.947-961.

James, B. and Hudgins, A., 2016. Failure analysis with case studies from the oil and gas industry.

Jia, D., 2012. Slug flow induced vibration in a pipeline span, a jumper and a riser section. In: Offshore Technology Conference. OTC.

Jia, D., 2013. Effect of boundary conditions, flow rate, slug length, and slug frequency on slug flow induced vibration in a pipeline span. In: Offshore Technology Conference. OTC.

Khan, U., Pao, W. and Sallih, N., 2022. A review: Factors affecting internal two-phase flow-induced vibrations. Applied Sciences, 12(17), p.8406.

Li, W., Li, J., Yin, G., Ong, M. C., 2023. Experimental and numerical study on the slug characteristics and flow-induced vibration of a subsea rigid M-shaped jumper. Journal of Applied Sciences, pp. 1-23.

Liang, F., Zheng, H., Yu, H. and Sun, Y., 2016. Gas–liquid two-phase flow pattern identification by ultrasonic echoes reflected from the inner wall of a pipe. Measurement Science and Technology 27, p. 035304.

Lie, H. and Kaasen, K.E., 2006. Modal analysis of measurements from a large-scale VIV model test of a riser in linearly sheared flow. Journal of fluids and structures, 22(4), pp.557-575.

Liu, G. and Wang, Y., 2018. Study on the natural frequencies of pipes conveying gas-liquid two-phase slug flow. International Journal of Mechanical Sciences, 141, pp.168-188.

Liu, G., Hao, Z., Wang, Y. and Ren, W., 2021. Research on the dynamic responses of simply supported horizontal pipes conveying gas-liquid two-phase slug flow. Processes, 9(1), p.83.

Liu, G., Li, H., Qiu, Z., Leng, D., Li, Z. and Li, W., 2020. A mini review of recent progress on vortex-induced vibrations of marine risers. Ocean Engineering, 195, p.106704.

Liu, Y., Miwa, S., Hibiki, T., Ishii, M., Morita, H., Kondoh, Y. and Tanimoto, K., 2012. Experimental study of internal two-phase flow induced fluctuating force on a 90 elbow. Chemical Engineering Science, 76, pp.173-187.

Ma, B. and Srinil, N., 2020. Planar dynamics of inclined curved flexible riser carrying slug liquid–gas flows. Journal of Fluids and Structures, 94, p.102911.

Ma, B. and Srinil, N., 2022, June. Influence of internal slug flow on vortex-induced vibration of flexible riser with variable curvature. In International Conference on Offshore Mechanics and Arctic Engineering (Vol. 85925, p. V007T08A024). American Society of Mechanical Engineers.

Hossain, M, Chinenye-Kanu, N. M, Droubi, M, Islam, S. Z., 2019. Investigation of slug-churn flow induced excitation forces at pipe bend. Journal of Fluids and Structures., pp. 1-28.

Mandhane, J.M., Gregory, G.A. and Aziz, K., 1974. A flow pattern map for gas-liquid flow in horizontal pipes. International Journal of Multiphase Flow 1, pp. 537-553.

Maribus, 2014. World ocean review 3: Marine Resources - Opportunities and Risks.

Matsui, G., 1984. Identification of flow regimes in vertical gas-liquid two-phase flow using differential pressure fluctuations. International journal of multiphase flow 10, pp. 711-719.

Meng, Shuai, Zhang, Xiaoqing, Che, Chidong and Zhang, Weijing, 2017. Cross-Flow Vortex-Induced Vibration of a Flexible Riser Transporting an Internal Flow from Subcritical to Supercritical. Ocean Engineering. Vol. 139: pp. 74-84.

Meng, S., Song, S., Che, C. and Zhang, W., 2018. Internal flow effect on the parametric instability of deepwater risers. Ocean Eng. 149, 305–312.

Meng, S., Chen, Y. and Che, C., 2020. Slug flow's intermittent feature affects VIV responses of flexible marine risers. Ocean Engineering, 205, p.106883.

Mi, L. and Zhou, Y., 2022. Natural frequency analysis of horizontal piping system conveying low viscosity oil–gas–water slug flow. Processes, 10(5), p.992.

Miranda, J.M.C. and Paik, J.K., 2019. Two-phase flow induced vibrations in a marine riser conveying a fluid with rectangular pulse train mass. Ocean Eng. 174, 71–83.

Mohmmed, A.O., Al-Kayiem, H.H., Nasif, M.S. and Time, R.W., 2019. Effect of slug flow frequency on the mechanical stress behavior of pipelines. International Journal of Pressure Vessels and Piping, 172, pp.1-9.

Monprapussorn, T., Athisakul, C. and Chucheepsakul, S., 2006. Nonlinear vibrations of an extensible flexible marine riser carrying a pulsatile flow. ASME. J. Appl. Mech. 74 (4), 754–769.

Montoya-Hernández, D.J., Vázquez-Hernández, A.O., Cuamatzi, R. and Hernandez, M.A., 2014. Natural frequency analysis of a marine riser considering multiphase internal flow behavior. Ocean Engineering, 92, pp.103-113.

Morooka, C.K. and Tsukada, R.I., 2013. Experiments with a steel catenary riser model in a towing tank. Applied Ocean Research 43, pp. 244-255.

Mukundan, H., Modarres-Sadeghi, Y., Dahl, J.M., Hover, F.S. and Triantafyllou, M.S., 2009. Monitoring VIV fatigue damage on marine risers. Journal of Fluids and structures, 25(4), pp.617-628.

Ortiz-Vidal, L.E., Mureithi, N.W. and Rodriguez, O.M., 2017. Vibration response of a pipe subjected to two-phase flow: Analytical formulations and experiments. Nuclear Engineering and Design, 313, pp.214-224.

Patel, M. and Syed, F., 1989. Internal flow-induced behaviour of flexible risers. Eng. Struct 11, 266–280

Parameshwaran, R., Dhulipalla, S.J. and Yendluri, D.R., 2016. Fluid-structure interactions and flow induced vibrations: a review. Procedia Engineering. 144:1286-1293.

Porter, K., Pereyra, E., Mesa, J. and Sarica, C., 2023. Experimental investigation of induced vibrations in horizontal Gas-Liquid flow. Experimental Thermal and Fluid Science, 149, p.111015

Riley, K.F., Hobson, M.P. and Bence, S.J., 1998. Mathematical methods for physics and engineering. Cambridge University Press, Cambridge.

Riverin, J., and Pettigrew, M. J., 2006. Vibration Excitation Forces Due to Two-Phase Flow in Piping Elements. ASME. J. Pressure Vessel Technol. February 2007; 129(1): 7–13.

Safrendyo, S., and Srinil, N., 2018. Slug flow-induced oscillation in subsea catenary riser experiencing VIV. ASME 2018 37th International Conference on Ocean, Offshore and Arctic Engineering.

Santillan, S.T. and Virgin, L.N., 2011. Numerical and experimental analysis of the static behavior of highly deformed risers. Ocean Engineering, 38(13), pp.1397-1402.

Sarpkaya, T., 2004. A critical review of the intrinsic nature of vortex-induced vibrations. Journal of Fluids and Structures 19, pp. 389-447.

Shou Chen, Zheng, Joan Kim, Wu, and Bo Xiong, Cong, 2012. Effect of Upward Internal Flow on Dynamics of Riser Model Subject to Shear Current. Ocean Engineering. Vol. 26: pp. 95–108.

Song, J.N., Lu, L., Teng, B., Park, H.I., Tang, G.Q. and Wu, H., 2011. Laboratory tests of vortex-induced vibrations of a long flexible riser pipe subjected to uniform flow. Ocean Eng. 38 (11–12), 1308–1322.

Srinil, N., and Bakis, K. N., 2019. Internal flow-induced instability analysis of catenary risers. The 8th conference on computational methods in marine engineering, Gothenburg.

Srinil, N., 2010. Multi-mode interactions in vortex-induced vibrations of flexible curved/ straight structures with geometric non-linearities. J. Fluids. Struct. 26, 1098–1122.

Srinil, N., Wiercigroch, M. and O'Brien, P., 2009. Reduced-order modelling of vortex-induced vibration of catenary riser. Ocean Engineering, 36(17-18), pp.1404-1414.

Sumer, B.M. and Fredsøe, J., 2006. Hydrodynamics Around Cylindrical Structures. World Scientific Publishing, London.

Taitel, Y. and Dukler, A.E., 1976. A model for predicting flow regime transitions in horizontal and near horizontal gas-liquid flow. American Institute of Chemical Engineers Journal 22, pp. 47-55.

Taitel, Y., Bornea, D. and Dukler, A.E., 1980. Modelling flow pattern transitions for steady upward gas-liquid flow in vertical tubes. AIChE Journal 26, pp. 345-354.

Thorsen, M.J., Challabotla, N.R., Sævik, S. and Nydal, O.J., 2019. A numerical study on vortex-induced vibrations and the effect of slurry density variations on fatigue of ocean mining risers. Ocean Engineering, 174, pp.1-13.

Torres, L., Verde, C. and Vázquez-Hernández, O., 2015. Parameter identification of marine risers using Kalman-like observers. Ocean Engineering, 93, pp.84-97.

Vandiver, J.K., Jaiswal, V. and Jhingran, V., 2009. Insights on vortex-induced, traveling waves on long risers. Journal of fluids and structures, 25(4), pp.641-653.

Violette, R., de Langre, E. and Szydlowski, J., 2010. A linear stability approach to vortex-induced vibrations and waves. Journal of Fluids and Structures, 26(3), pp.442-466.

Vince, M.A., Lahey, R.T., Commission, U.S.N.R., Rensselaer Polytechnic, I., 1980. Flow regime identification and void fraction measurement techniques in two-phase flow. The Commission: Available from GPO Sales Program, Division of Technical Information and Document Control, U.S. Nuclear Regulatory Commission; National Technical Information Service, Washington, D.C.: Springfield, Va.

Wallis, G.B., 1969. One-Dimensional Two-Phase Flow. McGraw-Hill.

Wang, E. and Xiao, Q., 2016. Numerical simulation of vortex-induced vibration of a vertical riser in uniform and linearly sheared currents. Ocean Engineering, 121, pp.492-515.

Wang, L., Yang, Y., Li, Y. and Wang, Y., 2018. Dynamic behaviours of horizontal gas-liquid pipes subjected to hydrodynamic slug flow: modelling and experiments. Int. J. Pressure Vessels Piping 161, 50–57.

Wang, L., Yang, Y., Liu, C., Li, Y. and Hu, Q., 2018. Numerical investigation of dynamic response of a pipeline-riser system caused by severe slugging flow. International Journal of Pressure Vessels and Piping, 159, pp.15-27.

Williamson, C., and Govardhan, R., 2004. Vortex-induced Vibration. Annual review of fluid mechanics.

Wu, M.C. and Lou, J.Y.K., 1991. Effects of rigidity and internal flow on marine riser dynamics. Appl. Ocean Res. 13 (5), 235–244.

Wu, X., Ge, F. and Hong, Y., 2012. A review of recent studies on vortex-induced vibrations of long slender cylinders. Journal of Fluids and Structures 28, pp. 292-308.

Xie, W., Gao, X., Wang, E., Xu, W. and Bai, Y., 2019. An investigation of the nonlinear dynamic response of a flexible pipe undergoing vortex-induced vibrations and conveying internal fluid with variable-density. Ocean Engineering, 183, pp.453-468.

Yang, W., Ai, Z., Zhang, X., Chang, X. and Gou, R., 2018. Nonlinear dynamics of three-dimensional vortex-induced vibration prediction model for a flexible fluid-conveying pipe. International Journal of Mechanical Sciences, 138, pp.99-109.

Zaldivar, M., 2014. Quantification of flow rate during slug flow. SPEI flow assurance technical section.

Zanganeh, H. and Srinil, N., 2016. Three-dimensional VIV prediction model for a long flexible cylinder with axial dynamics and mean drag magnifications. Journal of Fluids and Structures, 66, pp.127-146.

Zanganeh, H., Kurushina, V. and Srinil, N., 2021. iSLUG - Identification of Steady Slug Flow Characteristics. Newcastle University. Software.

Zhang, H.Q., Wang, Q., Sarica, C. and Brill, J.P., 2003. A unified mechanistic model for slug liquid holdup and transition between slug and dispersed bubble flows. International journal of multiphase flow, 29(1), pp.97-107.

Zhang, H.Q., Wang, Q., Sarica, C. and Brill, J.P., 2003. Unified model for gas-liquid pipe flow via slug dynamics—part 1: model development. J. Energy Resource. Technol., 125(4), pp.266-273.

Zhu, H., Gao, Y. and Zhao, H., 2018a. Experiment investigation on the flow-induced vibration of a free-hanging flexible riser by internal unstable hydrodynamic slug flow. Ocean Eng. 164, 488–507.

Zhu, H., Gao, Y. and Zhao, H., 2019. Coupling vibration response of a curved flexible riser under the combination of internal slug flow and external shear current. Journal of Fluids and Structures, 91, p.102724.

Zhu, H., Gao, Y., Hu, J., Zhao, H. and Bao, Y., 2022. Temporal-spatial mode competition in slug-flow induced vibration of catenary flexible riser in both in plane and out of plane. Applied Ocean Research, 119, p.103017.

Zhu, H., Gao, Y., Srinil, N. and Bao, Y., 2021. Mode switching and standing-travelling waves in slug flow-induced vibration of catenary riser. Journal of Petroleum Science and Engineering, 203, p.108310.

Zhu, H., Hu, J., Gao, Y., Ji, C. and Zhou, T., 2022. Experimental investigation on flow-induced vibration of a flexible catenary riser conveying severe slugging with variable gas superficial velocity. Journal of Fluids and Structures, 113, p.103650.

Zhu, H., Zhao, H. and Gao, Y., 2018b. Experimental investigation of vibration response of a free-hanging flexible riser induced by internal gas-liquid slug flow. Ocean Eng. 32, 633–645.

Appendix A. Finite Difference Scheme

The nonlinear dimensionless equations (11) – (20) were discretised using a standard finite difference scheme of the second order in both space and time domains following Gao et al., (2019). The total time t_{total}, and the cylinder span ratio (L_D) were subdivided into n and i segments, respectively, such that each time step can be obtained as $\Delta T_m = t_{total}/n$ and each space elements can be obtained as $\Delta Y = L/(D \times i)$. The distinct space locations and time were expressed as $Y = Y_i$ and $T_m = T_{mn}$ where $i = 0, 1, 2, 3 \ldots\ldots, i_{end}$ and $n = 0, 1, 2, 3, \ldots\ldots, n_{end}$. The dimensionless parameters $U, V, W, p,$ and q at location Y_i with time T_{mn} are depicted as U_n^i, V_n^i, W_n^i, p_n^i, and q_n^i respectively. The resulting finite difference derivatives with respect to U, V, W, p and q are expressed as:

$$\frac{\partial^2 U}{\partial T_m^2} = \frac{U_{n-1}^i - 2U_n^i + U_{n+1}^i}{\Delta T_m^2}$$

$$\frac{\partial U}{\partial T_m} = \frac{U_{n+1}^i - U_{n-1}^i}{2\Delta T_m}$$

$$\frac{\partial U}{\partial Y} = \frac{U_{n+1}^{i+1} - U_{n+1}^{i-1}}{2\Delta Y}$$

$$\frac{\partial^2 U}{\partial Y^2} = \frac{U_{n+1}^{i+1} - 2U_{n+1}^i + U_{n+1}^{i-1}}{\Delta Y^2}$$

$$\frac{\partial^4 U}{\partial Y^4} = \frac{6U_{n+1}^{i} - 4U_{n+1}^{i+1} + U_{n+1}^{i+2} - 4U_{n+1}^{i-1} + U_{n+1}^{i-2}}{\Delta Y^4}$$

$$\frac{\partial^2 U}{\partial Y \partial T_m} = \frac{U_{n+1}^{i+1} - U_{n+1}^{i-1} - U_{n-1}^{i+1} + U_{n-1}^{i-1}}{4\Delta T_m \Delta Y}$$

$$\frac{\partial^2 V}{\partial T_m^2} = \frac{V_{n-1}^{i} - 2V_{n}^{i} + V_{n+1}^{i}}{\Delta T_m^2}$$

$$\frac{\partial V}{\partial T_m} = \frac{V_{n+1}^{i} - V_{n-1}^{i}}{2\Delta T_m}$$

$$\frac{\partial V}{\partial Y} = \frac{V_{n+1}^{i+1} - V_{n+1}^{i-1}}{2\Delta Y}$$

$$\frac{\partial^2 V}{\partial Y^2} = \frac{V_{n+1}^{i+1} - 2V_{n+1}^{i} + V_{n+1}^{i-1}}{\Delta Y^2}$$

$$\frac{d^4V}{\partial Y^4} = \frac{6V_{n+1}^{i} - 4V_{n+1}^{i+1} + V_{n+1}^{i+2} - 4V_{n+1}^{i-1} + V_{n+1}^{i-2}}{\Delta Y^4}$$

$$\frac{\partial^2 V}{\partial Y \partial T_m} = \frac{UV_{n+1}^{i+1} - V_{n+1}^{i-1} - V_{n-1}^{i+1} + V_{n-1}^{i-1}}{4\Delta T_m \Delta Y}$$

$$\frac{\partial^2 W}{\partial T_m^2} = \frac{W_{n-1}^{i} - 2W_{n}^{i} + W_{n+1}^{i}}{\Delta T_m^2}$$

$$\frac{\partial W}{\partial T_m} = \frac{W_{n+1}^{i} - W_{n-1}^{i}}{2\Delta T_m}$$

$$\frac{\partial W}{\partial Y} = \frac{W_{n+1}^{i+1} - W_{n+1}^{i-1}}{2\Delta Y}$$

$$\frac{\partial^2 W}{\partial Y^2} = \frac{W_{n+1}^{i+1} - 2W_{n+1}^{i} + W_{n+1}^{i-1}}{\Delta Y^2}$$

$$\frac{\partial^4 W}{\partial Y^4} = \frac{6W_{n+1}^{i} - 4W_{n+1}^{i+1} + W_{n+1}^{i+2} - 4W_{n+1}^{i-1} + W_{n+1}^{i-2}}{\Delta Y^4}$$

$$\frac{\partial^2 W}{\partial Y \partial T_m} = \frac{W_{n+1}^{i+1} - W_{n+1}^{i-1} - W_{n-1}^{i+1} + W_{n-1}^{i-1}}{4\Delta T_m \Delta Y}$$

$$\frac{\partial^2 q}{\partial T_m^2} = \frac{q_{n-1}^{i} - 2q_{n}^{i} + q_{n+1}^{i}}{\Delta T_m^2}$$

$$\frac{\partial q}{\partial T_m} = \frac{q_{n-1}^{i} - q_{n+1}^{i}}{2\Delta T_m}$$

$$\frac{\partial^2 p}{\partial T_m^2} = \frac{p_{n-1}^{i} - 2p_{n}^{i} + p_{n+1}^{i}}{\Delta T_m^2}$$

$$\frac{\partial p}{\partial T_m} = \frac{p_{n+1}^{i} - p_{n-1}^{i}}{2\Delta T_m}$$

(A1)

Substituting the finite difference derivatives (A1) in equations (11) – (20), one can obtain a system of nonlinear equations which is solved using the *FSolve* function in MATLAB. As an example, equation (11) can be expressed as:

$$\frac{(M_n^i+1)(U_{n-1}^i-2U_n^i+U_{n+1}^i)}{\Delta T_m^2}-\frac{E_A\left(\frac{(V_{n+1}^{i+1}-V_{n+1}^{i-1})(U_{n+1}^{i+1}-2U_{n+1}^i+U_{n+1}^{i-1})}{2\Delta Y^3}+\frac{(U_{n+1}^{i+1}-U_{n+1}^{i-1})(V_{n+1}^{i+1}-2V_{n+1}^i+V_{n+1}^{i-1})}{2\Delta Y^3}\right)}{L_D}-$$
$$\frac{E_A\left(\frac{3(U_{n+1}^{i+1}-U_{n+1}^{i-1})^2(U_{n+1}^{i+1}-2U_{n+1}^i+U_{n+1}^{i-1})}{4\Delta Y^4}+\frac{(V_{n+1}^{i+1}-V_{n+1}^{i-1})^2(U_{n+1}^{i+1}-2U_{n+1}^i+U_{n+1}^{i-1})}{4\Delta Y^4}+\frac{(W_{n+1}^{i+1}-W_{n+1}^{i-1})^2(U_{n+1}^{i+1}-2U_{n+1}^i+U_{n+1}^{i-1})}{4\Delta Y^4}+\frac{(U_{n+1}^{i+1}-U_{n+1}^{i-1})(V_{n+1}^{i+1}-V_{n+1}^{i-1})(V_{n+1}^{i+1}-2V_{n+1}^i+V_{n+1}^{i-1})}{2L_D\Delta Y^4}+\frac{(U_{n+1}^{i+1}-U_{n+1}^{i-1})(W_{n+1}^{i+1}-W_{n+1}^{i-1})(W_{n+1}^{i+1}-2W_{n+1}^i+W_{n+1}^{i-1})}{2L_D\Delta Y^4}\right)}{2L_D}-$$
$$\frac{{T_n}_n^i(U_{n+1}^{i+1}-2U_{n+1}^i+U_{n+1}^{i-1})}{\Delta Y^2}+\frac{E_I(6U_{n+1}^i-4U_{n+1}^{i+1}+U_{n+1}^{i+2}-4U_{n+1}^{i-1}+U_{n+1}^{i-2})}{\Delta Y^4}-\frac{M_n^i(U_{n-1}^i-U_{n+1}^i)}{2\Delta T_m}-\frac{{T_n}_n^i(U_{n+1}^{i+1}-U_{n+1}^{i-1})}{2\Delta Y}-\frac{\zeta(U_{n-1}^i-U_{n+1}^i)}{\Delta T_m}-$$
$$\frac{C_{\bar{d}}\left(\frac{Vr_i}{2p_n^i}+\frac{U_{n-1}^i-U_{n+1}^i}{2\Delta T_m}\right)\left(\left(\frac{Vr_i}{2p_n^i}+\frac{U_{n-1}^i-U_{n+1}^i}{2\Delta T_m}\right)^2+\frac{(V_{n-1}^i-V_{n+1}^i)^2}{4\Delta T_m^2}+\frac{(W_{n-1}^i-W_{n+1}^i)^2}{4dT_m^2}\right)^{\frac{1}{2}}}{2mu}-\frac{M_n^iU_r(U_{n-1}^i-U_{n+1}^i)}{2\Delta T_m}+\frac{M_n^iU_r(U_{n+1}^{i+1}-U_{n+1}^{i-1})}{2\Delta Y}+\frac{M_n^iU_r^2(U_{n+1}^{i+1}-U_{n+1}^{i-1})}{2\Delta Y}+\frac{M_n^iU_r^2(U_{n+1}^{i+1}-2U_{n+1}^i+U_{n+1}^{i-1})}{\Delta Y^2}-$$
$$\frac{C_{d0}p_n^i\left(\frac{Vr_i}{2p_n^i}+\frac{U_{n-1}^i-U_{n+1}^i}{2dT_m}\right)\left(\left(\frac{Vr_i}{2p_n^i}+\frac{U_{n-1}^i-U_{n+1}^i}{2dT_m}\right)^2+\frac{(V_{n-1}^i-V_{n+1}^i)^2}{4dT_m^2}+\frac{(W_{n-1}^i-W_{n+1}^i)^2}{4dT_m^2}\right)^{\frac{1}{2}}}{4\mu}-\frac{M_n^iU_r(U_{n-1}^{i+1}-U_{n-1}^{i-1}-U_{n+1}^{i+1}+U_{n+1}^{i-1})}{2\Delta T_m\Delta Y}+\frac{C_lq_n^i(W_{n-1}^i-W_{n+1}^i)\left(\left(\frac{Vr_i}{2p_n^i}+\frac{U_{n-1}^i-U_{n+1}^i}{2dT_m}\right)^2+\frac{(V_{n-1}^i-V_{n+1}^i)^2}{4dT_m^2}+\frac{(W_{n-1}^i-W_{n+1}^i)^2}{4dT_m^2}\right)^{\frac{1}{2}}}{8\Delta T_m\mu} \tag{A2}$$

The values at U_0^i, V_0^i, W_0^i, p_0^i, and q_0^i can be obtained from the initial conditions of U, V, W equal to zero and wake variables p and q equal to 2. However, the initial conditions of $\frac{\partial U}{\partial T_m}=0$, $\frac{\partial V}{\partial T_m}=0$, $\frac{\partial W}{\partial T_m}=0$, $\frac{\partial p}{\partial T_m}=0$ and $\frac{\partial q}{\partial T_m}=0$ must be used when determining the values at U_1^i, V_1^i, W_1^i, p_1^i and q_1^i. From these initial conditions one can have:

$$U_{-1}^i = U_1^i$$

$$V_{-1}^{i} = V_{1}^{i}$$

$$W_{-1}^{i} = W_{1}^{i}$$

$$p_{-1}^{i} = p_{1}^{i}$$

$$q_{-1}^{i} = q_{1}^{i} \tag{A3}$$

Substituting equations (A3) into equations similar to (A2) will result in a new system of nonlinear equations which its solution will provide U_1^i, V_1^i, W_1^i, p_1^i and q_1^i. A detailed description of this discretisation method can also be found in Riley et al., (1998).